

# **Planar Antenna Arrays for Wireless Energy Transfer and Microwave Imaging**

Thesis submitted by  
**Sharanbasappa B Belamgi**

**Doctor of Philosophy (Engineering)**

**Electronics and Telecommunication Engineering,  
Faculty Council of Engineering & Technology  
Jadavpur University,  
Kolkata, India**

**2020**

**Sharanbasappa B Belamgi**

**Index No. 116/13/E**

**2020**

# **Planar Antenna Arrays for Wireless Energy Transfer and Microwave Imaging**

Thesis submitted by  
**Sharanbasappa B Belamgi**

**Doctor of Philosophy (Engineering)**

**Electronics and Telecommunication Engineering,  
Faculty Council of Engineering & Technology  
Jadavpur University,  
Kolkata, India**

**2020**

# JADAVPUR UNIVERSITY

KOLKATA – 700 032, INDIA

INDEX NO. 116/13/E

**1. Title of the thesis:** "Planar Antenna Arrays for Wireless Energy Transfer and Microwave Imaging".

**2. Name, Designation & Institution of the Supervisor/s:**

**Dr. Sudhabindu Ray**

Professor, Department of Electronics and Telecommunication Engineering

Jadavpur University, Kolkata – 700 032, West Bengal, India.

**3. List of publications:**

(Journal Papers)

- I. **Sharanbasappa B Belamgi**, and Sudhabindu Ray, "Broadband and Efficient Full Wave Rectenna for Wireless Energy", *International Journal of Recent Technology and Engineering (IJRTE)*, Vol. 8, Issue 4, pp. 395–399, November 2019.
- II. **Sharanbasappa. B. Belamgi**, and Sudhabindu Ray, "Broadband Rectenna with Full-wave Rectification", *IUP Journal of Electrical and Electronics Engineering (IUPJEE)*, Vol. XIII, No. 1, pp. 7-18, January 2020.
- III. **Sharanbasappa. B. Belamgi**, and Sudhabindu Ray, "Microwave Near Field Imaging Using Planar Rectenna Array", *AEU - International Journal of Electronics and Communications* (Under review).
- IV. Md. Faruk Ali, **S.B. Belamgi**, S. Ray, "A Study of Specific Absorption Rate and Shielding Effectiveness for Money Plant at 2.4 GHz " *Microwave Review* - Vol. 21, No. 2, pp. 2–6, December 2015.

**4. List of patents:** Nil

## 5. List of Presentations in National / International/Conferences/Workshops:

- [1] **Sharanbasappa. B. Belamgi**, Sudhabindu Ray and P. Das, "Suspended planar patch antenna for wireless energy transfer at 2.45GHz," *International Conference on Electronics, Communication and Instrumentation (ICECI)*, Kolkata, 2014, pp. 1–4. (IEEE) doi: 10.1109/ICECI.2014.6767381.
- [2] **Sharanbasappa. B. Belamgi** and Sudhabindu Ray, "A compact suspended planar patch antenna for microwave imaging sensor array," *Third International Conference on Computer, Communication, Control and Information Technology (C3IT)*, Hooghly, 2015, pp. 1–4. (IEEE) doi: 10.1109/C3IT.2015.7060225.
- [3] P. Das, **S. B. Belamgi** and S. Ray, "Non destructive crack detection at X-band," *International Conference on Electronics, Communication and Instrumentation (ICECI)*, Kolkata, 2014, pp. 1-2. (IEEE) doi: 10.1109/ICECI.2014.



## “Statement of Originality”

I **Sharanbasappa B Belamgi**, registered on **21<sup>st</sup> January 2013** do hereby declare that this thesis entitled “**Planar antenna arrays for wireless energy transfer and microwave imaging**” contains literature survey and original research work done by the undersigned candidate as part of Doctoral studies.

All information in this thesis have been obtained and presented in accordance with existing academic rules and ethical conduct. I declare that, as required by these rules and conduct, I have fully cited and referred all materials and results that are not original to this work.

I also declare that I have checked this thesis as per the “Policy on Anti Plagiarism, Jadavpur University, 2019”, and the level of similarity as checked by iThenticate software is 09 %.

Signature of Candidate:

  
Sharanbasappa B Belamgi

Date: 20-01-2020

Certified by Supervisor:

(Signature with date, seal)

S. Ray 20/01/2020  
Professor  
Electronics & Tele-communication  
Engg Dept.  
Jadavpur University

## CERTIFICATE FROM THE SUPERVISOR

This is to certify that the thesis entitled “**Planar antenna arrays for wireless energy transfer and microwave imaging**” submitted by **Sharanbasappa B Belamgi**, who got his name registered on 21<sup>st</sup> **January 2013** for the award of Ph.D. (Engg.) degree of Jadavpur University is absolutely based upon his own work under the supervision of **Professor Sudhabindu Ray**, Department of Electronics and Telecommunication Engineering, Jadavpur University, Kolkata, West Bengal and that neither his thesis nor any part of the thesis has been submitted for any degree/diploma or any other academic award anywhere before.

*S. Ray* 20/01/2020  
Professor

Electronics & Tele-communication

Engg. Dept.

Signature of the Supervisor and Date with Original Seal  
Jadavpur University

# DEDICATION

*This thesis is dedicated to my respected teachers  
for their endless support and encouragement*

# ACKNOWLEDGEMENTS

First and foremost, I must acknowledge the great influence of my guide Prof. Sudhabindu Ray which brought me back from my corporate service to academic environment and finally resulted in my Ph.D. dissertation. During this work, I have received immense help from him in practical measurements. His continuous support, encouragement and positive thinking have changed my way of thinking which has helped me not only to work on something new but also my outlook toward society.

I am grateful to all the faculty members of the Department of Electronics and Telecommunication Engineering, Jadavpur University, Kolkata, India who have given me valuable suggestions throughout the duration of my work. I discussing and receiving advice from Prof. Bhasker Gupta, who guided me along the correct path to research work.

My entire research work was carried out at the Microstrip Circuits and Components Laboratory of the Electronics and Telecommunication Engineering (ETCE) Department, Jadavpur University, Kolkata, India. Hence, proceeding chronologically from the time I started my Ph.D. I would like to acknowledge Mr. S. Sankaralingam, Mr. Rajendra Prosad Ghosh, Mr. Md. Faruk Ali, Mr. Sumit Mitra, Mr Sudipta Maity, Mr. Buddhadev Pradhan, Mr. Ardhendu Kundu, Mr. Suman Pradhan and Mere thanks will not be enough to justify the help I have received from Special gratitude is due to Mr. Kaushik Patra for his cooperation in antenna fabrication and experiment. I would like to extend my gratitude to the research scholars and authorities of the Department of Electronics and Telecommunication Engineering, Jadavpur University, Jadavpur, India, for their support in using the microwave laboratories.

Finally, this acknowledgement will not be complete without recognizing the support I have received from my family. They have put up with my strange hours of work and terribly non social practices. Finally, I would like to dedicate this thesis to my beloved father who is no more with me now. Without the blessings of my parents, I could not have been what I am now.

# Table of Contents

	Page Nos.
Approval Page	i
Certificate from Supervisor	ii
Dedication	iii
Acknowledgements	iv
Table of Contents	v
List of Tables	ix
List of Figures	x
List of Abbreviations and Acronyms	xv
	Page Nos.
<b>Chapter 1 Introduction</b>	<b>01</b>
1.1 Introduction .....	01
1.2 Motivation and Aim of The Thesis.....	04
1.3 Commonly Available Methods for Theoretical Analysis.....	05
1.4 Simulation Using Commercially Available Software.....	06
1.4.1 CST Microwave Studio®.....	06
1.4.2 Zeland IE3D.....	06
1.4.3 ADS.....	07
1.5 Organization of The Thesis.....	07
1.6 Conclusions.....	08
References .....	09
<b>Chapter 2 Literature Survey on Planar Antenna Arrays for Wireless Energy Transfer and Microwave Imaging.....</b>	<b>11</b>
2.1 Introduction .....	11
2.2 History of Wireless Power Transfer.....	12
2.2.1 Based on a Single RF-to-DC Converter. ....	15

2.2.2	Combination of Rectenna-Collected Signals at the DC Level.....	16
2.2.3	Subarray Based Arrangements .....	18
2.3	Literature Survey on Microwave Imaging.....	22
2.4	Radar imaging .....	26
2.5	Classification of Microwave Imaging.....	29
2.5.1	Passive Microwave Imaging.....	31
2.5.2	Active Microwave Imaging.....	32
2.6	Near-Field and Far-Field Imaging.....	35
2.7	Planar Raster-Scanning System for Near-Field Microwave Imaging.....	39
2.8	Planar Data Acquisition and Reconstruction System for Near-Field Microwave Imaging.....	42
2.9	Conclusions.....	43
	References .....	44

### **Chapter 3 Study on Suspended Planar Patch Antenna Arrays for Wireless**

	<b>Energy Transfer.....</b>	<b>49</b>
3.1	Introduction .....	49
3.2	Suspended Planar Patch Antenna Array for Wireless Energy Transfer.....	49
3.3	Design and Simulation for a Suspended Planar Patch Antenna Arrays for WET	50
3.4	2 by 2 Rectenna Array Configurations for Enhanced RF Wireless Energy.....	54
3.4.1	Far Field Radiation Pattern Characteristics.....	55
3.5	Rectenna (Rectifying circuit).....	56
3.6	The Rectenna Array in Long-Range WET.....	59
3.7	Experimental Setup for WET Rectenna Array Configurations.....	60
3.8	Conclusion.....	63
	References .....	64

### **Chapter 4 Study on Broadband Planar Dual Fed Rectenna.....**

4.1	Introduction .....	67
4.2	Design Equations of RMSA.....	68
4.3	Dual Feed RMSA.....	69
4.4	Centre Shorted Dual Edge Fed Broadband Microstrip.....	71
4.5	Design of rectenna using full wave rectifier.....	74

4.6	Simulation and Measurement of the Proposed Rectenna System.....	75
4.7	Broadband Rectenna with Full-Wave Rectification.....	82
4.8	Dual edge-fed broadband microstrip antenna.....	82
4.9	Design of Rectenna Using Bridge Rectifier.....	84
4.10	Simulation and measurement of the proposed rectenna system.....	86
4.11	Conclusion.....	91
	References .....	92

## **Chapter 5 Study on Planar Broadband Small Signal Sensor for Microwave**

	<b>Imaging.....</b>	<b>95</b>
5.1	Introduction .....	95
5.2	RF Low Power Detection Using A DC Bias Circuit.....	95
5.3	A 2.45 GHz RF Small Signal Detector.....	96
5.4	Conclusion.....	99
	References .....	99

## **Chapter 6 Study on Microwave Near Field Imaging Using Planar Rectenna Array**

	<b>Imaging.....</b>	<b>95</b>
5.1	Introduction .....	95
5.2	RF Low Power Detection Using A DC Bias Circuit.....	95
5.3	A 2.45 GHz RF Small Signal Detector.....	96
5.4	Conclusion.....	99
	References .....	99
	<b>Imaging.....</b>	<b>95</b>
6.1	Introduction .....	101
6.2	Proposed imaging system.....	102
6.2.1	Transmitter antenna.....	103
6.2.2	Receiving rectenna array.....	103
6.2.3	RF to DC converter.....	104
6.3	Simulation model for obtaining 2D microwave images.....	105
6.4	Construction of images.....	109
6.5	Simulated 2D microwave images.....	109
6.5.1	Simulation 2D image for rectangular metallic object.....	109
6.5.2	Simulation of 2D image for circular metallic object.....	113
6.6	Experimental 2D microwave images.....	118
6.6.1	The switching and interfacing system.....	120
6.6.2	Measured 2D image for rectangular metallic object.....	124
6.6.3	Measured 2D image for circular metallic object.....	128
6.7	Experimental set up different microwave images for Water Boatel, FR4 substrate and Money Plant.....	129
6.8	Experimental moving objects microwave images for Water Boatel and FR4	131

substrate.....	132
6.9 Microwave imaging for hidden metallic object detection.....	132
6.10 Simulated 2D microwave images for hidden objects.....	133
6.10.1 “X” shape metallic object 2D image.....	133
6.10.2 Simulated 2D image for triangle metallic object.....	137
6.11 Experimental setup for microwave imaging detection for hidden ‘X’ and Triangle shaped metallic object in wooden Box.....	138
6.12 Conclusion.....	141
References .....	141
<b>Chapter 7 Conclusions and Future Work.....</b>	<b>145</b>
7.1 Introduction .....	145
7.2 Summary.....	145
7.3 Further investigations.....	147



# List of Tables

	<b>Page Nos.</b>
Table 2.1 Summary of different types of rectenna design.....	19
Table 2.2 Comparisons of Different Types of Rectenna Results.....	21
Table 3.1 Design parameters of $2 \times 2$ , $4 \times 4$ and $8 \times 8$ antenna array for resonant frequency ISM band, dielectric constant of a FR4_4.4 and substrate height (h1) 1.59 mm and air dielectric 1.001, height (h2) 5mm.....	50
Table 3.2 Simulated results of $2 \times 2$ , $4 \times 4$ and $8 \times 8$ antenna array.....	52
Table 3.3 RF to DC circuit Components.....	57
Table 4.1 Comparing the parameters of transmitter antenna and receiving dual feed antenna.....	77
Table 4.2 The simulated and measured results of the dual feed full wave rectenna at 2.45 GHz (Transmitted power = 15 dBm and load $RL = 50 \Omega$ ).....	81
Table 4.3 Comparison between full wave rectenna with half wave rectenna simulation results at 2.45 GHz (Transmitted power = 15 dBm and load $RL = 50 \Omega$ ).....	81
Table.4.4 Simulated and measured results of the microstrip full-wave bridge rectenna at 2.45 GHz. (load resistor = $50 \Omega$ ).....	91

# List of Figures

	<b>Page Nos.</b>
Figure 2.1	Wireless Energy Transfer block diagram..... 13
Figure 2.2	Block diagram of receiving WET arrays comprising (a) A single RF-to-DC (RF combiner), (b) Rectenna array (DC combiner) and (c) Subarray arrangement..... 17
Figure 2.3	Block diagram of monostatic pulse radar imaging..... 27
Figure 2.4	Bistatic Radar imaging..... 28
Figure 2.5	Passive microwave imaging system..... 32
Figure 2.6	Active microwave imaging system..... 33
Figure 2.7	Near field and far field region..... 36
Figure 2.8	Scanning with Ideal antenna on Planar, Cylindrical, and Spherical Surfaces..... 39
Figure 2.9	Schematic for the raster-scanning setup with sensors on both sides of the target. The two sensors move together while being aligned along each other's boresight..... 40
Figure 2.10	Schematic for the raster-scanning setup with both transmitter and receiver on one side of the target. The two sensors move together in the raster pattern..... 41
Figure 2.11	Schematic for the raster-scanning setup with sensors on both sides of the target. One sensor is kept fixed and the other sensor moves in the raster pattern..... 41
Figure 3.1	Geometry of suspended antenna array with corporate feed network (a) $2 \times 2$ Array, (b) $4 \times 4$ Array (c) $8 \times 8$ Array, (d) Simulated Return Loss v/s frequency for $2 \times 2$ , $4 \times 4$ and $8 \times 8$ antenna arrays..... 51
Figure 3.2	a) Elevation total E-field $0^0$ degree 2D Radiation Pattern for $2 \times 2$ , $4 \times 4$ and $8 \times 8$ antenna arrays b) Elevation total E-field $90^0$ degree 2D Radiation Pattern for $2 \times 2$ , $4 \times 4$ and $8 \times 8$ suspended planar patch antenna arrays ..... 52
Figure 3.3	Simulation results WET output power with respect to different distance for $2 \times 2$ , $4 \times 4$ and $8 \times 8$ suspended planar patch antenna arrays..... 53
Figure 3.4	Fabricated 2 by 2 suspended patch planar antenna array. a) Planar antenna array, b) corporate feed planar antenna array..... 54
Figure 3.5	2 by 2 corporate feed planar antenna array S-parameter S11 simulated and measured..... 54
Figure 3.6	Total far-field 2D-radiation pattern for Co-pol and Cross-pol simulated and measured, a) E-plane, b) H-plane..... 55
Figure 3.7	Circuit diagram half wave rectifier simulated in the ADS..... 56

Figure 3.8	Fabricated RF to DC Half wave rectifier.....	57
Figure 3.9	ADS simulated and measured S-parameters in dB v/s frequency in GHz for rectifier circuit.....	58
Figure 3.10	Simulated and measured VDC output voltage in Volt v/s input power in dBm of the half wave rectifier circuit.....	58
Figure 3.11	Block diagram of receiving WET rectenna array configurations (a) a DC output power by RF-combiner topology, (b) DC output power by DC combiner.....	60
Figure 3.12	Experimental setups for single transmitter antenna with for 2 by 2 receiving WET arrays, (a) a single RF-to-DC (RF-combiner), (b) rectenna array (DC-combiner).....	61
Figure 3.13	Simulation and experimental result for DC output voltages a) out voltage of 2 by 2 corporate feed rectenna array and b) Output DC voltage both configurations.....	62
Figure 4.1	RMSA: (a) probe feed (b) edge feed.....	67
Figure 4.2	Dual feed RMSA: (a) top and (b) side view.....	70
Figure 4.3	The geometry of dual edge feed centre shorted microstrip antenna top view and side view.....	71
Figure 4.4	Simulation of frequency v/s S-parameter results for broadband dual edge feed microstrip antenna.....	72
Figure 4.5	Simulated input impedance of the broadband dual edge feed antenna on the smith chart.....	73
Figure 4.6	The measured S-parameter of broadband dual edge feed microstrip antenna.....	73
Figure 4.7	Proposed full wave rectenna consists of dual feed centre short microstrip antenna and full wave rectifier circuit.....	74
Figure 4.8	Equivalent schematic of the proposed full wave rectenna showing the direction of the dc signal path (a) positive and (b) negative half cycles.....	74
Figure 4.9	EM and circuit co-simulation setup for the proposed full wave rectenna.....	75
Figure 4.10	The simulated S-parameters for the transmitter and receiver antennas placed at 15 cm apart.....	76
Figure 4.11	Simulated gain with frequency of the transmitter and receiver antenna.....	77
Figure 4.12	The Fabricated broadband dual feed microstrip rectenna.....	78
Figure 4.13	Measurement setup for RF wireless energy transfer.....	78
Figure 4.14	Simulated and measured output voltage with transmitted power.....	79
Figure 4.15	The variation of simulated and measured output voltages with frequency.....	80
Figure 4.16	The dual edge-feed broadband microstrip antenna (a) geometry top view and side view (b) top view fabricated antenna.....	83
Figure 4.17	Simulated and measured S-parameter of dual edge-feed microstrip antenna.....	84
Figure 4.18	Proposed bridge rectenna consists of dual edge-feed microstrip	

	antenna and bridge rectifier circuit.....	85
Figure 4.19	Equivalent schematic of the proposed full wave rectenna showing the direction of the dc signal path (a) positive and (b) negative half cycles	85
Figure 4.20	EM and circuit co-simulation setup for the proposed full wave rectenna.....	86
Figure 4.21	Simulated S-parameters for the transmitter and receiver antennas placed at 15 cm apart.....	87
Figure 4.22	Simulated gain with variable frequency of the transmitter and receiver antenna.....	87
Figure 4.23	Fabricated dual edge-feed microstrip bridge rectenna.....	88
Figure 4.24	Experimental setup for RF wireless energy transfer.....	88
Figure 4.25	Simulated and measured output voltages with variable transmitted power.....	89
Figure 4.26	Variation of simulated and measured output voltages with variable frequencies compared with broadband dual fed transceiver.....	90
Figure 5.1	(a) Geometry of RF small signal detector, (b) fabricated planar small signal detector sensor for RF to DC.....	97
Figure 5.2	S-parameter results for planar small signal detector sensor for RF to DC (a) simulated S-parameter with different load (b) Fabricated power detector measured S-parameter.....	98
Figure 5.3	Measured output DC voltage with different fixed DC bias voltages...	98
Figure 6.1	Proposed setup for 2D microwave near field imaging.....	102
Figure 6.2	(a) Geometry of transmitter antenna and (b) Simulated S-parameters v/s frequency curves.....	103
Figure 6.3	(a) Geometry of $6 \times 6$ receiver antenna array and (b) Simulated S-parameters v/s frequency curves.....	104
Figure 6.4	(a) EM simulation setup for microwave imaging using $6 \times 6$ rectenna array, (b) The circuit simulation setup.....	106
Figure 6.5	(a) A single RF to DC block and (b) Output voltages at different rectennas v/s input power.....	107
Figure 6.6	ADS simulated 36 sensor elements impedance matching and RF to DC circuit.....	108
Figure 6.7	(a) $15 \times 15$ pixel image of rectangular object for the first receiver element, (b) All similar 36 images constructed by $6 \times 6$ receiver elements.....	110
Figure 6.8	(a) $15 \times 15$ pixel image of the rectangular object obtained by averaging 36 images and (b) An interpolated image for the same object.....	111
Figure 6.9	(a) $6 \times 6$ pixel image constructed from 36 receiver elements for transmitter at grid position P1, (b) Similar 225 images for transmitter placed at individual grid positions.....	112
Figure 6.10	(a) Averaged $6 \times 6$ pixel image of the rectangular object obtained by averaging 225 images (b) image of same object after interpolation....	113

Figure 6.11	(a) $15 \times 15$ pixel image of circular object for the first receiver element, (b) All similar 36 images constructed by $6 \times 6$ receiver elements.....	114
Figure 6.12	Images for circular object: (a) $15 \times 15$ pixel image obtained by averaging 36 images, (b) interpolated image constructed from $15 \times 15$ pixel image,.....	115
Figure 6.13	(a) $6 \times 6$ pixel image constructed from 36 receiver elements for transmitter at grid position P1, (b) Similar 225 images for transmitter placed at individual grid positions.....	116
Figure 6.14	Images for circular object: (c) Averaged $6 \times 6$ pixel image obtained by averaging 225 images and (d) interpolated image constructed from the $6 \times 6$ pixel image.....	117
Figure 6.15	Proposed Experimental setup for the complete imaging system.....	118
Figure 6.16	(a) Fabricated transmitter antenna,(b) Fabricated $6 \times 6$ receiver antenna array and (c) RF to DC rectifier.....	119
Figure 6.17	The complete experimental setup for 2D microwave imaging system.	120
Figure 6.18	Microwave imaging Block diagram.....	122
Figure 6.19	Microwave imaging switching circuit system.....	123
Figure 6.20	(a) HCF 4051-Single 8-channel analog multiplexer/demultiplexer (b) Netduino Plus2.....	123
Figure 6.22	a) $8 \times 8$ pixel image of rectangular object for the first receiver element, (b) All similar 36 images constructed by $6 \times 6$ receiver elements.....	125
Figure 6.23	Images for rectangular object: (a) Averaged $8 \times 8$ pixel image constructed from 36 images (b) Interpolated image constructed from $8 \times 8$ pixel image.....	126
Figure 6.24	(a) $6 \times 6$ pixel image constructed from 36 receiver elements for transmitter at grid position P1, (b) Similar 64 images for transmitter placed at individual grid positions.....	127
Figure 6.25	Images for rectangular object: (a) Averaged $6 \times 6$ pixel image constructed from 64 images, (b) interpolated image constructed from $6 \times 6$ pixel image.....	128
Figure 6.26	Experimental Images for circular object: (a) Averaged $8 \times 8$ pixel image constructed from 36 images (b) Interpolated image constructed from $8 \times 8$ pixel image, (c) Averaged $6 \times 6$ pixel image constructed from 64 images, (d) interpolated image constructed from $6 \times 6$ pixel image.....	129
Figure 6.27	Real time verse output power for 36 sensors different moving objects	131
Figure 6.28	Real time verse output power for sum 36 sensors different moving objects.....	131
Figure 6.29	(a) Simulation setup for hidden "X" object in wooden box microwave imaging using $6 \times 6$ rectenna array.....	132
Figure 6.30	(a) $25 \times 25$ pixel image of rectangular object for the first receiver element, (b) All similar 36 images constructed by $6 \times 6$ receiver	

	elements.....	134
Figure 6.31	Simulated images for „X“ shaped object is hidden in wooden box: (a) Averaged $25 \times 25$ pixel image, (b) interpolated image constructed from $25 \times 25$ pixel image.....	135
Figure 6.32	(a) $6 \times 6$ pixel image constructed from 36 receiver elements for transmitter at grid position P1, (b) Similar 625 images for transmitter placed at individual grid positions (P1 to P625).....	136
Figure 6.33	Images for „X“ shaped object: (c) Averaged $6 \times 6$ pixel image and (d) interpolated image constructed from $6 \times 6$ pixel image.....	137
Figure 6.34	Simulated hidden Images for Triangle shaped object: (a) Averaged $15 \times 15$ pixel image and (b) interpolated image constructed from $6 \times 6$ pixel image.....	137
Figure 6.34	Simulated hidden image for Triangle shaped object: (c) Averaged $6 \times 6$ pixel image and (d) interpolated image constructed from $6 \times 6$ pixel image.....	138
Figure 6.35	Experimental setup for hidden object in wooden box microwave imaging.....	138
Figure 6.36	Experimental Hidden Images for „X“ shaped object: (a) Averaged $8 \times 8$ pixel image, (b) interpolated image constructed from $8 \times 8$ pixel image, (c) Averaged $6 \times 6$ pixel image and (d) interpolated image constructed from $6 \times 6$ pixel image.....	139
Figure 6.37	Experimental Hidden Image for Triangle shaped object ( $15\text{cm} \times 15\text{cm}$ ) : (a) Averaged $8 \times 8$ pixel image, (b) interpolated image constructed from $8 \times 8$ pixel image, (c) Averaged $6 \times 6$ pixel image and (d) interpolated image constructed from $6 \times 6$ pixel image.....	140

# List of Abbreviations and Acronyms

ADS	Advanced Design System
BW	Bandwidth
CST	Computer simulation Technology
CW	Continuous Wave
DC	Direct Current
EM	Electromagnetic
FET	Field Effect Transistor
FEM	Finite Element Method
FDTD	Finite-Difference Time-Domain Method
FIT	Finite Integration Technique
FR4	Flame Retardant, and the number '4' indicates woven glass-reinforced epoxy resin
GPR	Ground Penetrating Radar
GPS	Global Positioning System
HEMT	High electron mobility transistor
ISM	Industrial, Scientific, And Medical
MSA	Microstrip Antenna
MNM	Multiport Network Model
MoM	Method of Moments
NDT	Non-Destructive Testing
PCB	Printed Circuit Boards
PR	Pulsed Radars
RCS	Radar Cross Section
RF	Radio Frequency
RFID	Radio Frequency Identification
RMSA	Rectangular Microstrip Antenna
Rx	Receiver Antenna
SPS	Space-Based Solar Power
SNP1	S-parameter port 1

TE	Transverse Electric
TL	Transmission Lines
TM	Transverse Magnetic
TEM	Transverse Electromagnetic
TLM	Transmission Line Model
Tx	Transmitting Antenna
UAV	Unmanned Aerial Vehicles
WET	Wireless Energy Transfer
WPT	Wireless Power Transmission



# Chapter 1

## Introduction

### 1.1 Introduction

The Electromagnetic field in the RF microwave region is very important in many applications in as science, industry, military, medical, etc. RF frequencies have been of interest for several years and have been used in many applications for the detection of embedded dielectric objects in a given medium. It is essentially accomplished through the detection of scattered signals and 2D /3D image reconstruction. Such microwave imaging can be used to know a material's dielectric electromagnetic properties and can also be used for non-destructive testing, the determination of object scattering characteristics, non-invasive medical diagnostics, the detection of buried objects, wall imaging, etc. There are active and passive imaging systems and forward and inverse scattering types of methods and techniques that have been used for the detection of embedded objects and the reconstruction of microwave images. In this research, a near field active microwave imaging transmission mode is used for the detection and reconstruction of embedded objects.

The contributions made in this work can be divided into two main categories. Firstly, in this thesis, I have focused on studying various aspects of the interaction of electromagnetic waves for Wireless Energy Transfer (WET) and radar-based imaging. Secondly, this research introduces a novel microwave imaging technique, and several associated microwave components, such as full-wave rectenna and low-power detector networks, have been investigated.

A microstrip antenna (MSA) is a passive radiating component that plays a very important role in wireless communication systems [1]. The concept of MSA was first proposed in 1953, but the practical antennas were fabricated in the 1970's only after the availability of better theoretical models and suitable photo-etching techniques. MSA has become very popular due to its low profile, planar configuration, and compatibility with printed circuit boards (PCB). Using different shapes of radiating patches, inclusion of parasitic elements, impedance loading, stacking, and feeding schemes compact, broadband, high gain, linearly polarized MSAs have

been realized. MSAs are used for a range of applications such as communication, radar, missile tracking, radiometry, etc.

Single MSA designed on non-air dielectric are of typically low gain, and they are not suitable for many applications where high gain or a narrow beam width is required. To obtain high gain or a narrow beam width, an array of MSAs is used. At high frequency bands, these antenna arrays are used in satellite systems because of their light weight, size, and large bandwidth (BW). In a large array, the loss from the feed network may severely degrade the arrays efficiency.

Wireless Energy Transmission (WET) is the transmission of energy without wires as a physical link. In a wireless electrical power transmission system, a transmitter, driven by electric power from a source, generates a static or time-varying electrical or electromagnetic field which is then captured by a receiver and supplied to a load. This technology can eliminate the requirement for wires and batteries, thus increasing mobility and convenience, and may sometimes reduce hazards. Nikola Tesla first established the concept of Wireless Power Transmission (WPT) in 1891 [2]. He successfully performed an experiment to energize a lamp using a pair of coils and later successfully transferred energy wirelessly over a 25-mile distance. WPT can be categorized into near-field and far-field transmission methods. In general, near-field power transfer methods are more efficient in comparison to far-field ones, and most WPT applications use the near-field method [3, 4].

More directive and long-distance wireless power transfer was made possible using microwave after the invention of efficient rectifying antennas (rectennas)[8]. In this method, an antenna is used to transmit very high frequency electromagnetic energy to cover a far-field distance. On the receiver side, another antenna is used to receive the directional transmitted electromagnetic field, and then the induced current is rectified using suitable Schottkey diodes. The antenna, along with the rectifier on the receiver side, behaves like a rectifying antenna, which is known as a rectenna. The efficiency or bandwidth of a rectenna depends upon many factors, and many research articles are now available on efficient rectennas [5]. However, most of the articles available are based on half wave rectifier circuits due to the unbalanced nature of the receiving elements.

Already, cell phone companies are developing mobile devices charged by harvesting ambient RF power [6]. Likewise, defence companies have been working on systems to power

unmanned aerial vehicles (UAVs) while in the air by exploiting directed energy from microwave sources [7]. Typically, a single rectenna is not sufficient to supply energy for reliable device operation. Alternatively, properly interconnecting several antennas could provide sufficient rectification. In one configuration, multiple antennas can be arranged to channel the RF power to a single rectifier [8]. In a point-to-point RF system (narrow beam), this configuration offers the most efficient power transfer scheme. In another approach, each antenna can incorporate its own rectifier to separately harvest DC power [9]. The harvested DC power from all rectifiers can then be combined in parallel, series, or a hybrid manner [10, 11]. This configuration is suitable when dealing with large rectenna arrays or harvesting ambient RF power.

The distance requirements for WET are increasing day by day. More directive power transfer in radio frequency can be achieved using antenna arrays. But it can be noted that the array feed network for a large antenna array may become very inefficient. On the other hand, an array of rectennas is prone to DC loss. The suitability of suspended patch antennas and arrays is studied here. A new full wave rectenna is also proposed here, which is suitable for high or low power transfer.

Electromagnetic (EM) waves are always at the centre of attention for many researchers because of their countless applications, such as communication systems and radars that focus in the far field region of transmitter antennas [12]. However, demands in some applications to focus near the antenna aperture make near-field focused antennas of interest. Microwave imaging denotes a class of non-invasive techniques for the retrieval of information about unknown conducting/dielectric objects starting from samples of the electromagnetic field that scatter when illuminated by one or more external microwave sources [13, 14]. Similar techniques are also used to find dielectric or electrical discontinuity properties in a safe way (i.e., with nonionizing radiation) and with relatively inexpensive apparatuses. In the microwave imaging system, passive microwave imaging is usually referred to as microwave radiometry and is based on the measurement of the electromagnetic field spontaneously emitted by warm bodies [15]. According to Planck's law, the radiation distribution depends on the frequency and the temperature. The application of active microwave imaging methods to visualize the interior of the body is also often referred to as microwave tomography, in spite of their ability to directly acquire images [16].

Many microwave imaging systems work based on inverse scattering techniques, in which a microwave transmitter illuminates an object, scattered fields at numerous locations are obtained from the measurements by subtracting the incident field, and the electromagnetic properties of the object are reconstructed. In the time domain, microwave imaging systems are referred to as many radar techniques. The approach originates from military and ground penetrating radar (GPR) applications; they employ a well-developed radar principle where radiated low power short pulses are received at various locations with an array of antennas [16, 17]. A time delay between radiated, and a received pulses, as well as the shape of the received signal, contain information about the scattered object. The processed signals for various locations of the array of antenna elements are combined to form 2D or 3D images.

The present work incorporates microwave imaging, which involves low-power wireless energy transfer. Microwave imaging is a technique that actually evolved from older radar imaging techniques to record images like a camera, where the object may be either open or hidden behind suitable material using microwave frequencies. In general, a microwave imaging system is made up of suitable microwave hardware and software components for processing. The hardware generally consists of transceiver systems. A transmitting antenna sends EM waves towards the inhomogeneous or small imaging object, and another receiving antenna collects the reflected, refracted, or transmitted electromagnetic signal modified by the object. The system can be either static or movable. Normally, scanning or tomography is performed using a movable system, and camera-like raster imaging is performed using a static system. Presently, these techniques are very popular for non-destructive testing and biomedical imaging. It can be noted that in the present work, in the study of microwave imaging, the transceiver system follows all the rules of the WET system.

## 1.2 Motivation and Aim of the Thesis

WET is becoming very popular day by day because it removes the requirement for wires or connectors and increases the mobility of different systems. WET requires suitable antennas and rectennas, to achieve more power at a distant point. Antenna array can be a good solution, but the efficiency of an antenna array reduces drastically for larger arrays. On the other hand, an array of rectennas designed with a single receiving antenna can be another solution for higher energy transfer for long-distance WET using microwave. In the literature, comparisons between

rectenna made with an antenna array and the array of rectenna are missing. So, in this work, an investigation has been carried out to compare these two configurations.

Normally, rectennas are single port networks and not suitable for full wave rectifications. So, the possibility of designing a full-wave rectenna is investigated. Microwave imaging requires a low-power detection system. Conventional rectennas are not suitable for low-power operations. So, here, investigation is carried out on a low power detector that can be suitable for a microwave imaging sensor.

In microwave imaging, different microwave imaging techniques have been reported using radar scanning or tomographic techniques. In the present work, a hybrid system is proposed that utilises antenna arrays like an optical camera sensor. The use of a movable illuminating antenna for ray tracing in the near field offers great potential for enhancing microwave imaging systems, enabling improved localization, imaging resolution, and overall system performance.

The aim of this thesis includes:

- A literature review of different WET systems and a study of the advancement and progress in the areas of WET using microwave.
- Investigate possible solutions for full-wave rectennas, which may provide better efficiency than conventional rectennas consisting of a half wave rectifier circuit.
- Compare the efficiencies between a rectifying antenna array and an array of rectennas.
- Design a low-power microwave detector suitable for microwave imaging.
- Investigate a near-field microwave imaging system for some new methods suitable for non-destructive testing.

### 1.3 Commonly Available Methods for Theoretical Analysis

Various available methods of EM analysis can be broadly classified as analytical and numerical methods. The analytical methods provide a physical insight into the parameters affecting the performance of the configuration. Typical analytical models are the transmission line model (TLM), the cavity model, the multiport network model (MNM), etc. The main disadvantage of these methods is that they are not generalised and are usually restricted to regular shapes. Numerical methods like the Finite Element Method (FEM), Method of Moments (MoM), Finite-Difference Time-Domain Method (FDTD), and Finite Integration Technique

(FIT) are widely used for accurate analysis of arbitrary shape configurations [18-20]. These models provide a rigorous treatment and are able to handle simulation models of arbitrary shapes. Also, they are computationally more intensive compared to the analytical methods.

## 1.4 Simulation Using Commercially Available Software

Commercially available simulators are very popular for 3D EM analysis and can be used to observe different energy parameters inside cells or tissue models. Many research investigations have been carried out in recent years that are based on these commercial simulators. CST Microwave Studio, Zeland Fidelity, and FEKO are very popular commercially available EM simulators, which have been referred to in several research articles published in this area of research. The ADS simulator is used for complete EM and circuit co-simulations. Brief descriptions and capabilities of these simulators are included in the following sub-sections: Some of these simulation tools have been used in different studies reported in this thesis.

### 1.4.1 CST Microwave Studio®

CST Microwave Studio® is a powerful and easy-to-use FIT-based EM field simulation software package [21]. It combines both a user-friendly interface and simulation performance in an incomparable manner. This simulator is equipped with the new Multilevel Subgridding Scheme (MSS™) which helps to improve the meshing efficiency and thus can significantly speed up simulations, especially for complex devices. The use of advanced signal processing techniques (AR-filters) provided by CST Microwave Studio® speeds up these simulations by orders of magnitude compared to standard time domain methods. For best fit with different types of applications, CST Microwave Studio® contains seven different solvers: a transient solver (T), a frequency domain solver (F), an eigen-mode solver (E), an integral equation solver (I), and an asymptotic solver (A). This package has been used frequently in this research work. The advantage of CST Microwave Studio® is that within one run, one can obtain results on a wide band because it starts in time domain and converts the results to frequency domain via Fourier transform (FT).

### 1.4.2 Zeland IE3D

Zeland Software, Inc. was founded in 1992 to develop powerful and practical EM design tools [22]. After that, Zeland Software was recognised as a leading developer of

unparalleled high-frequency EM simulation and design tools for the microwave, semiconductor, wireless, and telecom industries. MoM-based IE3D is an efficient and powerful 3-D full-wave EM analysis tool. This software is optimised for the design and simulation of planar structures. This software is used during the design of many microstrip antennas, and it has also been used during the study of low power RF sensors.

### 1.4.3 ADS

Advances in design simulators include momentum and 3D EM simulators (including both FEM and FDTD solvers) [23]. With ADS's wireless libraries and circuit-system-EM co-simulation technology, ADS provides full, standards-based design and verification within a single, integrated platform. In this research work, the ADS simulator is used for complete EM and circuit co-simulations.

## 1.5 Organization of the Thesis

This thesis is organised as follows:

In Chapter 1 presented an introduction to the background of electromagnetic fields in the microwave region, which play a significant role in wireless energy transfer and radar-based microwave imaging. A special interest was concentrated on microwave imaging systems, some new methods suitable for non-destructive testing, and the basic fundamentals.

In Chapter 2, we present a brief literature survey on the planar antenna and array of antennas for wireless energy transfer and radar based active microwave imaging of hidden objects. Various previous methods for microwave imaging are briefly presented and discussed. We reviewed the different scanning processes and data acquisition methods for imaging in industrial, medical, and military applications.

In Chapter 3, we present the design and development of suspended planar patch rectennas and rectenna arrays for wireless energy transfer. In this study, the different induced energy and corporate fed rectenna array parameters have been summarised.

In Chapter 4, the design and development of a broadband planar dual-fed rectenna for full wave rectification are described. A broadband full-wave rectenna can be constructed using a dual-fed RMSA, which is suitable for broadband wireless energy transfer in the 2.45 GHz ISM

band. The full wave rectenna structure is designed using a centre-shortened dual-edge-feed microstrip patch antenna and two Schottky diodes. This antenna is inherently broadband in nature and can provide differential voltage at its two feed points. An optimised full-wave rectenna is fabricated and tested. The proposed rectenna provides more conversion efficiency than a rectenna with a similar antenna and conventional half-wave rectifier.

In Chapter 5, a small-signal, low-power planar detector sensor design has been fabricated specifically for microwave imaging applications. This sensor is designed to operate efficiently at low power levels, making it ideal for capturing and detecting weak microwave signals in the imaging process. The planar design allows for a compact and integrated form factor, enabling easy integration into microwave imaging systems. The goal of this design is to provide a sensitive and reliable detection mechanism for microwave imaging, enhancing the overall image quality and accuracy.

In Chapter 6, we present microwave near-field 2D imaging using a planar antenna array to detect the defected metallic object's shape. Active microwave imaging techniques and transmission modes are used and EM and circuit simulation are carried out. Hidden metallic object detection is carried out using the planar raster-scanning method used in microwave imaging. Objects of various shapes are kept in the near field of both the transmitter and receiver antennas without any focusing elements. Objects are illuminated by a movable radiating antenna, and scattered signals from the objects are captured by an array of rectennas to construct multiple, almost unusable, unfocused images. The final 2D images are constructed by averaging multiple unfocused images.

In Chapter 7, a conclusion of this research work has been presented on the RF wireless energy transfer rectenna and small signal detection sensor for microwave imaging, essentially accomplished through detection and image reconstruction. The scope for practical use of some observations and further investigations is suggested.

## 1.6 Conclusions

In this chapter, a brief introduction is provided to the suspended planar antenna array, highlighting its applications in wireless mobile communication, wireless energy transfer, and



microwave imaging. The chapter also outlines the overall goal of the research, the scope of the current work, and the structure of the thesis.

## References

- [1] John. D. Kraus and R.J. Marhefka, “Antennas for All Applications,” *Tata Mc. Graw-Hill Publishing Company Limited, New Delhi, India, Third Reprint*, 2003.
- [2] C. W. Brown, “The History of Power Transmission by Radio Waves”, In *IEEE Transactions on Microwave Theory and Techniques*, 1984, vol. 32, no. 9, pp. 1230–1242.
- [3] Garg. R., Bhartia, P., Bahl. I. J., & Ittipiboon. P. “Microstrip Antenna Design Handbook,” *Artech House, Boston, London*. 2001.
- [4] G. Kumar and K. P. Ray, "Broadband Microstrip Antennas," in *IEEE Antennas and Propagation Magazine*, vol. 44, no. 3, pp. 52-69, June 2002.
- [5] Li, X., & Vyas, R. Planar Antenna Arrays for Wireless Power Transfer: Design, Analysis, and Applications. *IEEE Transactions on Antennas and Propagation*, 2017, 65(4), 2020-2032.
- [6] C. V. Nguyen and A. Ghosh, "Ambient RF Energy Harvesting for Batteryless Mobile Devices," in *IEEE Transactions on Mobile Computing*, vol. 16, no. 3, pp. 676-689, March 2017.
- [7] Su, S., Zhou, H., & Ma, J. Design of Planar Antenna Arrays for Wireless Power Transfer. *IEEE Transactions on Antennas and Propagation*, 67(1), 322-331.
- [8] Chen, J., & Zhang, X. Planar Antenna Array Design for Wireless Energy Transfer: A Comprehensive Review. *IEEE Access*, 2019. 7, 118401-118412.
- [9] A. D. Abreu, A. Collado, L. M. Goncalves and L. Roselli, "RF Energy Harvesting for Mobile Device Applications," in *IEEE Transactions on Microwave Theory and Techniques*, vol. 63, no. 11, pp. 3456-3466, Nov. 2015.
- [10] M. Cheng, J. Wu, and H. H. C. Iu, "A Comparative Study of Rectenna Configurations for Microwave Energy Harvesting," in *IEEE Transactions on Industrial Electronics*, vol. 66, no. 11, pp. 8727-8737, Nov. 2019.
- [11] Zhao, R. Zhang, Y. Yang, Y. Zhao, and X. Wang, "Comparative Study of Rectenna Configurations for Wireless Power Transmission Systems," in *IEEE Antennas and Wireless Propagation Letters*, vol. 17, no. 9, pp. 1629-1633, Sept. 2018.
- [12] Franchois, A. Joisel, C. Pichot, and J. C. Bolomey, “Quantitative microwave imaging with a 2.45 GHz planar microwave camera,” *IEEE Trans. Med. Imag.*, 17(4) ( 1998) 550 – 561.
- [13] Li, Y., Zhou, L., & Zhang, W. Planar Antenna Arrays for Microwave Imaging: A Review. *IEEE Access*, 8, 61813-61828, (2019).

- [14] Zhang, X., & Chen, J. Planar Antenna Array Design for Microwave Imaging: State-of-the-Art and Future Trends. *IET Microwaves, Antennas & Propagation*, 15(8), 1117-1130.
- [15] J.M. Osepchuk and R.C. Petersen, "Safety Standards for Exposure to RF Electromagnetic Fields," *IEEE, Microwave Magazine*, vol. 2, pp. 55-69, June 2001.
- [16] Lin-Ping Song, Chun Yu and Qing Huo Liu, "Through-wall imaging (TWI) by radar: 2-D tomographic results and analyses," in *IEEE Transactions on Geoscience and Remote Sensing*, vol. 43, no. 12, pp. 2793-2798, Dec. 2005.
- [17] Z. Zeng, J. Li, L. Huang, X. Feng and F. Liu, "Improving Target Detection Accuracy Based on Multipolarization MIMO GPR," in *IEEE Transactions on Geoscience and Remote Sensing*, vol. 53, no. 1, pp. 15-24, Jan. 2015.
- [18] K.S. Kunz, R.J. Luebbers, "The Finite-Difference Time-Domain Method," *Boca Raton, FL: CRC.*, pp. 448, 1993.
- [19] K.S. Yee and J.S. Chen, "The Finite-Difference Time-Domain (FDTD) and the Finite-Volume Time-Domain (FVTD) Methods in Solving Maxwell's Equations," *IEEE Trans. Antennas Propagation*, vol. 45, No. 3, pp. 354-363, March 1997.
- [20] T. Weiland, "A discretization method for the solution of Maxwell's equations for six-component fields," *Electronics and Comms. AEU*, vol. 31, No. 3, pp. 116-120, 1977.
- [21] CST-Computer Simulation Technology, Available at: <http://www.cst.com>.
- [22] Zeland Software, Inc., Available at: <http://www.zeland.com>.
- [23] Agilent Advanced Design System, 2009, Agilent Technologies, USA.

## Chapter 2

# Literature Survey on Planar Antenna Arrays for Wireless Energy Transfer and Microwave Imaging

## 2.1 Introduction

The past few years have witnessed significant advancements in a wide range of portable electronic devices. These devices include not only consumer gadgets like smartphones but also find applications in industries such as wireless sensor networks. The prevailing trend is towards the miniaturization of these devices to enhance their portability and integration into various environments. However, one of the primary challenges that needs to be addressed is ensuring a reliable energy supply, considering that the nature of these devices often makes the use of electrical wires impractical. Currently, most portable electronic devices heavily rely on batteries for power. However, for small and compact devices, batteries tend to occupy a significant portion of the available volume. This not only hinders further miniaturization but also adds weight and cost. Additionally, the autonomy of these devices is limited due to the trade-off between battery size and power density. Batteries require periodic replacement or recharging, and the disposal of used batteries poses environmental concerns as they are highly polluting. Furthermore, battery recycling is a complex and expensive process. In the case of rechargeable batteries, the charging process typically relies on a wall plug charger, which restricts the portability of wireless devices.

To address these challenges, wireless power transfer systems are being developed. These systems aim to improve the availability, reliability, and user friendliness of portable electronic devices. The evolution of power transfer mirrors the progression of information transfer, with the ultimate goal of eliminating the need for physical cords and ushering in an era of wireless technology.

## 2.2 History of Wireless Power Transfer

More than 100 years ago, Nikola Tesla introduced and demonstrated the concept of wireless power transmission [1]. He described a method of harnessing effects transmitted through natural media. Although Tesla was unable to implement his wireless power transmission systems for commercial use, he managed to transmit power from his oscillators, operating at 150 kHz, to illuminate two light bulbs. The main reason for his lack of success was that the transmitted power was radiated in all directions as a 150 kHz radio wave with a wavelength of 20 km, resulting in low efficiency.

The development of microwave tubes during World War II paved the way for the rectification of microwave signals to supply DC power through wireless transmission. Research on high-power beaming using microwave signals gained momentum in the 1950s. B. C. Brown, at Raytheon Company, played a crucial role in advancing wireless power transmission and ushering in the modern era [2, 3]. By 1958, a 15 kW average power-band cross-field amplifying tube had been developed, exhibiting an impressive overall DC to RF conversion efficiency of 81%. In the early 1960s, the first efficient receiving device for microwave power, known as a rectifying antenna or rectenna, was developed by Raytheon.

The rectenna consisted of a half-wave dipole antenna with a balanced bridge or a single semiconductor diode placed above a reflecting plane. The output of the rectenna element was connected to a resistive load. At this time, the 2.45 GHz frequency gained popularity for wireless transmission due to its technological advancements, its location within the industrial, scientific, and medical (ISM) band, and its minimal atmospheric attenuation, even in heavy rainstorms. The conversion efficiency of the rectenna increased at this frequency during the 1960s and 1970s.

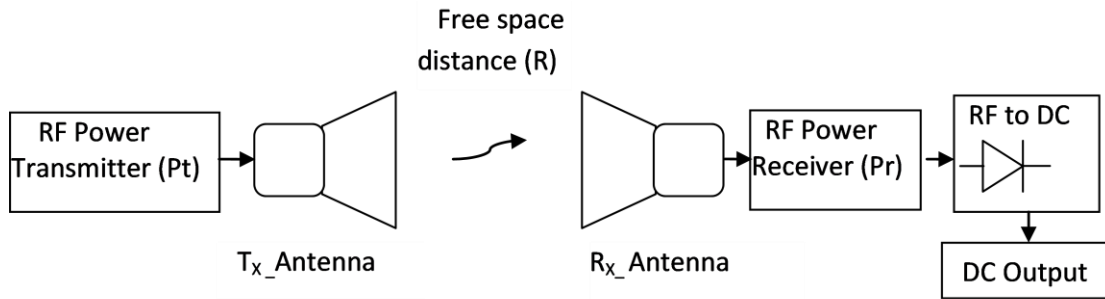


Fig.2.1 Wireless Energy Transfer block diagram

The Frii's transmission equation relates the power received ( $P_r$ ) to the power transmitted ( $P_t$ ) between two antennas separated by a distance ( $R$ ) greater than  $2d^2/\lambda$ , where 'd' represents the largest dimension of either antenna.

The Frii's transmission formula is given as:

$$\frac{P_r}{P_t} = \frac{G_t G_r \lambda^2}{(4\pi R)^2} \quad (1)$$

Where,  $P_r$  is the power received,  $P_t$  is the power transmitted,  $G_t$  is the gain of the transmitting antenna,  $G_r$  is the gain of the receiving antenna,  $\lambda$  is the wavelength of the transmitted signal,  $R$  is the distance between the antennas. It is important to note that the Friis transmission equation assumes free space propagation, meaning that there are no obstacles or interference affecting the signal propagation between the antennas.

In the past two decades, numerous wireless systems have been developed and widely adopted worldwide. Notable examples include cellular mobile radio and Wi-Fi systems. Similar to radio and television broadcasting systems, these wireless systems emit electromagnetic waves into the surrounding environment. However, a substantial amount of energy is often wasted in the process. Consequently, the concept of harvesting and recycling ambient wireless electromagnetic energy has gained significant interest.

One of the most promising methods for harvesting wireless energy is through the use of a rectenna, which combines a rectifier and an antenna. Figure 2.1 illustrates a typical block diagram of a rectenna. The antenna is responsible for capturing the wireless energy, which is

then directed to rectifying diodes through filters and a matching circuit. The rectifying diodes convert the received wireless energy into direct current (DC) power. A low-pass filter is employed to match the load with the rectifier and to suppress the high-order harmonics generated by the diode. The aim is to achieve high energy conversion efficiency, which is a critical parameter for such a device. By utilizing rectenna, it becomes possible to harness and convert ambient wireless electromagnetic energy into usable electrical power, thereby reducing wastage and promoting energy efficiency. This has led to increased research and development in the field of rectenna technology.

Rectennas offer several advantages over traditional power sources, such as batteries. Two notable advantages are:

(i) Unlimited Lifetime: Rectennas have an almost unlimited lifespan and do not require replacement like batteries. This longevity is advantageous as it ensures a long-lasting and reliable power source.

(ii) Environmentally Friendly: Rectennas are considered environmentally friendly as they do not contribute to pollution or environmental degradation. Unlike batteries, which require proper disposal due to their toxic components, rectennas do not produce any waste or deposition that can harm the environment.

The world's first rectenna, developed by Brown in 1963, utilized a normal bridged rectifier [2]. It operated at a frequency of 2.45 GHz, which falls within the industrial, scientific, and medical (ISM) band. This rectenna was designed as part of a fuel-free helicopter experiment in 1964 and produced a power output of 7 W at approximately 40% efficiency, using four point-contact diodes. Brown further developed the first single-shunt rectenna [5], focusing on low-cost production. This rectenna design was also employed in a 1.6-mile microwave power transmission (MPT) field experiment in Goldstone in 1975 [8]. Brown's advancements led to the development of a large rectenna array measuring 3.4 m × 7.2 m. In the field experiment, the microwave power transmitted from the klystron source was 450 kW at a frequency of 2.388 GHz, resulting in rectified DC power of 30 kW with 82.5% rectifying efficiency. Subsequent to Brown's achievements, further progress was made to increase rectenna efficiency. One approach involved utilizing a full-wave rectifier with a 0° to 180° combination through an antenna [10]. This rectifier employed a reverse-phase microwave combination to achieve full-wave

rectification. Overall, Brown's pioneering work laid the foundation for rectenna development, and subsequent improvements and innovative approaches have been explored to enhance their efficiency.

The antenna used in a rectenna can take various forms, including a dipole, a Yagi-Uda antenna, a microstrip antenna, a monopole, a coplanar patch, a spiral antenna or even a parabolic antenna [6-14]. Similarly, the rectifying circuit in a rectenna can be of different types, such as a single shunt full-wave rectifier, a full-wave bridge rectifier, or other hybrid rectifiers [15-18]. The choice of circuit, particularly the diode used, plays a significant role in determining the radio frequency (RF) to direct current (DC) conversion efficiency. Recent developments have seen the emergence of rectennas using Field effect transistor (FET) or High electron mobility transistor (HEMT) diodes [19-22].

The current world record for RF-DC conversion efficiency among developed rectennas is approximately 90% at an input power of 8 W and a frequency of 2.45 GHz [23]. As depicted in Fig. 2.1, the RF-DC conversion efficiency of a rectenna with a diode depends on the intensity of the microwave power input and the optimal connected load. When the power is low or the load is not properly matched, the efficiency can significantly decrease. Additionally, the characteristics of the diode, such as its junction voltage and breakdown voltage, also affect the efficiency. If the input voltage to the diode is below the junction voltage or exceeds the breakdown voltage, the diode will not exhibit rectifying characteristics. Consequently, the RF-DC conversion efficiency decreases when the input voltage deviates from the optimum range.

In Japan, in the early 21st century, several trials were conducted as part of the development of high-efficiency phased arrays, primarily for space-based solar power (SPS) applications. These trials involved transmission at a frequency of 5.77 GHz. In 2009, Kyoto University's research group conducted a field experiment on microwave power transmission (MPT) from an airship to the ground using two phased-controlled magnetrons [24-26].

### 2.2.1 Based on a Single RF-to-DC Converter.

In the design of a receiving antenna for long-range wireless power transfer (WPT), one approach is to use a classical phased array configuration connected to a single RF-to-DC converter at its output port, as shown in Figure 2(a). This type of architecture is known for its

high reception efficiencies because it coherently sums up the impinging power. To achieve this, the receiving antenna includes an RF combining network that combines the incoming waves in phase. However, such architectures require the receiving array to track the incident beam in real time, making them more suitable for "fixed" applications such as ground-to-ground WPT.

WPT receiving array consisting of four patch antennas connected to a single RF-to-DC converter was proposed. This arrangement was designed for an 8 GHz compact application with high reception gain. The proposed rectenna arrangement achieved a broadside gain of 15.07 dBi, resulting in high end-to-end efficiency for the overall system. To further enhance the performance, a focusing reflector array was introduced, resulting in a total gain of 18.60 dBi. Similarly, a 2x2 microstrip antenna array connected to a single diode was demonstrated. At a frequency of 2.45 GHz, the rectenna achieved an overall gain of 6.8 dBi [6]. These examples highlight the use of a single RF-to-DC converter in conjunction with a receiving antenna array, allowing for efficient wireless power transfer and significant gains in reception.

### 2.2.2 Combination of Rectenna-Collected Signals at the DC Level

The commonly used arrangement for wireless power transfer (WPT) reception is the combination of signals received and converted by each antenna at the DC level, as depicted in Figure 2.1(b). This approach offers the advantage of simplicity. Unlike coherent combination methods, there is no need for RF alignment across the receiving aperture, making deployment, interconnection, and calibration of the antennas much simpler. Additionally, this architecture provides increased degrees of freedom (DoFs) for element displacement, as no phase correction is required.

However, it is important to note that this non-coherent combination of signals results in a lower overall efficiency compared to coherent reception, as rectification is performed on an individual antenna basis.

Fig. 2.2 represents the block diagrams of different receiving arrays for wireless energy transfer (WET). Here is a description of each arrangement:



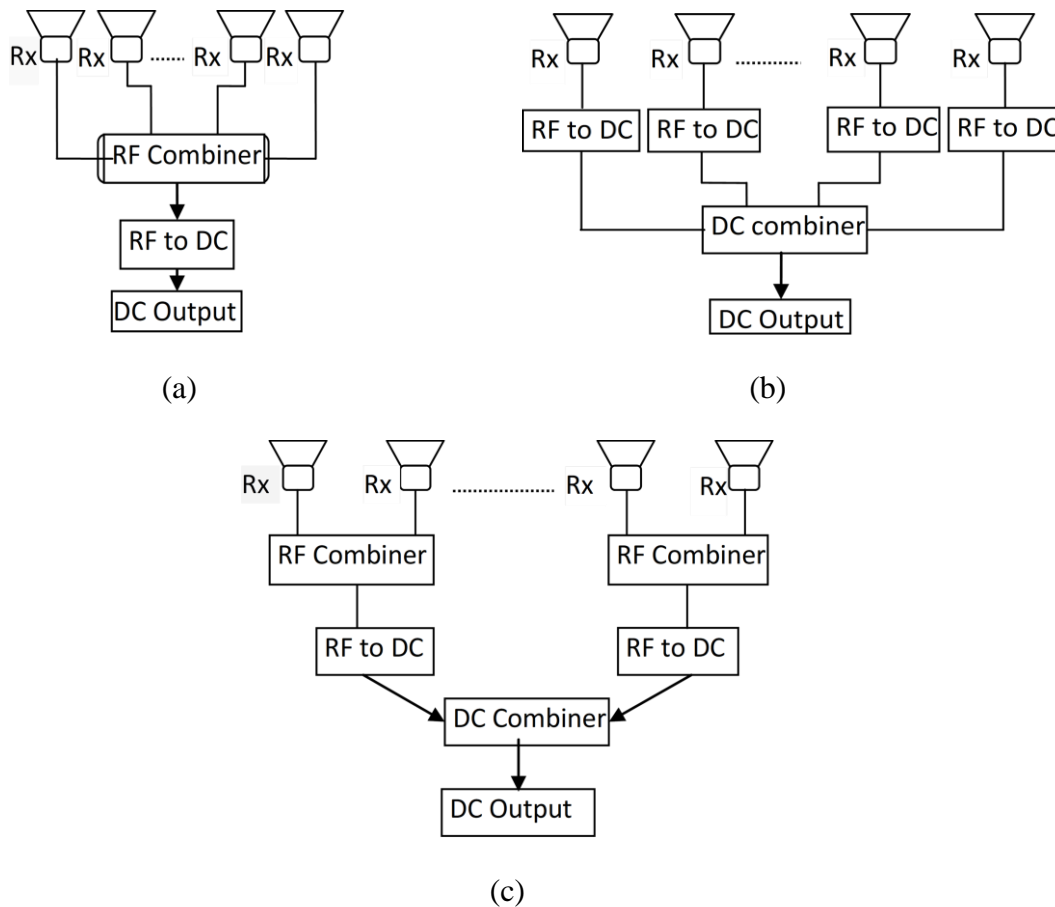


Fig.2.2 Block diagram of receiving WET arrays comprising (a) A single RF-to-DC (RF combiner), (b) Rectenna array (DC combiner) and (c) Subarray arrangement.

(a) Single RF-to-DC Combiner: In this configuration, the received signals from multiple antennas are combined at the RF-to-DC converter stage. The signals are first converted from RF (radio frequency) to DC (direct current) individually by each antenna's rectenna. Then, the DC outputs from the rectennas are combined into a single DC output through an RF-to-DC combiner. This allows for the non-coherent combination of signals and simplifies the system design.

(b) Rectenna Array: In this arrangement, the receiving array consists of multiple rectennas, with each rectenna comprising an antenna and a rectifier. The signals received by each antenna are rectified individually, converting them into DC power. The DC outputs from the rectennas can be used independently or combined further downstream in the system.

(c) Subarray Arrangement: The subarray arrangement involves dividing the receiving array into smaller subarrays. Each subarray consists of a group of antennas and rectennas. The signals received by the antennas in each subarray are rectified individually, generating DC power. The DC outputs from the rectennas in each subarray can be combined within the subarray or further combined with outputs from other subarrays. These different arrangements provide flexibility in designing the receiving arrays for WET, allowing for different levels of signal combinations and system complexity.

### 2.2.3 Subarray Based Arrangements.

It seems that subarray-based architectures have been proposed to address the limitations of the single RF-to-DC converter approach. Here's a description of the subarray-based architecture Fig. 2.2(c). In subarray-based architectures, the overall receiving layout is divided into subarrays. Each subarray comprises a group of antennas and rectennas. The signals collected by the antennas within each subarray are combined at the RF level using an RF network. The combined RF signal from each subarray is then converted to DC using an RF-to-DC converter specific to that subarray. The DC output from each subarray is connected to an overall combiner, which is responsible for power summation. The overall combiner combines the DC outputs from all the subarrays to generate the final DC output of the WPT system. By using subarrays, the architecture achieves a modular structure with a lower complexity RF network and RF-to-DC converter for each subarray. This approach reduces the need for a full RF feed network and allows for localized signal combinations. It also improves robustness by isolating the power conversion process, reducing the impact of diode failures. In a specific example mentioned in [28], a set of four folded dipole antennas operating at 5.8 GHz were combined in a dual-rhombic loop antenna (DRLA) subarray at the RF level. This subarray was then connected to a single high-efficiency RF-to-DC circuit. Multiple instances of this subarray were replicated and combined in DC to form an overall 4 x 16 receiving array. The simplicity of the RF combination network, along with the subarray-based approach, allowed for a high collecting efficiency of 82%.

The widely deployed WPT receiving arrangement, as mentioned earlier, is a combination of rectenna-collected signals at the DC level. This approach involves converting the RF signals received and rectified by each antenna into DC power, which is then straightforwardly combined

at the DC level. This non-coherent combination of received signals simplifies the system design, eliminates the need for RF alignment, and provides enhanced degrees of freedom for element displacement. Fig. 2.2(b). The main advantage of such a choice is its simplicity. This is because there is no need for RF alignment across the receiving aperture, thanks to the non-coherent combination of the received signals Fig. 2.2(b).

Table: 2.1 Summary of different types of rectenna design

References	Year	Author s	Antenna type	Rectifier element	Remarks
[4]	2018	E. Adami, P. Proynov, G.S. Hilton, et al.	Flexible fabric antenna	SMS7632	Self-powered boost converter with 150-nA quiescent consumption is demonstrated to match the rectenna with over 95% matching efficiency across the entire usage range. The maximum end-to-end efficiency is 28.7% at -7 dBm
[5]	2017	P. Pereira, R. C. M. Pimenta, et	Rectangular patch antenna	HSMS2860 Half wave rectifier	Antenna geometry is optimized to match the complex impedance of the rectifier.
[6]	2017	P. Wouchoum , P. Janpangner n, et al.,	2 × 2 rectangular patch rectifying antenna array	SMS7630 Voltage doubler	Rectangular patch rectifying antenna array for WPT. Voltage doubler rectifying circuit achieved at distance of 1m, the output of 1.5 Volt and 0.05mA current with 1M load resistance and a Tx power of 34.6dBm.
[7]	2012	Erez falkenstein	Dual linear polarized patch antenna	SMS7630-79 Schottky diode	Source-pull RF-to-DC configuration is applied to obtain the best diode impedance.
[8]	2014	Mohamed Adel Sennouni	3 × 3 array antenna with circular polarization property	HSMS-2820 Schottky diode	Circular polarized and high efficiency rectenna is designed. However, 3 × 3 array antenna has resulted in a large size of the rectenna.
[9]	2011	Ugur Olgun	Fractal planar array antenna	Greinacher rectifier	Integration of array antenna with Zero-bias diodes rectifier is used. But, the design has large size.
[10]	2006	Jamal Zbitou,	Linear polarized 4-element patch array antenna	HSMS2820 Schottky Zero-bias (ZB) diode	High electron-mobility transistor is used to reduce the overall rectenna dimensions but due to the array antenna adoption, the rectenna size still large.
[11]	2013	Yong Huang	NA	MOSFET,	Buck-Boost converter is used for high

## Planar Antenna Arrays for Wireless Energy Transfer and Microwave Imaging

				Schottky diode,	conversion efficiency of the rectifying circuit.
[12]	2015	Mei-Juan Nie	broadband slot antenna fed by GCPW	Schottky diode of HSMS-2862	Ground coplanar waveguide integrated with voltage doubler rectifier is used to achieve high efficiency.
[13]	2012	Onur Kazanc	Miniaturized tag antenna	NMOS bridge	NMOS bridge rectifier is used for maximum power transfer that consists of BSIM model of zero-VT transistors.
[14]	2014	Chou, J. H., Lin	Dual circularly polarized patch antenna	HSMS282c diode	Slotting technique of T and U shapes is used to achieve circular polarization and harmonic rejection properties.
[15]	2008	Tzong-Chee Yo	Circularly polarized Patch antenna	Tow pair of HSMS-282c Schottky diodes	The size of the rectenna is reduced by 12% due to the use of circular shape slots and double layer structure techniques implementation.
[16]	2010	Gianfranco Andia Vera	Square coupled patch with a cross shaped slot	SMS7630 Schottky diode	The size of the patch side is reduced by 32.5% as an advantage of cross shaped slot adaption.
[17]	2010	H. Takhedmit	linearly polarized patch antenna	Two HSMS2860 Schottky diodes	The rectenna design is suitable for wireless sensor applications as it does not require a low pass filter.
[18]	2012	Fu-Jhuan Huang	Microstrip antenna with peripheral cuts and slits	NA	The output voltage is higher with LP than with CP. However, the LP output voltage is affected by rectenna rotation.
[19]	2012	Jui-Hung	T-shape slot dual circular polarized patch antenna	HSMS-282c Schottky detector diode	T-shape slot technique is applied to the antenna for circular polarization property so that more signals can be captured.
[20]	2012	S. Vinoth Kumar	Microstrip patch antenna	HSMS-282c diode	This design has a low conversion efficiency which can be improved by using voltage doubler.
[21]	2012	Vlad Marian	Single-pole 4 Throw (SP4T) switch integrated structure antenna	HSMS2860 Schottky diode	The series-mounted diode rectenna, bridge configuration rectenna and shunt-connected diode rectenna are considered for very low input power level, large input power range and mid-range, respectively.
[22]	2012	H. Takhedmit, L. Cirio	Antenna with shorted annular ring –slot	HSMS2850 zero bias Schottky diode	Rectifier is designed at the back side of the antenna, which makes the structure more compact and lower cost.
[23]	2013	Wen Huang	Microstrip dipole antenna	HSMS-282 Schottky diode	The design structure at 2.45 GHz limits the compatibility of the rectenna for some wireless sensor applications.
[24]	2010	H.	Linear polarized	Bridge rectifier	This rectenna has low cost and good

Chapter 2 Literature Survey on Planar Antenna Arrays for Wireless Energy Transfer and Microwave Imaging

		Takhedmit,	microstrip patch antenna	consists of four Schottky diodes	performance but the output DC voltage need to be further improved.
[25]	2010	A. Georigiadis	Square aperture-coupled patch antenna	SMS7630 Schottky diode	Thevenin equivalent circuit of antenna is used for receiving signals. However, the total conversion efficiency is low.
[26]	2008	Douyere, A, Lan Sun Luk	Square model patch antenna	HSMS2860 Schottky diode	In this design, equivalent circuit model formed of antenna and rectifier is studied. This design achieves efficiency of 75 % with no need for any electromagnetic simulation software.

Table: 2.2 Comparisons of Different Types of Rectenna Results

Author/year	Frequency (GHz)	Antenna Gain	Input impedance	Input power	Output load resistance	Output power	$\eta$ %
E. Adami, P. Proynov, G.S. Hilton, et al., 2018	2.45	8.1 dBi	50 $\Omega$ 20+j260 $\Omega$	-2 dBm -35dBm -24.3 dBm	3 k $\Omega$ 7.2 k $\Omega$ 4 k $\Omega$	150 $\mu$ W @ 2m distance	64.6%
P. Pereira, R. C. M. Pimenta, et al., 2017	2.45	3.386 dBi	50 $\Omega$ /48.61+j1.17 $\Omega$	-20 dBm	1 k $\Omega$	1.243mV@ 2m distance	9.6%
Seung-Tae Khang, Dong-Jin Lee, et al., 2017.	2.45	5.9 dBi single antenna	50 $\Omega$	10W/40dBm 250mW/20 dBm	NA	12 dBm	6.4%
S. Ahmed, Z. Zakaria, et al., 2017	2.45	7 dBi	50 $\Omega$	20dBm	2 k $\Omega$	2.016V	75.04%
P. Wouchoum, P. Janpangngern, et al., 2017	2.45	14 dBi	50 $\Omega$	34.6 dBm	1M $\Omega$	1.5V, 0.15mA@ 1meter	21.8%
T. Mitani, S. Kawashima, et al., 2017	2.45	1.62 dBi	75 $\Omega$	19.6mW/ 12.9 dBm	VD_469 $\Omega$ HWR-101 $\Omega$	0.8V @100 $\Omega$ (6V & 2.6V @10k $\Omega$ )	56.9%
Mei-Juan Nie, 2015	2.45	10 dBi	64.2+j9.8 $\Omega$	15dBm	900 $\Omega$	13 dBm/ 3.2 V	72.5%
M. Adel Sennouni, 2014	2.45	9.14 dBi		20dBm		7.02V	65.8%
Chou, J. H., Lin, 2014	2.45	7.9 dBi		0.158 W		11.42 V	82.3%
Yong Huang, 2013	2.45	NA		82mW		NA	60%
Wen Huang, 2013	2.45	5.2 dBi		20dBm		7.1 W	67.6%
Erez Falkenstein,	2.45	6 dBi		25-200		0.1 W	54%

## Planar Antenna Arrays for Wireless Energy Transfer and Microwave Imaging

2012				$\mu\text{W}/\text{cm}^2$			
Onur Kazanc, 2012	2.45	6.5 dBi		0dBm / -6 to 6dBm		560 $\mu\text{W}$	75%
Fu-Jhuan Huang, 2012	2.45	3.6 dBi		25dBm		2.76 V	37.8%
Jui-Hung, 2012	2.45	8 dBi		24dBm		NA	78.45%
S.Vinoth Kumar, 2012	2.45	NA		2dBm		1 V	NA
Vlad Marian, 2012	2.45	NA		0dBm		2.1 V	50%
H. Takhedmit, L. Cirio, 2012	2.45	5.25 dBi		10 $\mu\text{W}/\text{cm}^2$		1.1 V	50%
Ugur Olgun, 2011	2.45	4.5 dBi		-5dBm		NA	68%
Zied Harouni, Laurent Cirio, 2011	2.45	5.7 dBi	50-j284 $\Omega$ HSMS2860	10 dBm	1.6k $\Omega$	2.85 V	63%
Gianfranco Andia Vera, 2010	2.45	7.5 dBi		-10dBm		NA	42.1%
H. Takhedmit, 2010	2.45	6.2 dBi		10dBm/ 0.01 W		3.1 V	83%
H. Takhedmit, Merabet, 2010	2.45	4.7 dBi		10dBm 0.15mW/ cm <sup>2</sup>		3.64V/ 12.6mW	52%
A. Georgiadis, 2010	2.45	8.25 dBi		1.5 W/cm <sup>2</sup>		NA	38.2%
Tzong-Chee Yo, 2008	2.45	3.36 dBi		20dBm		15.8V	70.6%
Douyere, A., Lan Sun Luk, 2008	2.45	NA		32mW		NA	75%

### 2.3 Literature Survey on Microwave Imaging

Research on imaging systems and methods began in the history of humanity as early as the first investigations into the human visual system, namely the eye [27]. It is the most important sensing organ of humans and can intercept light to construct images of objects at varying distances. Therefore, early investigations were focused on the visible spectrum, where light can be easily detected by the naked eye. However, it was believed for many years that the eye emits rays of infinite velocity and receives them back to perceive an image. Over time, several physicians and mathematicians contributed to building a solid foundation for the wave picture of light. Among them, great credit goes to Fresnel (1788-1827), who explained diffraction phenomena based on Huygens' theory. This made it possible to calculate the existence of light in the shadow region caused by diffraction at edges.

Parallel to the research on light, thorough investigations into electricity and magnetism were in progress. The physical laws governing electric and magnetic forces were observed experimentally and formulated mathematically by many scientists, such as Ampere (1775-1836), Gauss (1777-1855), Faraday (1791-1867), and Weber (1804-1891). These quantitative formulations were first completed by the work of James Clerk Maxwell (1831-1879) after the introduction of the displacement current. He compiled his theories in his book "A Treatise on Electricity and Magnetism," published in 1873. By introducing the displacement current term to the previously available equations describing the actions made by electric and magnetic fields, Maxwell formulated the fundamental four differential equations of electromagnetism, known as Maxwell's equations. Additionally, the polarization of light could be explained due to the transverse wave nature of the propagating electromagnetic fields. This formulation could describe, for the first time, that electromagnetic signals can propagate in space with a velocity exactly equal to the experimentally known speed of light. It became evident then that light itself, as the visible part of the electromagnetic spectrum, also possesses the same wave nature.

In the early 20th century, advances in physics led to the declaration of light's duality, possessing both wave and particle natures. Max Planck's (1858-1947) experiments on black body radiation resulted in the postulation of quantized energy particles, later named photons. Each of these particles carries a fixed amount of energy depending on the frequency of radiation. This new theoretical framework was extensively developed throughout the 20th century and became widely known as modern physics.

The progress in microwave imaging has been strongly influenced by advancements in radar systems. Radar serves as the fundamental front-end component of an imaging system, and as a result, any technological advancement in radar performance or miniaturization can directly enhance imaging capabilities. Throughout the 20th century, considerable progress was made in the development of range radar for navigation and remote sensing applications, and it continues to undergo continuous improvement by pushing towards higher frequencies with wider bandwidths, such as the terahertz (THz) range.

Most radar systems operate in a monostatic configuration, where the transmitter and receiver are co-located or slightly separated for improved isolation. This configuration is often chosen due to practical constraints, such as mechanical limitations, connectivity requirements, or cost considerations. Advanced methods utilizing bistatic radar did not initially emerge but were

later developed during the Second World War and are credited to the Germans. Imaging with microwave frequencies, typically ranging from 0.3 to 300 GHz or wavelengths between 1 m and 1 mm, offers the advantage of penetration capabilities for non-metallic materials. However, due to the relatively long wavelengths involved, achieving high resolution in microwave imaging requires the use of large apertures. The construction of such mechanically large apertures has historically hindered the development of microwave imaging systems.

The first concepts for synthetic aperture were developed in the 1950s for passive observation of the sky. The realization of this imaging technique heavily relies on the availability of suitable recording media and efficient computational power. Currently, Synthetic Aperture Radar (SAR) is extensively utilized in airborne and spaceborne imaging systems [add citation], primarily in monostatic configuration. More recently, bistatic acquisition has become feasible through advances in signal synchronization between satellites and their position tracking using the Global Positioning System (GPS) [28].

Electromagnetic wave theory has proven to provide a theoretical framework for the development of microwave imaging systems. Microwave images can be classified as operating in the far-field or near-field range, depending on the relative aperture size to the imaged distance. They can also be categorized as active or passive, depending on the source of illumination. Active microwave images have the capability for full coherent imaging, encompassing both spatial and temporal information.

Among the various classes of imaging systems, multistatic imaging operating at close ranges is particularly rich. Multistatic imaging offers significant diversity in correlated information about the scattering of the imaged object, as well as flexibility in the choice of transmitting and receiving apertures. However, this increased flexibility also adds complexity to the design process, as it requires making challenging decisions regarding the imaging system architecture and array configuration.

Close range operation enhances object visibility and enables imaging with a high signal-to-noise ratio. Multistatic operation inherently indicates active imaging, where transmitters illuminate the imaged object from different directions, and receivers collect the scattered field from other directions. Active illumination is essential for many imaging problems to ensure a high dynamic range and independence from surrounding illumination. In image processing applications, the image's dynamic range becomes a crucial factor for stable operation.



Microwave imaging is primarily utilized for its capability to penetrate optically opaque surfaces. Active illumination is therefore necessary to ensure sufficient signal power reaches behind the surface of the object. However, using active illumination can introduce challenges related to specular reflections and shadowing effects. Understanding the nature of these phenomena is important to either avoid or reduce them, depending on the specific application. The flexibility offered by the synthesis of multistatic arrays allows for dedicated geometrical adaptation to match the imaged object, optimizing the imaging performance.

Image reconstruction serves as the core of any synthetic focusing system. Synthetic focusing is crucial for harnessing the optimal performance of multistatic arrays. With the advent of modern technologies, the digitization of signals and the digital processing of data have revolutionized radar imaging systems. The digital beam forming technique plays a pivotal role in the success of this modern technology. Fourier imaging methods have been established for many years to support microwave imaging techniques employing synthetic focusing. Although multistatic arrays can accommodate various geometries, planar multistatic arrays are particularly desirable due to practical considerations.

In the case of planar arrays, reflection imaging is emphasized, wherein both illumination and reception occur on the same side relative to the imaged object. While transmission imaging may be preferred in certain applications, it often faces challenges when objects are not fully transparent to microwave signals, leading to strong shadows. On the other hand, reflection imaging enables penetration through the outer layers of the object and allows signal reception from the same side, making it a suitable choice for many practical scenarios. The capabilities of multistatic imaging find numerous applications and can effectively replace other technologies currently used in microwave imaging systems, such as monostatic imagers, scanning phased arrays, or mechanical scanners.

One notable application is personnel screening with millimetre-waves, particularly at airport security checkpoints. Millimetre-wave imagers, which utilize non-ionizing radiation, are preferred over X-ray methods due to their safety. They also outperform conventional metal detector gates by detecting not only metallic objects but also dielectric objects like plastic explosives and ceramic knives. Commercialized devices and on-going developments cover a range from passive to active and from close-range to stand-off imagers. Microwave imaging's capabilities also extend to material characterization and non-destructive testing (NDT), making it

valuable for various research purposes. Therefore, when studying microwave imaging theories, it is important to maintain a sufficient level of generalization to adapt the acquired knowledge to different situations.

Recent years have witnessed significant development results, with some advancements even pushing into the THz domain. On-going research aims to further improve imaging methods and identify potential applications that can benefit from the performance of multistatic arrays. To achieve this, a deeper understanding of the unique aspects of multistatic imaging is essential. Planar multistatic arrays are particularly suitable for applications that require high-resolution imaging and a wide image dynamic range.

## 2.4. Radar imaging

Radars can be classified into different categories based on their deployment and specific characteristics. They are commonly categorized as ground-based, airborne, spaceborne, or ship-based radar systems, depending on where they are located or installed [29].

In addition to deployment, radars can also be classified based on various characteristics such as frequency band, antenna type, and waveforms utilized. One common classification method is based on the type of waveform used or the operating frequency.

Considering waveform types, radars can be categorized as Continuous Wave (CW) or Pulsed Radars (PR). CW radars continuously emit electromagnetic energy without modulation and utilize separate transmit and receive antennas. Unmodulated CW radars are capable of accurately measuring target radial velocity (Doppler shift) and angular position. On the other hand, pulsed radars use a train of pulsed waveforms, often with modulation. Pulsed radars are primarily used to measure target velocity. These classifications based on waveform types help differentiate the operational characteristics and capabilities of different radar systems [29, 30].

Monostatic radars are radar systems that use the same antenna for both transmitting and receiving signals [30]. In a simplified block diagram of a pulsed radar system as shown in Fig. 2.3, several components work together to enable radar operation.

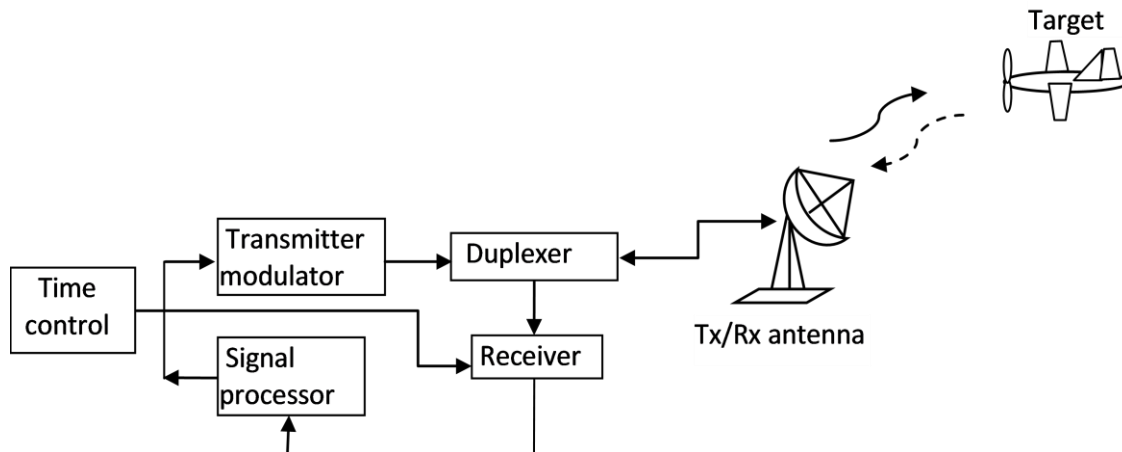


Fig.2.3. Block diagram of monostatic pulse radar imaging

The time control box is responsible for generating the synchronization timing signals required throughout the radar system. These timing signals ensure proper coordination of different operations. The modulator/transmitter block generates a modulated signal that is then sent to the antenna. The modulated signal carries the radar waveform and is responsible for transmitting electromagnetic energy into the environment.

The duplexer plays a crucial role in monostatic radar systems. It controls the switching of the antenna between transmitting and receiving modes. During transmission, the duplexer directs the radar electromagnetic energy towards the antenna for emission. On the other hand, during reception, it redirects the received radar echoes from the antenna to the receiver for further processing.

The receiver amplifies the weak radar returns (echoes) received by the antenna. It prepares the received signals for subsequent signal processing. The signal processor block performs various operations on the received signals to extract target information. This includes analysing the radar returns to determine the range of targets. The range is typically computed by measuring the time delay it takes for a radar pulse to travel the two-way path between the radar system and the target. Overall, these components work together in a pulsed radar system to enable the transmission, reception, amplification, and processing of radar signals for target detection and range measurement.

When radar radiated energy reaches a target, it interacts with the target's surface and induces surface currents. These induced currents then radiate electromagnetic energy in various

directions, including back towards the radar system. The amount of energy reflected back to the radar system depends on several factors, such as the size, orientation, physical shape, and material properties of the target.

To quantify the effectiveness of a target in reflecting radar energy, a parameter called the Radar Cross Section (RCS) is used. The RCS represents the target's ability to scatter and reflect radar signals back towards the radar system. It is defined as the ratio of the power reflected back to the radar system to the power density incident on the target. The RCS is usually denoted by the symbol  $\sigma$ . In other words, the RCS provides a measure of how much radar energy is scattered back to the radar system relative to the intensity of the incident radar energy on the target. It encapsulates various target properties that influence the scattering behaviour, allowing for a simplified representation of the target's interaction with radar waves. By quantifying the RCS of different targets, radar operators and engineers can assess and compare the detectability and visibility of various objects in a radar system. It plays a crucial role in radar system design, target recognition, and radar performance evaluation [31, 32].

Bistatic radars are characterized by using separate transmit and receive antennas that are located in different positions or platforms. In bistatic radar systems, the transmitted signal originates from the transmitter antenna and is received by the receiver antenna, which can be located at a considerable distance away [33].

The geometry associated with bistatic radars is depicted in Fig. 2.4, where the transmitter and receiver antennas are shown to be spatially separated. The angle  $\beta$ , referred to as the bistatic angle, represents the angle between the transmitter-receiver baseline and the direction of the target being observed.

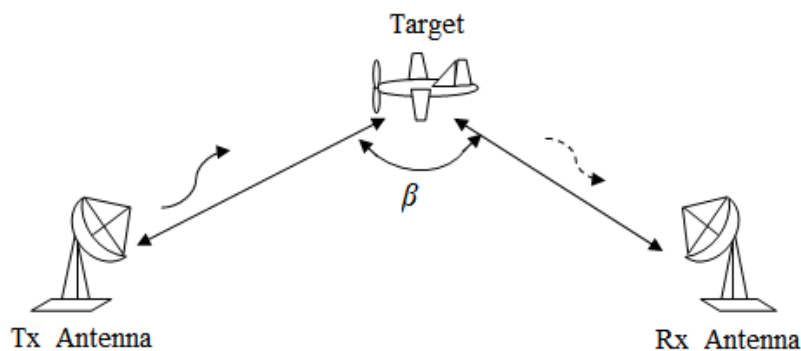


Fig.2.4. Bistatic Radar imaging

In order to maximize the receiver's knowledge of the transmitted signal and extract maximum target information, a synchronization link between the transmitter and receiver is necessary in bistatic radar systems. This synchronization ensures that the receiver has precise information about the transmitted signal, allowing for accurate processing and analysis.

One important distinction between monostatic and bistatic radar operations is related to the measured bistatic target Radar Cross Section (RCS), denoted by  $\sigma\beta$ . When the bistatic angle  $\beta$  is small, the bistatic RCS is similar to the monostatic RCS, which represents the target's ability to scatter radar energy. However, as the bistatic angle approaches  $180^\circ$  degrees (or becomes close to the backscattering direction), the bistatic RCS can become significantly larger [34, 35].

This increase in bistatic RCS for larger bistatic angles is due to the different scattering characteristics of the target when observed from different angles. The target's shape, orientation, and surface properties play a significant role in determining the bistatic RCS at different angles. Therefore, bistatic radar systems can provide valuable information about target properties and behaviour that may not be easily obtained with monostatic radar systems.

## 2.5. Classification of Microwave Imaging

Microwave imaging systems can be classified into two major categories: active and passive systems.

i). Active Systems: In active microwave imaging, the sensing is accomplished by probing the biological object with self-generated energy. This means that the imaging system itself emits electromagnetic waves and detects the response from the object. Active systems can employ different scattering schemes:

a). Forward Scattering: The system images the structure under inspection by detecting the reflected scattered signals from the object. The transmitted energy interacts with the object, and the scattered signals are analyzed to form an image.

b). Backward Scattering: The system images the structure by detecting the scattered signals transmitted through the object. The transmitted energy passes through the object, and the scattered signals on the other side are collected and processed to form an image.

ii). Passive Systems: In passive microwave imaging, the object itself generates the electromagnetic energy used for imaging. The system detects the naturally emitted or radiated

energy from the object. Passive systems rely on the object's own emissions or external radiation sources (such as natural or artificial background radiation) for imaging.

Another classification criterion for microwave imaging systems is based on their antenna shape or configuration:

a). Retina Shape: This classification considers the shape or layout of the antenna system used in the imaging system. Different antenna configurations, such as planar arrays or non-planar geometries, can be employed based on the specific imaging requirements.

iii). Finally, microwave imaging systems can also be classified based on whether they operate in the near-field or far-field region:

a). Near-Field Imaging Systems: These systems operate at close distances to the object under inspection. The proximity allows for higher-resolution imaging but may require specialized techniques to account for near-field effects.

b). Far-Field Imaging Systems: These systems operate at larger distances from the object, where the radiation can be approximated as coming from a point source. Far-field imaging is commonly used for long-range or remote sensing applications.

iv). Within the active microwave imaging category, there are various methods based on different physical effects:

a). Microwave Tomography: This technique involves using multiple measurements of electromagnetic waves to reconstruct an image. It can provide information about the dielectric properties and internal structure of the object.

b). Ultra-Wideband (UWB) Radar Techniques: UWB radar utilizes extremely short pulses of electromagnetic energy to achieve high-resolution imaging and can penetrate through materials that are optically opaque.

c). Microwave Microscopy: This method focuses on high-resolution imaging at small scales, such as cellular or subcellular levels. It enables the detailed analysis of biological samples or materials.

d). Hybrid Modalities: Some microwave imaging systems combine multiple techniques or modalities to enhance imaging capabilities. These hybrid approaches can utilize complementary information from different physical effects to improve the accuracy and resolution of the images.

Overall, microwave imaging encompasses a range of techniques and approaches, each suited for specific applications and imaging objectives.

### 2.5.1. Passive Microwave Imaging:

Passive microwave imaging operates by utilizing existing sources of electromagnetic energy, such as solar microwave radiation or natural emissions from objects, as the source of illumination. The principle is similar to optical imaging, where upwelling radiation is detected and converted into a brightness value to form an image. Here is a breakdown of the components involved:

a). Antenna: The antenna in a passive microwave imaging system receives the incoming radiation from various sources. It is typically pointed towards a specific region of the Earth's surface.

b). Apparent Brightness Temperature (TB): The region being observed by the antenna has an apparent brightness temperature, which is a measure of the intensity of the radiation emitted by the objects within that region.

c). Atmospheric Radiation (TAD): The atmosphere itself emits radiation in all directions, including towards the antenna. The component of radiation directly radiated towards the antenna is represented as TAD.

d). Reflected Power from Earth (TAR): The earth's surface reflects radiation back towards the antenna. This reflected power contributes to the overall detected signal.

e). Side Lobe Noise: There may be additional noise powers entering the side lobes of the antenna from various sources, such as the sun or other external sources. These noise powers can interfere with the detected signal.

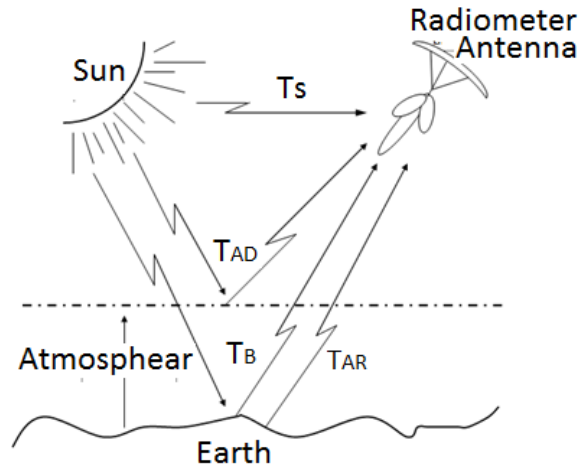


Fig.2.5. Passive microwave imaging system

In passive microwave imaging, the radiometer receives the combined signals from all these sources and processes them to form an image. The detected radiation, including the contributions from atmospheric radiation, reflected power from the Earth, and side lobe noise, is used to determine the apparent brightness temperature distribution in the observed region. This information is then used to create the final image.

Passive microwave imaging is particularly useful for applications such as sea, ice, or snow mapping, where the existing natural radiation can be utilized as an illumination source [37, 38]. It provides valuable information about the thermal properties and composition of the observed objects or regions.

### 2.5.2 Active Microwave Imaging

Active microwave imaging is a widely used scheme in which a signal of the desired frequency is generated and used as the source of illumination. It is particularly effective for near-field imaging of objects and finds applications in various fields, including non-destructive testing. Here is an overview of the components and processes involved in active microwave imaging:

a). Transmitter: The active microwave imaging system includes a transmitter that generates a continuous microwave signal at a specific frequency. This signal serves as the source of illumination for the imaging process.



b). Radiating Field: The continuous microwave signal generated by the transmitter is radiated into the environment, creating an illuminating field. This field interacts with the object under inspection.

c). Object Scattering: The illuminating field interacts with the object, causing scattering of the microwave signals. The scattered signals contain information about the object's properties, such as its shape, composition, and internal structure.

d). Receiver: A receiver is employed to capture the scattered signals after they have interacted with the object. The receiver may consist of an antenna or an array of antennas that detect the scattered signals and convert them into electrical signals.

e). Signal Processing: The electrical signals received by the receiver are processed to extract information about the object. Signal processing techniques, such as filtering, amplification, and modulation, are applied to enhance the desired signals and suppress noise.

f). Image Formation: The processed signals are used to create an image of the object. Various algorithms and imaging techniques are employed to reconstruct the object's properties based on the scattered signals. This can involve techniques such as beam forming, synthetic aperture radar (SAR), or tomographic reconstruction [39, 40].

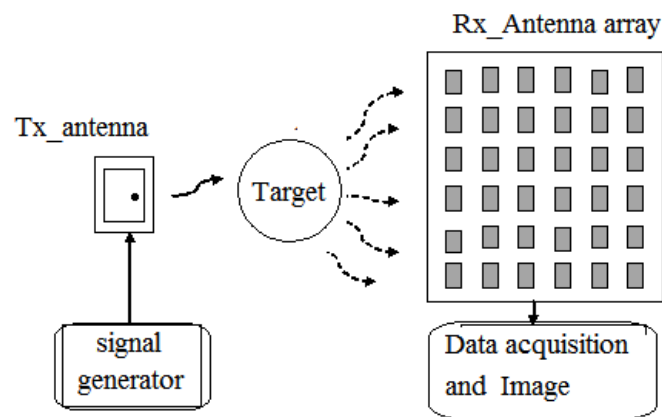


Fig.2.6. Active microwave imaging system

Active microwave imaging offers several advantages, including the ability to control the source of illumination and tailor it to specific imaging requirements. It allows for detailed imaging of objects in the near-field region, where high-resolution and accurate measurements are desired. This imaging scheme finds applications in diverse fields, such as medical imaging,

remote sensing, security screening, and non-destructive testing, where it enables the visualization and analysis of internal structures and properties of objects using microwave signals [41, 42]. An active microwave imaging system is shown in Fig.2.6.

Active microwave imaging, as you described, involves generating a signal of the desired frequency as the source of illumination. This method is widely used, especially in near-field imaging of objects, and finds applications in various fields, such as non-destructive testing. Let's discuss two schemes of active imaging:

a). Scattered Field Method: In this scheme, a continuous microwave signal is transmitted by the transmitter, which generates an illuminating field. The illuminating field interacts with the object, causing scattering of the microwave signals. The scattered field is then measured by the receiver, which consists of an array of antennas with individual detectors. The intensity of the received signal is highest where the scattered field is strongest. By plotting the signals received by each detector, an image of the object can be obtained. This scheme can involve multiple transmitters and receivers to illuminate the object from different positions and sample the scattered fields at multiple locations.

b). Backscattered Method: In this scheme, both the illumination source (transmitter) and the receiving sensor (antenna) are placed on one side of the object. The transmitter emits a continuous microwave signal that illuminates the object, and the antenna receives the backscattered electric field from the structure under study. By analyzing the characteristics of the backscattered signals, information about the object's structure and properties can be gathered. Different configurations and techniques can be used to extract the desired information from the received signals.

The other scheme of active imaging is based on the utilization of the reflected electric field from the structure under study, which is known as the back scattered method or radar effect. In this scheme, both the illumination source and the receiving sensor (antenna) are placed on one side of the object, and based on different configurations, information about the structure under test can be gathered.

Both schemes of active microwave imaging offer advantages in terms of control over the source of illumination and the ability to gather information about the object's properties. The choice of scheme depends on the specific imaging requirements and the nature of the object

under study. Active microwave imaging has proven to be valuable in various applications, including non-destructive testing, medical imaging, remote sensing, and more [43].

## 2.6 Near-Field and Far-Field Imaging

The antenna field zones can be divided into two principal regions: the near-field (Fresnel zone) and the far-field (Fraunhofer zone). Let's discuss these regions and their characteristics: Near-field (Fresnel Zone): The near-field region is located close to the antenna, typically within a few wavelengths. It can be further divided into two regions of interest: the reactive near-field and the radiating near-field.

a) Reactive Near-Field: The reactive near-field is the region in immediate vicinity to the antenna. In this region, the shape of the field pattern depends on the distance from the antenna. The electric and magnetic fields are not in phase, and their magnitudes and orientations vary spatially. The power flow is predominantly reactive, meaning that energy is stored in electric and magnetic fields rather than radiated as electromagnetic waves.

b) Radiating Near-Field: The radiating near-field region lies next to the reactive near-field region. In this region, the electric and magnetic fields are in phase, and their magnitudes and orientations also vary spatially. The power flow is a combination of reactive and radiated energy. The radiating near-field is characterized by complex wave fronts and non-uniform power distribution.

c). Far-field (Fraunhofer Zone): The far-field region is located at a large distance from the antenna, typically beyond a few wavelengths. In this region, the shape of the field pattern becomes independent of the distance and depends mainly on the antenna geometry and radiation characteristics. The far-field region is characterized by well-defined wave fronts, and the power flow is primarily in the form of a spherical wave expanding outward from the antenna.

In the near-field or Fresnel region, the shape of the field pattern is influenced by the distance from the antenna, and the longitudinal component of the electric field can be significant. The power flow in the near-field is not entirely radial, meaning that the energy distribution is more complex compared to the far-field region.

It's important to consider these near-field and far-field characteristics when designing and analysing antenna systems, as they can have implications for antenna performance, electromagnetic field interactions, and the interpretation of measurement data.

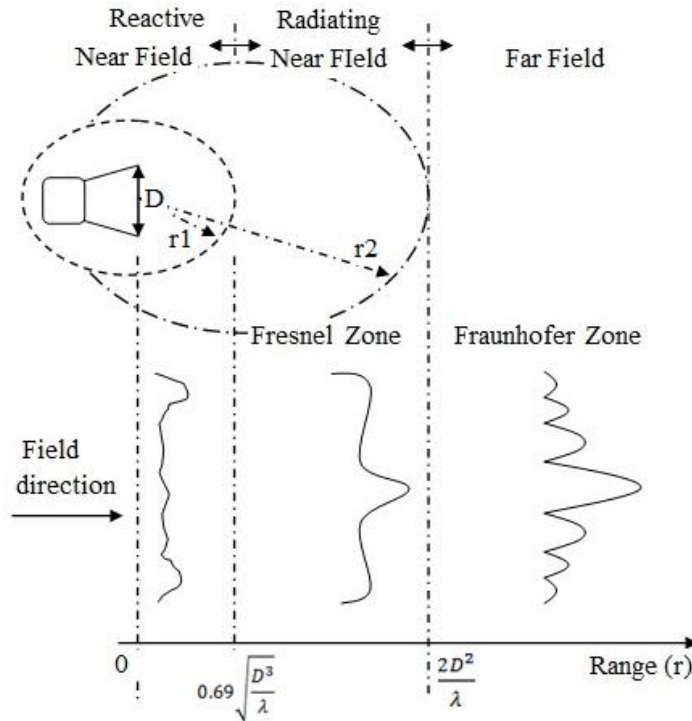


Fig.2.7. Near field and far field region

Reactive the Near-field region is the portion of the near-field region that starts immediately after the antenna. The reactive near field can be defined in terms of planar, cylindrical, or spherical modes. In this region, the reactive field dominates, meaning that the electric and magnetic fields are out of phase by 90 degrees [44, 45]. It is in this region that evanescent or near-field standing waves, which are known to have high frequency spatial information about the object of interest, exist. On the other hand, the radiating near-field, where the radiating fields begin to emerge, includes the region between the reactive near-field and the far-field region. However, unlike the far-field region, here the shape of the radiation pattern may vary significantly with distance. It is worth mentioning that if the maximum dimension of the antenna ( $d$ ) compared to the wavelength of the transmitted signal is not large enough, this region might not exist at all. To calculate the radius of these two regions ( $r_1$  and  $r_2$ ), Equations (1), (2) and (3) can be used.

$$\lambda = \frac{c}{f} \quad (2)$$

$$r1 \approx .62 \sqrt{\frac{d^3}{\lambda}} \quad (3)$$

$$r2 \approx \frac{2d^2}{\lambda} \quad (4)$$

Where,

d is the largest dimension of the antenna,

$\lambda$  is the wavelength of the signal,

r1 is radius of the reactive region and

r2 is radius of the radiating region

Far-field region of an antenna is defined as the region in which the radiating fields dominate. This means the electric and magnetic field planes are orthogonal to each other while the fields are in phase. Moreover, in this region shape of the radiation pattern does not depend on the distance from the antenna. These definitions can help understanding the basic difference between the far-field and near-field regions. Additionally, there are some other differences between these two types of imaging. For instance the antenna that is used in a typical near-field imaging system can be simple such as open-ended waveguide or coaxial line, while in far-field imaging, a high gain antenna should be adopted so that the signal would not disperse due to the distance. Moreover, near-field imaging technique allows considerable enhancement of the power compared to far-field imaging with the same wavelength. Radar cross section (RCS) imaging can be performed in the near field to examine military vehicles for their radar reflection properties due to their physical structure and radar absorbing material treatments [46, 47]. Active microwave and mm-wave imaging is now commonly used for concealed threat detection in high security areas including most domestic and international airports. This technology can be used to detect concealed metal and non-metal threats, including explosives, handguns, knives, or any concealed anomalous objects. Microwave and millimeter-wave imaging can be used to scan walls to reveal internal structure or to detect objects concealed in the walls [48-51]. Microwave imaging may be preferable to x-ray imaging for this application, because the technology is harmless to humans, and access to only one side of the wall is required. X-ray imaging frequently operates in a through-transmission mode, requiring access to both sides of the wall.

Active, two-dimensional, microwave or mm-wave imaging is highly effective for a number of near field imaging applications. These applications include concealed weapon detection in portals, standoff concealed weapon detection, RCS imaging, in-wall imaging, non-destructive evaluation imaging [52-54].

Near-field measurements play a crucial role in antenna testing and characterization. Understanding the theory behind near-field measurements is essential for conducting accurate and reliable measurements. While not everyone involved in near-field antenna measurements needs to be proficient in the theory, having at least one team member who possesses a competent and versatile knowledge of the theoretical formulation is important.

In near-field measurements, various scanning surfaces can be used, including planar, cylindrical, and spherical surfaces. These surfaces are depicted in Fig. 2.8, along with the representation of the electric field using a complete set of M and N eigen functions. The tangential electric field's amplitude and phase are measured over the scanning surface S.

To determine the unknown transmitting modal coefficients (TE<sub>m</sub>, TM<sub>m</sub>) of the antenna under test, orthogonal integration techniques are employed. The integration process, as illustrated in the Fig. 2.8, allows for the calculation of these coefficients based on the measured electric field data. By obtaining the modal coefficients, valuable information about the antenna's radiation characteristics, such as radiation patterns, beam width, and polarization, can be extracted. This information is essential for antenna design, optimization, and performance evaluation.

It is important to note that the specific details and equations involved in near-field measurements can vary depending on the measurement setup and the desired parameters to be extracted. Therefore, a solid understanding of the theoretical foundations and techniques is necessary to ensure accurate and meaningful near-field antenna measurements.

The mentioned references provide valuable resources for studying planar, cylindrical, or spherical near-field theory and techniques [55, 56]. Here is a summary of the references mentioned: Kerns' "translation": Kerns presents a streamlined and pedagogical development of planar near-field scanning and extrapolation techniques based on the plane-wave scattering matrix theory of antennas.

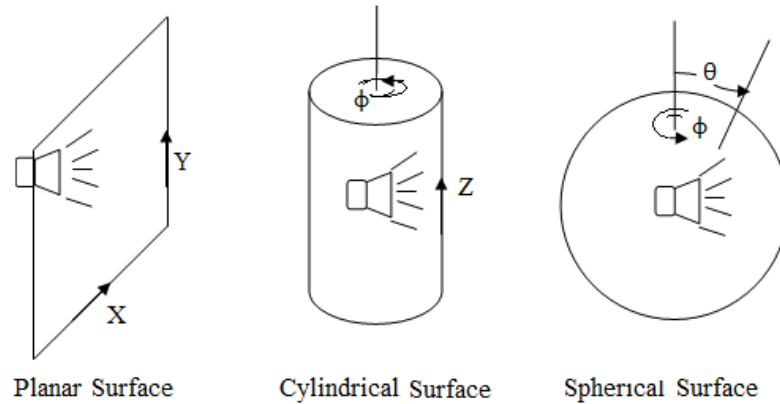


Fig.2.8. Scanning with Ideal antenna on Planar, Cylindrical, and Spherical Surfaces

This work offers a comprehensive understanding of planar near-field measurements. These papers provide brief descriptions and insights into planar near-field analysis, offering additional perspectives and practical considerations. Review paper [56] from GIT: This paper applies the Lorentz reciprocity theorem to derive the probe-compensated planar transmission formula. It provides an alternative approach to planar near-field measurements compared to the scattering-matrix approach. Appel-Hansen's review [57]: Appel-Hansen offers a useful review of probe-corrected planar, cylindrical, and spherical near-field measurements.

These references cover a range of topics related to near-field measurements, including theory, techniques, analysis methods, and probe compensation. They provide a solid foundation for understanding and applying planar, cylindrical, and spherical near-field measurements in antenna testing and characterization [58].

## 2.7 Planar Raster-Scanning System for Near-Field Microwave Imaging.

The implementations of active microwave imaging systems follow different techniques depending on the specific application. Here is a description of some of these techniques:

a). Sub-surface imaging: A pioneering imaging system proposed in 1973 used a radiating horn and an elemental dipole antenna as the transmitter/receiver. The data acquisition was performed by scanning the transmitter/receiver unit over a 2-D aperture on one side of the target. This approach was primarily focused on sub-surface imaging applications.

b). Medical applications: In 1979, Larsen et al. [59] developed a water-immersed imaging setup for medical applications. They successfully imaged a canine kidney using two horn antennas immersed in a water tank, aligned along each other's boresight. The object to be imaged was scanned in between the antennas in a raster pattern. Similar raster-scanning approaches have been proposed for sub-surface sensing and breast cancer detection [60, 61].

c). Raster scanning with sensors on both sides: In some imaging systems, such as those proposed for medical applications in the sensors are placed on both sides of the object to be imaged. This allows for obtaining both the scattered field and the transmitted field. During the measurements, the two antennas move together in a raster pattern as shown Fig.2.9.

d). Raster scanning with sensors on the same side: In other systems proposed for sub-surface sensing and a specific medical application, the transmitter and receiver are located on the same side of the target and move simultaneously during measurements as shown Fig.2.10. In this configuration, only the scattered field can be obtained.

e). Special case of raster scan: In a special case proposed in, sensors are located on both sides of the target. However, during the scan, one of the sensors remains fixed while the other one moves in the raster pattern as shown Fig.2.11. The schematics illustrate these different scanning setups for active microwave imaging systems. Each of these approaches has its advantages and is tailored to specific imaging requirements and applications.

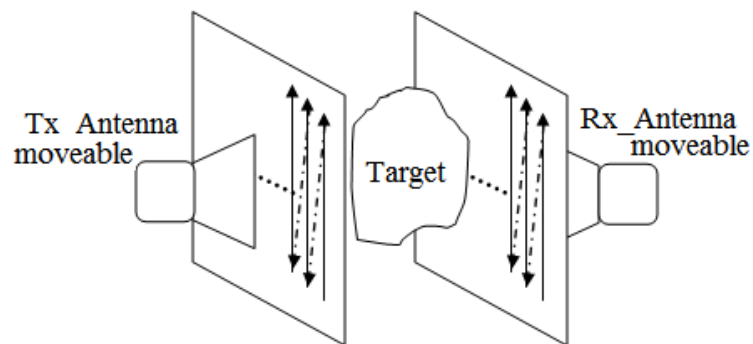


Fig.2.9 The schematic for the raster-scanning setup with sensors on both sides of the target, the two sensors move together while being aligned along each other's boresight.



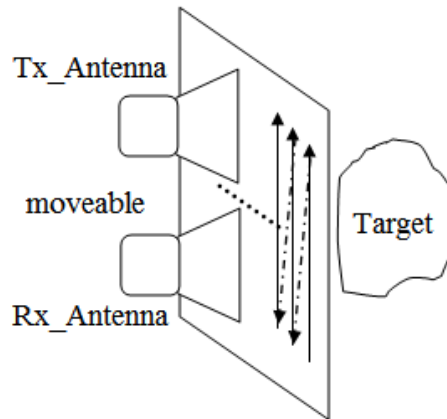


Fig. 2.10 The schematic for the raster-scanning setup with both the transmitter and receiver on one side of the target, the two sensors move together in the raster pattern.

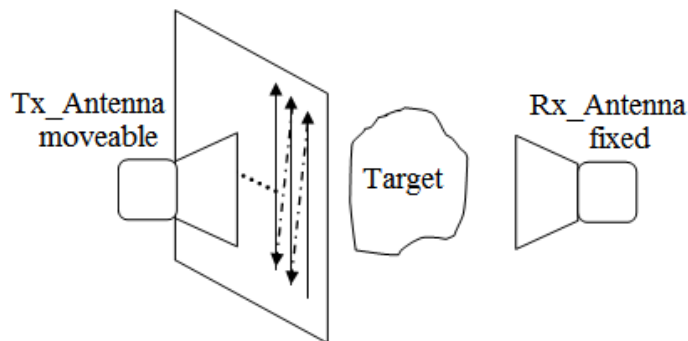


Fig. 2.11 The Schematic for the raster-scanning setup with sensors on both sides of the target. One sensor is kept fixed and the other sensor moves in the raster pattern

In the field of microwave imaging, there are various approaches to data acquisition, including scanning and multi-static approaches. Some specific implementations are described below:

Multi-static approach for breast cancer detection: The system described in is designed for breast cancer detection. Imaging sensors are placed on a hemispherical surface, which helps constrain the breast being imaged. This approach allows for multi-static measurements, where multiple combinations of transmitter and receiver antennas are used to collect data from different perspectives. Array-scan hybrid approach for concealed weapon detection: In [61], an array-scan hybrid approach is proposed for concealed weapon detection. The system consists of a fixed, linear array of transceivers parallel to the ground. The array scans in the vertical direction, and

with electronically switched array components, the system can acquire data over the full 2-D plane.

Both the scanning and multi-static approaches have their advantages and considerations: Scanning Approach: Requires only one set of transmitter or receiver antennas, leading to a lower cost compared to antenna array techniques. Adjustable spatial sampling rate controlled by the scanning mechanism. Suitable when the sensors are large or larger than the required spatial sampling rate.

Challenges of the scanning approach: Mechanical scanning complicates the design of the imaging system. Moving parts introduce uncertainties in the measurements, potentially affecting the overall dynamic range. Slower data acquisition compared to electronically switched antenna arrays.

While the scanning approach has benefits such as cost-effectiveness and adjustable spatial sampling, it also presents challenges related to mechanical design and slower data acquisition. The choice between scanning and antenna array techniques depends on specific imaging requirements, system constraints, and trade-offs between cost, speed, and design complexity. Items 1 and 2 are manageable by carefully designing the system. Item 3 is an intrinsic problem in applications that require very quick data acquisition. The biggest drawback in multi-static approach on the other hand, is the impossibility to adjust spatial sampling rate, or to employ relatively large sensors. Thus, in our case, we select the scanning approach and implement a complete imaging system based on it. In particular, we used in this thesis a planar raster-scanning imaging system.

## 2.8 Planar Data Acquisition and Reconstruction System for Near-Field Microwave Imaging

In near-field microwave imaging, the planar data acquisition and image reconstruction system is essential for obtaining accurate and high-resolution images [62-65]. The system typically involves the following components and processes:

- a). Data acquisition:

**Transmitter:** A microwave source that generates the desired frequency signal for illumination. **Receiver:** Antennas or sensor arrays that capture the scattered fields from the object under investigation.

**Scanning Mechanism:** A mechanism that controls the movement of the transmitter and receiver antennas or arrays in a planar scanning pattern can be implemented. **Data Sampling:** Measurement of the amplitude and phase of the received signals at different scanning positions. **Data pre-processing:** calibration and noise reduction techniques applied to the acquired data.

b). **Image Reconstruction:**

**Data Processing:** Processing the acquired data to extract relevant information and features. **Reconstruction Algorithm:** Utilizing mathematical algorithms to convert the measured data into an image representation. **Image Formation:** Mapping the processed data onto a 2D or 3D grid to generate the reconstructed image. **Visualization:** Displaying the reconstructed image for analysis and interpretation.

The reconstruction process typically involves solving an inverse problem, where the scattered field measurements are inverted to estimate the object's properties and spatial distribution. Various techniques can be employed for image reconstruction, such as: **Fourier Transform-based Methods:** Utilizing the Fourier Transform to convert the measured data from the spatial domain to the frequency domain, where image reconstruction is performed. **Iterative Methods:** Iteratively optimizing the estimated object properties based on a forward model that relates the measured data to the object.

**Regularization Techniques:** Incorporating prior knowledge or constraints to stabilize the reconstruction process and improve image quality. The effectiveness of the planar data acquisition and image reconstruction system depends on factors such as the antenna design, scanning resolution, data processing algorithms, and system calibration. Optimizing these components contributes to achieving accurate and detailed near-field microwave images.

## 2.9 Conclusion

This chapter presents a brief literature survey on RF wireless power transmission and the development of rectenna technology for rectifying RF microwave signals to supply DC power through wireless transmission. The antenna is responsible for capturing wireless energy, which is then directed to rectifying diodes through filters and a matching circuit. The rectifying diodes

convert the received wireless energy into direct current (DC) power. Various methods, such as RF and DC combiners, are employed for rectenna array combination to achieve maximum DC output.

The second literature survey focuses on microwave imaging, specifically active microwave imaging and passive microwave imaging. Advancements in radar systems have strongly influenced the progress of microwave imaging. Microwave images can be categorized into far-field imaging and near-field imaging, depending on the relative aperture size to the imaged distance. The near-field imaging technique offers significant power enhancement compared to far-field imaging using the same wavelength. A literature survey is conducted on the Planar Raster-Scanning System for Near-Field Microwave Imaging, which highlights the importance of a planar data acquisition and image reconstruction system in achieving accurate and high-resolution images in near-field microwave imaging.

## References

- [1] A. S. Marincic, "Nikola Tesla and the Wireless Transmission of Energy," in *IEEE Transactions on Power Apparatus and Systems*, vol. PAS-101, no. 10, pp. 4064-4068, Oct. 1982.
- [2] W.C.Brown, "The history of power transmission by radio waves," *IEEE Trans. Microwave Theory Tech.*, vol. MTT-32, pp. 1230-1242, Sept. 1984.
- [3] W. C. Brown, "An experimental low power density rectenna," in *Microwave Symposium Digest, 1991.*, *IEEE MTT-S International*, 1991, pp. 197-200.
- [4] S. -E. Adami et al., "A Flexible 2.45-GHz Power Harvesting Wristband With Net System Output From  $-24.3$  dBm of RF Power," in *IEEE Transactions on Microwave Theory and Techniques*, vol. 66, no. 1, pp. 380-395.
- [5] P. Pereira, R. C. M. Pimenta, R. Adriano, G. L. F. Brandão and Ú. C. Resende, "Antenna impedance correction for low power energy harvesting devices," *2017 SBMO/IEEE MTT-S International Microwave and Optoelectronics Conference (IMOC), Aguas de Lindoia, Brazil, 2017*, pp. 1-5.
- [6] E. Falkenstein, M. Roberg, and Z. Popovic, "Low-power wireless power delivery," *IEEE Trans. Microw. Theory Techn*, vol. 60, no. 7, Jul. 2012, pp. 2277–2286.
- [7] M. Adel, J. Zbitou, B. Abboud, A.Tribak, "Efficient Rectenna Design Incorporating New Circularly Polarized Antenna Array for WirelessPowerTransmissionat2.45GHz,"*IEEE Renewable and Sustainable Energy Conference (IRSEC)*, Oct. 2014, 577 - 581

- [8] U.Olgun, C.-C. Chen, and J. L. Volakis, "Investigation of rectenna array configurations for enhanced RF Power harvesting," *IEEE Antennas Wireless Propag.Lett.*, vol. 10, 2011, pp. 262–265.
- [9] J. Zbitou, M. Latrach, and S. Toutain, "Hybrid rectenna and monolithic integrated zero-biasmicrowave rectifier," *IEEE Trans. Microw. Theory Tech.*, vol. 54, no. 1, Jan. 2006, pp. 147–152.
- [10] Y. Huang, N. Shinohara, and T. Mitani" A Study on Low Power Rectenna Using DC-DC Converter to Track Maximum Power Point" *Asia-Pacific Microwave Conference Proceedings*, 2013.
- [11] M. Nie, X. Yang, G. Tan, and B. Han, "A Compact 2.45-GHz Broadband Rectenna Using Grounded Coplanar Waveguide," *IEEE Antennas and Wireless Propagation Letters*, Vol. 14, 2015.
- [12] O. Kazanc, F. Mazzilli, N. Joehl, F. Maloberti, C. Dehollain, "Miniaturized Antenna and Integrated Rectifier Design for Remote Powering of Wireless Sensor Systems", *IEEE Radio and Wireless Week, Santa Clara, USA*, Jan 2012.
- [13] Chou, J. H., Lin, D. B., Weng, K. L. and Li, H. J., "All Polarization Receiving Rectenna With Harmonic Rejection Property for Wireless Power Transmission," *IEEE Trans. Antennas Propag*, Vol. 62, No.10, Oct.2014, pp.5242-5249.
- [14] T.-C. Yo, C.-M. Lee, C.-M. Hsu, and C.-H. Luo, "Compact circularly polarized rectenna with unbalanced circular slots," *IEEE Trans. Antennas Propag.*, vol. 56, no. 3, Mar. 2008, pp. 882–886.
- [15] G. Vera, A. Georgiadis, A. Collado, and S. Via, "Design of a 2.45 GHz rectenna for electromagnetic (EM) energy scavenging," in *IEEE Radio Wireless Symp.*, 2010, pp. 61-64.
- [16] H. Takhedmit, L. Cirio, B. Merabet, B. Allard, F. Costa, C. Vollaie, and O.Picon, "Efficient 2.45GHz rectenna design including harmonic rejecting rectifier device," *Electron. Lett.* vol. 46, Jun. 2010, pp. 811– 812.
- [17] F.J. Huang, T.C. Yo, C.M. Lee, C.H. Luo, "Design of Circular Polarization Antenna With Harmonic Suppression for Rectenna Application," *IEEE Antenna and Wireless Propagation Letters*, , Vol. 11, 2012, pp 592- 595.
- [18] J.-H. Chou, D.-B.Lin, K.-L.Weng, and H.-J. Li, "Novel T-shape slot couple feed dual circular polarized rectenna," in *Proc. Int. Symp. Antennas Propog, Nagoya, Japan*, Nov. 2012, pp. 178 – 181.
- [19] S. V. Kumar, P. Patel, A. Mittal, "Design, Analysis and Fabrication of Rectenna for Wireless Power Transmission - Virtual Battery," *National Conference on Communication, Kharagpur India*, Feb 3-5, 2012, pp.1-4.
- [20] V. Marian, B. Allard, C. Vollaie, and J. Verdier, "Strategy for micro wave energy harvesting from ambient field or a feeding source," *IEEE Trans. Power Electron.*, vol. 27, no. 11, Nov. 2012, pp.4481– 4491.

- [21] H. Takhedmit, L. Cirio, S. Bellal, D. Delcroix, and O. Picon, "Compact and efficient 2.45GHz circularly polarized shorted ring-slot rectenna", *Electron. Lett.* vol. 48, no. 5, Mar. 2012, pp. 253–254.
- [22] Y. Huang, N. Shinohara, T. Mitani "A Study on Low Power Rectenna Using DC-DC Converter to Track Maximum Power Point," in *Proc. APMC2013*, Seoul, Nov. 2013, pp.83-85.
- [23] H. Takhedmit, B. Merabet, L. Cirio, B. Allard, F. Costa, C. Vollaïre, and O. Picon, "A 2.45-GHz low cost and efficient rectenna," in *Proc. 4th Eur. Antennas Propag. Conf.*, 2010, pp. 1–5
- [24] A. Georgiadis, G. Andia, and A. Collado, "Rectenna design and optimization using reciprocity theory and harmonic balance analysis for electromagnetic (EM) energy harvesting," *IEEE Antennas Wireless Propag Lett.*, vol. 9, 2010, pp. 444-446.
- [25] Douyere, A., Lan Sun Luk, J. D. and Alicalapa, F., "High efficiency microwave rectenna circuit: modeling and design," *Electr. Lett. Vol.* 44, No.24, Nov. 2008, pp.1409-1410
- [26] E. Levine, S. Shtrikman, and D. Treves, "Double-sided printed arrays with large bandwidth," *Microwaves, Antennas and Propagation, IEE Proceedings H*, vol. 135, pp. 54-59, 1988.
- [27] M. I. Skolnik, "Introduction to Radar Systems," *3rd Edition, McGraw-Hill Education*.
- [28] Z. Zeng, J. Li, L. Huang, X. Feng and F. Liu, "Improving Target Detection Accuracy Based on Multipolarization MIMO GPR," in *IEEE Transactions on Geoscience and Remote Sensing*, vol. 53, no. 1, pp. 15-24, Jan. 2015.
- [29] M. I. Skolnik, "Radar imaging," *Proceedings of the IEEE*, vol. 63, no. 2, pp. 174-181, February 1975.
- [30] R. J. Burkholder, I. J. Gupta, and J. T. Johnson, "Comparison of monostatic and bistatic radar images," *IEEE Antennas Propag. Mag.*, vol. 45, no. 3, pp. 41–50, Jun. 2003
- [31] De Maio and M. D. Migliore, "Bistatic radar imaging: Recent advances and future directions," *IEEE Aerospace and Electronic Systems Magazine*, vol. 30, no. 3, pp. 14-26, March 2015.
- [32] M. Vetterli, "Sampling theory and applications to radar imaging," *Proceedings of the IEEE*, vol. 80, no. 6, pp. 821-836, June 1992.
- [33] F. Zhang and Y. Huang, "Bistatic SAR: Principles and applications," in *Radar Imaging and Sensing*, 1st ed., CRC Press, 2019, pp. 243-282.
- [34] R. L. Moses, "Bistatic synthetic aperture radar," in *Radar Imaging for Maritime Observation*, 1st ed., Elsevier, 2019, pp. 57-83.
- [35] Y. Huang and W. Lin, "Bistatic SAR data processing: A review," *IEEE Journal of Selected Topics in Applied Earth Observations and Remote Sensing*, vol. 7, no. 7, pp. 2707-2722, July 2014.
- [36] H. W. Rihn and W. R. Frazier, "Bistatic radar imaging," *IEEE Transactions on Aerospace and Electronic Systems*, vol. 25, no. 5, pp. 656-664, September 1989.

- [37] M. Peichl, S. Dill, M. Jirousek and H. Suess, "Passive microwave remote sensing for security applications," 2007 *European Radar Conference, Munich, Germany, 2007*, pp. 32-35.
- [38] J. Wang et al., "A New Passive Imaging Technique Based on Compressed Sensing for Synthetic Aperture Interferometric Radiometer," in *IEEE Geoscience and Remote Sensing Letters*, vol. 17, no. 11, pp. 1938-1942, Nov. 2020,
- [39] Franchois, A. Joisel, C. Pichot , and J. C. Bolomey, "Quantitative Microwave Imaging with a 2.45 GHz Planar Microwave Camera," *IEEE Trans. Med. Imag.*, vol. 17, pp. 550-561, Aug. 1998.
- [40] F. Friederich et al., "THz Active Imaging Systems With Real-Time Capabilities," in *IEEE Transactions on Terahertz Science and Technology*, vol. 1, no. 1, pp. 183-200, Sept. 2011.
- [41] C. Bakerjian, "Active radar imaging: principles and applications," *Proceedings of the IEEE*, vol. 70, no. 2, pp. 105-120, February 1982.
- [42] C. R. Dietlein and D. A. DiFilippo, "Active Microwave Imaging: Techniques, Applications and Considerations," *IEEE Aerospace and Electronic Systems Magazine*, vol. 30, no. 9, pp. 10-19, September 2015.
- [43] L. Anitori, R. Cicchetti, and R. Guerriero, "An Overview of Active Microwave Imaging for Non-Destructive Testing and Diagnostic," *Sensors*, vol. 19, no. 14, 3177, July 2019.
- [44] M. H. Wengrovitz and J. E. Vranish, "Advances in Near-Field Microwave Imaging," *IEEE Transactions on Microwave Theory and Techniques*, vol. 63, no. 12, pp. 4393-4406, December 2015.
- [45] C. V. Jakobson and S. J. Buckner, "Through-Wall Imaging Technology: A Review," *IEEE Sensors Journal*, vol. 11, no. 1, pp. 73-83, January 2011.
- [46] N. Ida et al., "High-resolution Through-wall Imaging Radar for Moving Object Detection," *IEEE Transactions on Antennas and Propagation*, vol. 64, no. 3, pp. 931-941, March 2016.
- [47] G. Wu, H. Lu, and H. Zheng, "Review on near-field microwave imaging techniques for nondestructive testing," *IEEE Transactions on Instrumentation and Measurement*, vol. 66, no. 11, pp. 2984-2994, November 2017.
- [48] S. R. Aricò and M. Lucido, "Near-field and far-field imaging techniques for nondestructive testing of composite materials: A review," *Composites Part B: Engineering*, vol. 110, pp. 493-511, November 2017.
- [49] C. Orecchia, C. Falessi, and P. Rocca, "Microwave imaging techniques for non-destructive testing and evaluation," *Inverse Problems in Science and Engineering*, vol. 28, no. 12, pp. 1717-1756, 2020.
- [50] M. Llombart, A. Sierra-Castañer, and J. Romeu, "Review of near-field imaging techniques: Spatial and polarimetric information retrieval," *IEEE Transactions on Antennas and Propagation*, vol. 67, no. 7, pp. 4589-4604, July 2019.

- [51] M. H. Wengrovitz and J. E. Vranish, "Advances in near-field microwave imaging," *IEEE Transactions on Microwave Theory and Techniques*, vol. 63, no. 12, pp. 4393-4406, December 2015.
- [52] S. Caorsi, F. Gragnaniello, and M. Pastorino, "Microwave imaging approaches for non-destructive testing applications: A review," *Inverse Problems in Science and Engineering*, vol. 26, no. 11, pp. 1503-1530, 2018.
- [53] S. Gong and C. A. Balanis, "A review of microwave imaging with planar scanning," *IEEE Antennas and Propagation Magazine*, vol. 61, no. 4, pp. 14-32, August 2019.
- [54] L. Udpa and S. Udpa, "Through-wall imaging radar: An overview," *IEEE Potentials*, vol. 27, no. 4, pp. 21-25, October 2008.
- [55] M. Pasternack, T. Boerner, and M. Eisele, "Scanning near-field microwave microscopy for materials science," *Journal of Applied Physics*, vol. 127, no. 13, 130901, April 2020.
- [56] P. Zhang and H. Ling, "Scanning with an ideal antenna on a planar surface," *IEEE Transactions on Antennas and Propagation*, vol. 58, no. 6, pp. 1977-1981, June 2010.
- [57] A. J. Devaney, "Scanning with an ideal antenna on a cylindrical surface," *IEEE Transactions on Antennas and Propagation*, vol. 61, no. 1, pp. 114-120, January 2013.
- [58] L. Landesa and M. Guglielmi, "On scanning with an ideal antenna on a spherical surface," *IEEE Transactions on Antennas and Propagation*, vol. 66, no. 11, pp. 6133-6137, November 2018.
- [59] L. Crocco, R. Solimene, and T. Isernia, "Planar near-field microwave imaging: Theory and applications," *Inverse Problems*, vol. 28, no. 9, p. 094007, August 2012.
- [60] G. Oliveri et al., "A fast full-wave planar near-field-to-far-field transformation technique for microwave imaging," *IEEE Transactions on Antennas and Propagation*, vol. 62, no. 9, pp. 4742-4754, September 2014.
- [61] R. K. Amineh, M. Ravan, A. Trehan and N. K. Nikolova, "Near-Field Microwave Imaging Based on Aperture Raster Scanning With TEM Horn Antennas," in *IEEE Transactions on Antennas and Propagation*, vol. 59, no. 3, pp. 928-940, March 2011.
- [62] J. T. Case, M. T. Ghasr and R. Zoughi, "Nonuniform Manual Scanning for Rapid Microwave Nondestructive Evaluation Imaging," in *IEEE Transactions on Instrumentation and Measurement*, vol. 62, no. 5, pp. 1250-1258, May 2013.
- [63] M. Salucci et al., "A flexible and efficient planar scanning system for near-field microwave imaging," *IEEE Transactions on Microwave Theory and Techniques*, vol. 65, no. 8, pp. 2828-2839, August 2017.
- [64] F. Soldovieri et al., "Planar microwave imaging for nondestructive evaluation: Present and future," *IEEE Transactions on Microwave Theory and Techniques*, vol. 59, no. 10, pp. 2630-2643, October 2011.
- [65] A. Yarovoy et al., "A planar microwave imaging system for near-field and far-field applications," *IEEE Transactions on Antennas and Propagation*, vol. 59, no. 8, pp. 3097-3108, August 2011.



## Chapter 3

# Study on Suspended Planar Patch Antenna Arrays for Wireless Energy Transfer

### 3.1 Introduction

Planar antenna arrays provide symmetrical patterns with lower side lobes and higher directivity than a single antenna. Antenna arrays are widely used in wireless energy transfer (WET). In this chapter, wireless energy transferred using a single rectenna consists of an array and an array of rectennas is compared.

### 3.2 Suspended Planar Patch Antenna Array for Wireless Energy Transfer

A high gain suspended planar patch antenna array is presented for microwave energy transfer in the ISM band. The radiating patch of the antenna is placed at a height of 5 mm on an air dielectric substrate ( $\epsilon_r = 1.001$ ) between the radiating planar patch and the ground plane. The antenna is fed using a corporate feed network constructed with quarter-wavelength power dividers.  $2 \times 2$ ,  $4 \times 4$  and  $8 \times 8$  planar antenna arrays with  $0.6 \lambda_0$  inter element spacing are designed as shown in Fig. 3.1 (a), (b) and (c).

Extensive growth in the use of microstrip antennas can be observed in RF wireless energy transfer systems. In general, microstrip antennas are half-wavelength structures and are operated at the fundamental resonant mode TM<sub>01</sub> or TM<sub>10</sub>, with a resonant frequency [1, 2]. In this chapter, a corporate fed suspended planar patch antenna array is presented in ISM band.

A high gain antenna array is suitable for microwave wireless energy transfer application. The suspended method for planar patch antennas can offer several advantages, including achieving a wide impedance bandwidth and high efficiency. Microstrip patch antennas, suspended plate antennas, planar antennas [3]-[5] are various antennas used extensively in microwave wireless

energy transfer systems. Usually, they exhibit advantages such as simple structure, low cost, low profile, high polarization purity, high gain, high directivity, broad bandwidth, high efficiency, etc. In this work, a high gain suspended planar patch antenna array with corporate feed technique [6]-[8] and quarter wavelength power feed is designed for microwave wireless energy transfer at 2.45 GHz. The proposed structure was simulated using MoM-based commercial software IE3D to investigate various antenna characteristics. These characteristics include resonant frequency, bandwidth, return losses, characteristic impedance, E and H field polarizations, radiation parameters, gain, directivity, and antenna efficiency.

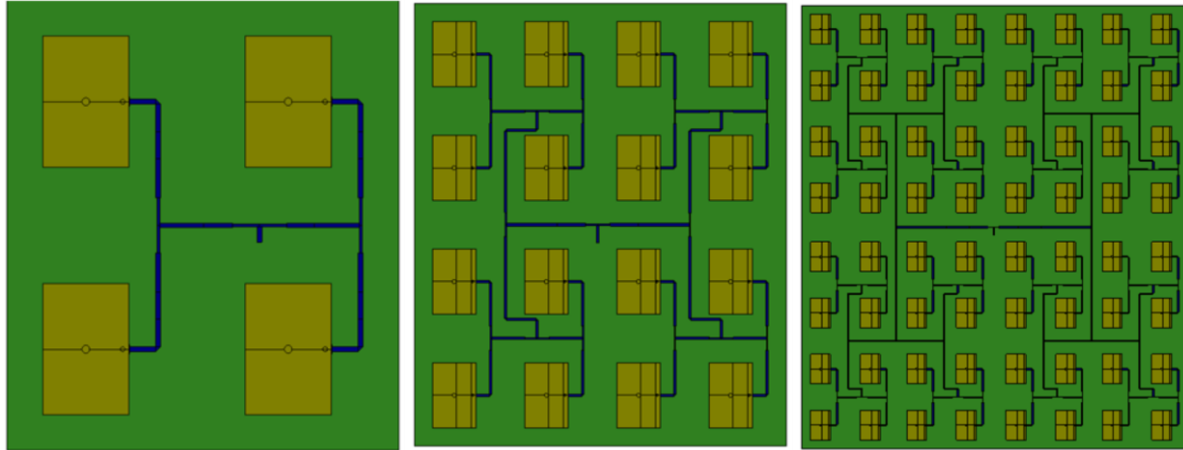
### 3.3 Design and Simulation for a Suspended Planar Patch Antenna Arrays for WET

The antenna arrays were designed and simulated to operate at 2.45 GHz, frequency for WET applications. The corporate feed, equally powered divider and coaxial probe were used to ensure uniform power distribution and efficient excitation of the antenna elements. The electromagnetic simulation was performed using the IE3D software, which is based on the Method of Moments (MoM) technique. The simulation analysis covered various performance parameters, including radiation pattern, gain, impedance, and S-parameters. The analysis encompassed different array configurations, such as  $2 \times 2$ ,  $4 \times 4$  and  $8 \times 8$ , to evaluate their performance and capabilities. Fig. 3.1(d) shown that the S-parameter characteristics of the antenna arrays, illustrating their performance within the ISM band.

Table3.1. Design parameters of  $2 \times 2$ ,  $4 \times 4$  and  $8 \times 8$  antenna array for resonant frequency ISM band, dielectric constant of a FR4\_4.4 and substrate height (h1) 1.59 mm and air dielectric 1.001, height (h2) 5mm.

<b>Array/ dimension</b>	<b><math>2 \times 2</math> Array</b>	<b><math>4 \times 4</math> Array</b>	<b><math>8 \times 8</math> Array</b>
Length of the patch	82.164mm	82.164mm	82.164mm
Width of the patch	54.469mm	54.469mm	54.469mm
Number. of antenna	04	16	64
Substrate dimension	1028.1 cm <sup>2</sup>	2564.64 cm <sup>2</sup>	10268.34 cm <sup>2</sup>
Feeding Technique	Corporate feed	Corporate feed	Corporate feed

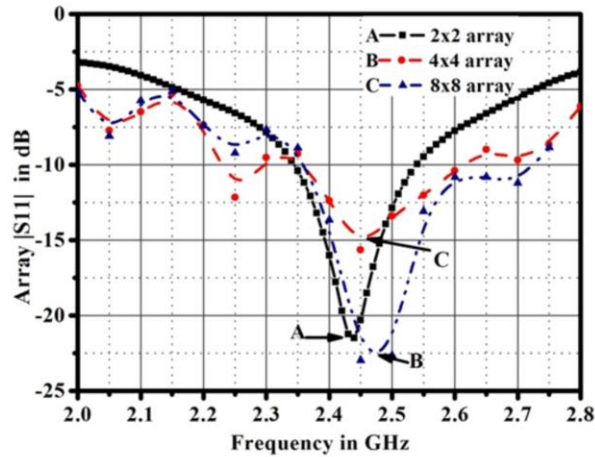
Feed impedance	50 Ohm , $\lambda/4$ wavelength transfer	50 Ohm , $\lambda/4$ wavelength transfer	50 Ohm , $\lambda/4$ wavelength transfer
inter element spacing $D_x$ and $D_y$	$D_x = 0.62 \lambda$ $D_y = 0.61 \lambda$	$D_x = 0.62 \lambda$ $D_y = 0.61 \lambda$	$D_x = 0.62 \lambda$ $D_y = 0.61 \lambda$



(a)

(b)

(c)



(d)

Fig.3.1. Geometry of suspended antenna array with corporate feed network (a)  $2 \times 2$  Array, (b)  $4 \times 4$  Array (c)  $8 \times 8$  Array, (d) Simulated Return Loss v/s frequency for  $2 \times 2$ ,  $4 \times 4$  and  $8 \times 8$  antenna arrays.

Elevation total E-field  $0^\circ$  degree 2D radiation patterns for  $2 \times 2$ ,  $4 \times 4$  and  $8 \times 8$  antenna arrays are shown in Fig. 3.2 (a). Elevation total E-field  $90^\circ$  degree 2D radiation patterns for  $2 \times 2$ ,  $4 \times 4$  and  $8 \times 8$  suspended planar patch antenna arrays are shown in Fig. 3.2 (b). The simulated gain of each antenna array is 14.02dBi, 18.91dBi and 25.15dBi respectively.

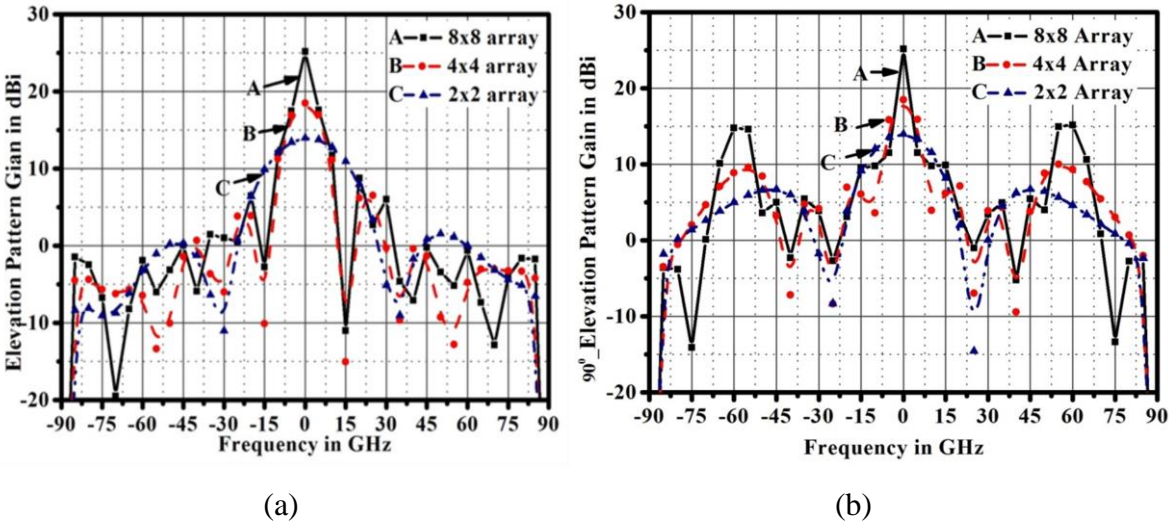


Fig. 3.2 a) Elevation total E-field 0° degree 2D Radiation Pattern for 2 × 2, 4 × 4 and 8 × 8 antenna arrays b) Elevation total E-field 90 degree 2D Radiation Pattern for 2 × 2, 4 × 4 and 8 × 8 suspended planar patch antenna arrays

Table3.2 Simulated results of 2 × 2, 4 × 4 and 8 × 8 antenna array

Array/ Parameters	2 × 2 Array	4 × 4 Array	8 × 8 Array
Return loss	-22.13 dB	-17.27 dB	-24.41dB
Bandwidth	0.32 GHz	0.34 GHz	0.39 GHz
Gain	14.021 dBi	18.912 dBi	25.15 dBi
Directivity	15.8 dBi	22.2dBi	27.4 dBi
Radiating efficiency	68.43 %	48.95 %	45.12 %

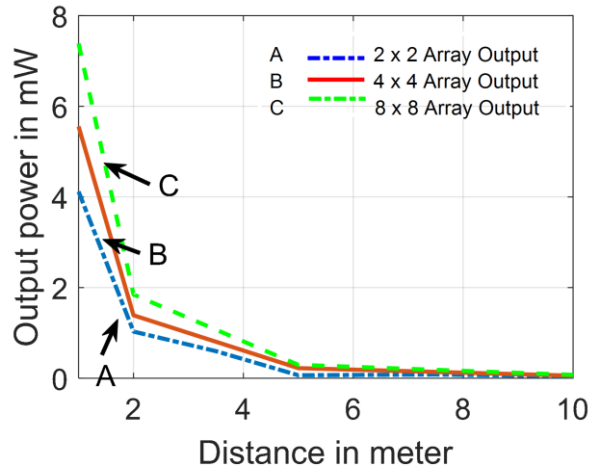


Fig.3.3 Simulation results WET output power with respect to different distance for  $2 \times 2$ ,  $4 \times 4$  and  $8 \times 8$  suspended planar patch antenna arrays

The simulations of WET for different suspended patch planar antenna array combinations are carried out for the measurement of output power. A single suspended patch planar antenna is used as the transmitter and at the receiving side, different combination of are used, like the corporate feed of a  $2 \times 2$ ,  $4 \times 4$  and  $8 \times 8$  suspended patch planar antenna array. The setup for measuring the output power at various distances is being established. First, simulation is carried out using EM simulation in IE3D, then s-parameter are collected in the form of touchstone files, and second, circuit simulation in ADS for 10dBm input power. The simulation results show WET output power with respect to different distances for  $2 \times 2$ ,  $4 \times 4$  and  $8 \times 8$  suspended planar patch antenna arrays, as shown in Fig. 3.3. The output power graph shows an exponential decay of power with respect to distance. These proposed antennas can efficiently be utilized for microwave wireless energy transfer over long distances.

### 3.4. 2 by 2 Rectenna Array Configurations for Enhanced RF Wireless Energy.

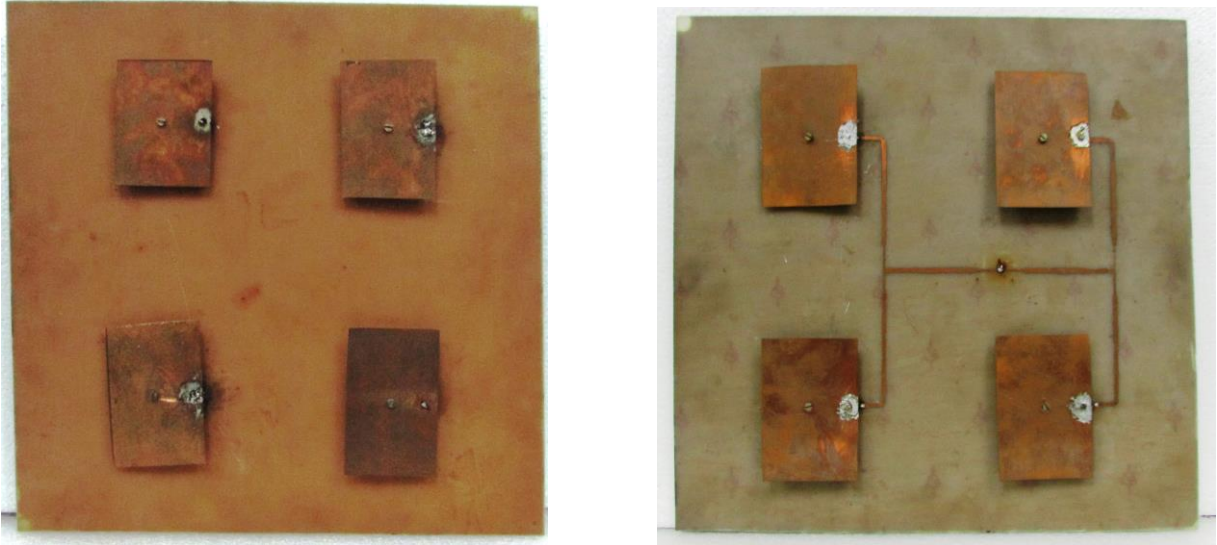


Fig.3.4 Fabriated 2 by 2 suspended patch planar antenna array. a) Planar antenna array, b) corporate feed planar antenna array

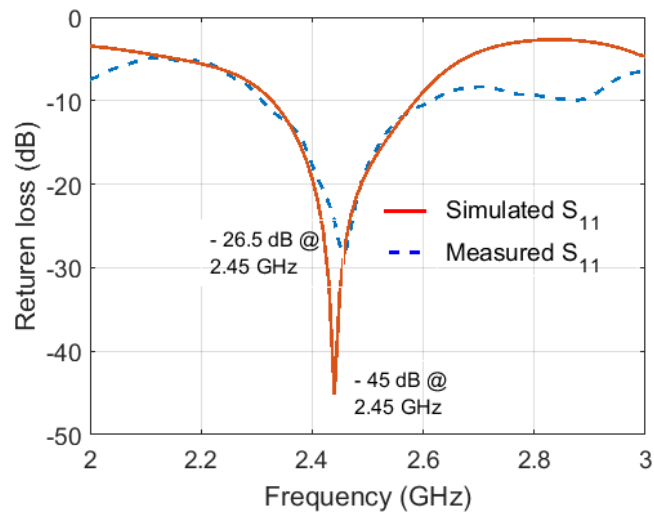


Fig.3.5. 2 by 2 corporate feed planar antenna array S-parameter  $S_{11}$  simulated and measured.

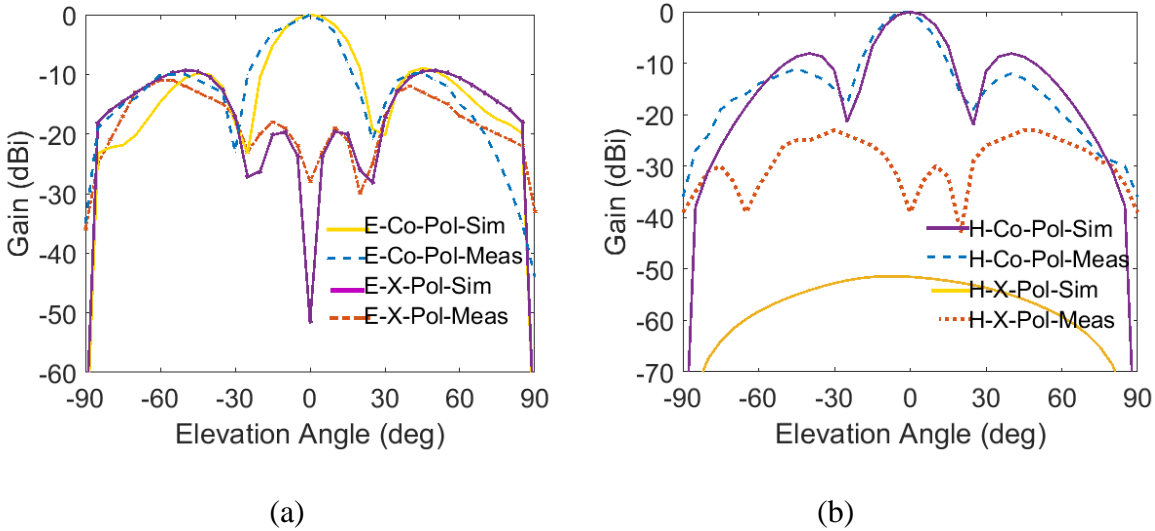


Fig.3.6. Total far-field 2D-radiation pattern for Co-pol and Cross-pol simulated and measured, a) E-plane, b) H-plane

### 3.4.1. Far Field Radiation Pattern Characteristics

The simulated and measured radiation patterns were obtained at a signal frequency of 2.45 GHz in the far field. The normalized radiation patterns for the E-plane and H-plane, considering both co-polarization and cross-polarization, are shown in Fig. 3.6 (a) and (b). The measured and simulated cross-polarization values for the E-plane are -27 dB and -52 dB, respectively, as shown in Fig. 3.6 (a). Similarly, for the H-plane, the measured and simulated cross-polarization values are -40 dB and -55 dB, respectively, as depicted in Fig. 3.6 (b). The fabricated antenna array was subjected to far-field radiation pattern measurements in a square, 8 by 8 feet shielded anechoic chamber.

In this investigation, two different rectenna architectures were compared for maximum RF to DC power conversion. A simple rectenna design consisting of a 2 by 2 planar antenna array will be presented. A single rectenna is not sufficient to supply enough energy for reliable device operation. Alternatively, properly interconnecting several antennas could provide sufficient rectification. In the first configuration, the antenna is fed using a corporate feed network, utilizing quarter-wavelength power transfer. A 2 by 2 antenna array can be arranged to direct the RF power to a single rectifier using an RF power combiner, as illustrated in Fig. 3.11 (a). In the second case, each individual antenna can incorporate its own rectifier to independently harvest DC power, known as a DC combiner, as shown in Fig. 3.11 (b). The DC

power generated from each rectifier can then be combined in parallel, series, or using a hybrid approach.

### 3.5 Rectenna (Rectifying circuit)

The concept of the rectenna, as well as the name itself, was conceived by W.C. Brown [9]. A rectenna is a passive element that consists of an antenna, a matching circuit with a low pass filter, a rectifying diode, and an output filter [10]-[16]. In this chapter, a surface mount Schottky diode HSMS2820 is used in the rectifying circuit due to its faster reverse recovery time, much lower forward voltage drop, and good RF characteristics. The development of a rectenna sensor, which is a sensitive zero-biased diode and serves as an essential part of the imaging front module, requires high RF responsively, high linearity, and low flicker noise in order to achieve good imaging quality in low contrast environments [17]-[21].

The proposed RF to DC rectifier circuit is illustrated in Fig. 3.7. The rectifier circuit is simulated and optimized on an FR4 substrate (dielectric constant  $\epsilon_r = 4.4$ ,  $h = 1.52\text{mm}$ ) using the Advanced Design System (ADS) software, which utilizes the harmonic balance method. It operates at a resonance frequency of 2.45 GHz, with a return loss of  $S_{11} = -55.65\text{ dB}$  and  $S_{22} = -56\text{ dB}$ . The impedance bandwidths achieved are 0.185 GHz (7.55%) and 0.409 GHz (16.69%) respectively. In terms of measurements, the operating resonance frequency is found to be 2.43 GHz, with a return loss of  $S_{11} = -24.4\text{ dB}$ . The impedance bandwidth is observed to be 2.38 GHz to 2.475 GHz (3.82%), as shown in Fig 3.9.

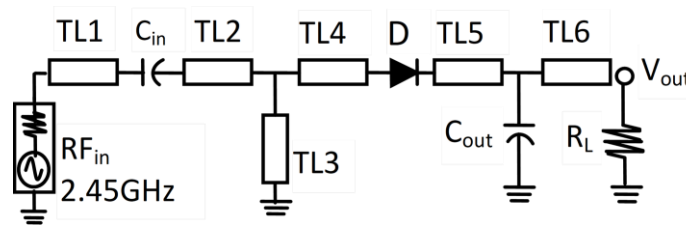


Fig. 3.7 Circuit diagram half wave rectifier simulated in the ADS.





Fig. 3.8 Fabricated RF to DC Half wave rectifier

The proposed prototype half wave rectifier circuit was fabricated on FR4 substrate, using surface mount components zero biased Schottky diode, capacitors  $C_{in}$ ,  $C_{out}$  and load resistance  $R_L$  and microstrip transmission lines TL1 to TL6 as shown in Fig. 3.7 The dimension of transmission lines and component values are given in the Table 3.4. The measurement setup, it consists of RF source Rohde & Schwarz SMR20 Signal generator, a conventional voltmeter is connected in parallel over the output resistive load to measure the output DC voltage.

Table 3.3 RF to DC circuit Components.

Components of Rectifier Circuit							
Diode		D	HSMS2820				
Capacitor		$C_{in}$	33 pf				
		$C_{out}$	3 pf				
Resistor		$R_L$	200 Ohm				
Microstrip line		TL1	TL2	TL3	TL4	TL5	TL6
Width	W mm	2.85676 mm					
Length	L mm	6	18.3	24	3	14.5	18.3

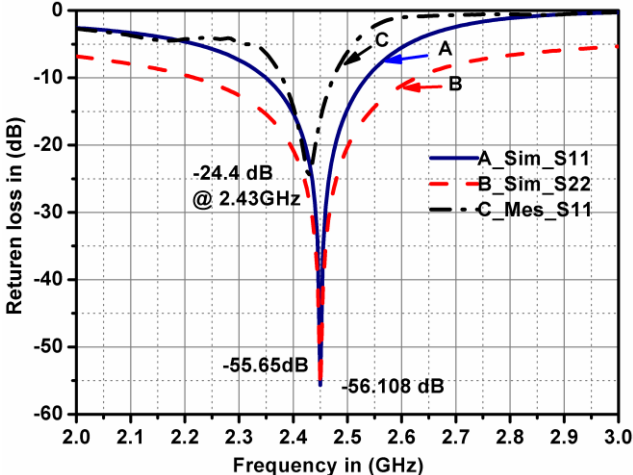


Fig. 3.9 ADS simulated and measured S-parameters in dB v/s frequency in GHz for rectifier circuit

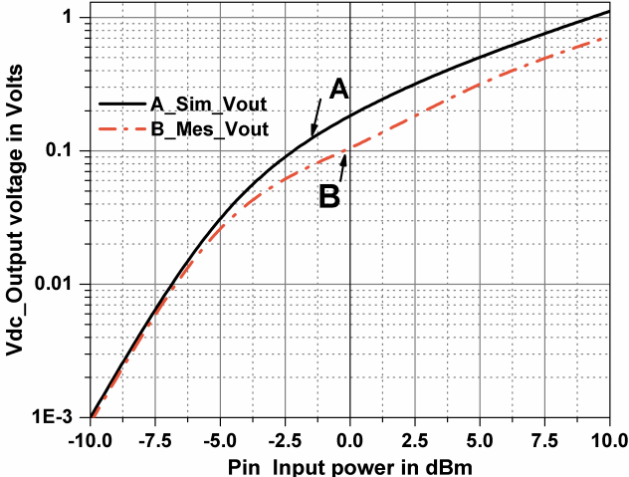


Fig. 3.10 Simulated and measured  $V_{DC}$  output voltage in Volt v/s input power in dBm of the half wave rectifier circuit.

The proposed RF to DC rectifier circuit is illustrated in Fig. 3.7. The rectifier circuit is simulated and optimized on an FR4 substrate. The prototype of the half-wave rectifier circuit has been characterized by examining the simulated and measured DC output voltage in volts versus the input power in dBm. The results are shown in Fig. 3.10. A fixed RF source is used at an operating frequency of 2.45 GHz, while the input power is varied in the range of -10 dBm to 10 dBm in step increments. As the input power increases, the output voltage also increases. At an input power of 0 dBm, the simulated output voltage is found to be 0.2 volts, while the measured

output voltage is 0.11 volts. A small discrepancy between the simulated and measured results is observed, which could potentially be attributed to factors such as improper soldering, misalignment, or loading issues during the experiment.

The circuit design and optimization were carried out using the Advanced Design System (ADS) software, which employs the harmonic balance method. The circuit operates at a resonance frequency of 2.45 GHz, with a return loss of  $S_{11} = -55.65$  dB and  $S_{22} = -56$  dB, indicating good impedance matching. The achieved impedance bandwidths are 0.185 GHz (7.55%) and 0.409 GHz (16.69%) respectively, indicating a wide frequency range over which the circuit performs effectively. In terms of measurements, the operating resonance frequency is found to be slightly lower at 2.43 GHz, with a return loss of  $S_{11} = -24.4$  dB. The measured impedance bandwidth is observed to be 2.38 GHz to 2.475 GHz (3.82%), which is slightly narrower than the simulated bandwidth. These results are shown in Fig. 3.9.

## 3.6 The Rectenna Array in Long-Range WET

### i) Single RF-to-DC Converter (RF combiner)

In the proposed architecture shown in Fig. 3.11 (a), a wireless energy transfer (WET) receiving array is composed of four patch antennas that are connected to a single RF-to-DC converter. This configuration is specifically designed for a compact application operating at 2.45 GHz, where high reception gain is required. By employing this arrangement, a remarkable 14-dBi broadside gain is achieved through the rectenna configuration. This significant gain contributes to the overall systems high end-to-end efficiency. The collecting arrangement is strategically designed to enhance the reception of signals at the desired frequency. In this architecture, the receiving layout is divided into sub-arrangements. Each sub-arrangement collects signals independently, and the gathered signals are then combined in the RF domain before being converted to DC. This allows for effective signal aggregation and optimal energy conversion from RF to DC.

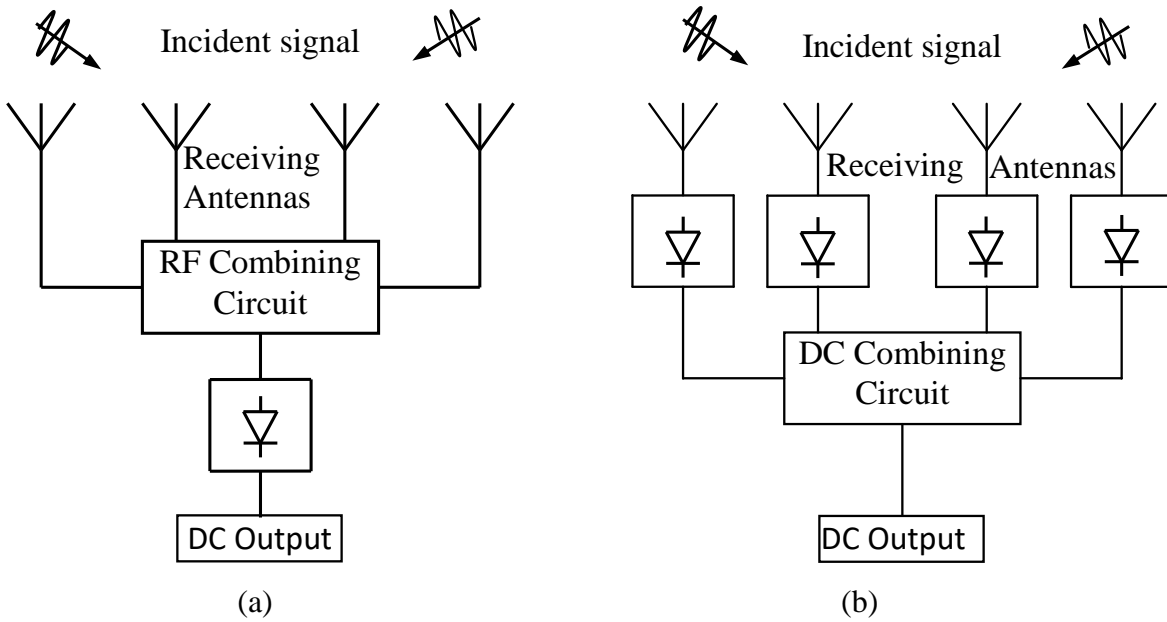


Fig.3.11. Block diagram of receiving WET rectenna array configurations (a) a DC output power by RF-combiner topology, (b) DC output power by DC combiner

### ii) Combination of Rectenna-Collected Signals at the DC Level (DC combiner)

In the architecture shown in Fig. 3.11 (b), the rectenna-collected signals are combined at the DC level. This approach is widely used in wireless power transfer (WPT) receiving arrangements. It involves straightforwardly combining the signals received and converted by each individual antenna at the DC output. One of the main advantages of this approach is its simplicity. Unlike coherent combination methods, such as RF combining, no precise RF alignment is required throughout the receiving aperture. The signals collected by each antenna are independently converted to DC, and then these DC signals are combined without the need for strict phase or amplitude matching. The non-coherent combination of the received signals simplifies the overall system design and reduces the complexity of the receiving circuitry.

## 3.9. Experimental Setup for WET Rectenna Array Configurations

WET rectenna array configurations are shown in anechoic chamber in Fig.3.12. The incident RF power impinging on the receiving antennas is output as DC power by the RF combiner and DC output power by the DC combiner. A 2 by 2 planar antenna array with  $0.6\lambda_0$  inter-element

spacing is designed and fabricated such that it can support both configurations as shown in Fig. 3.12 (a) and (b).



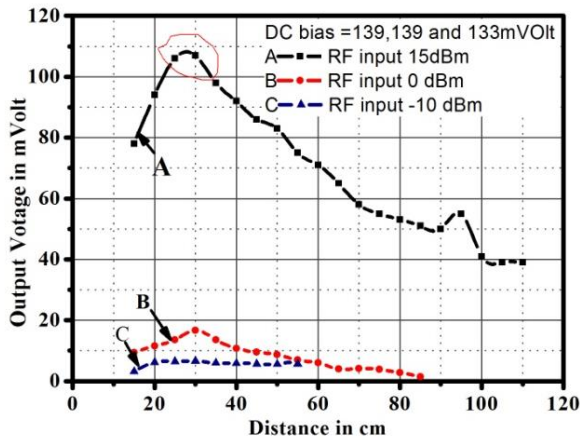
(a)



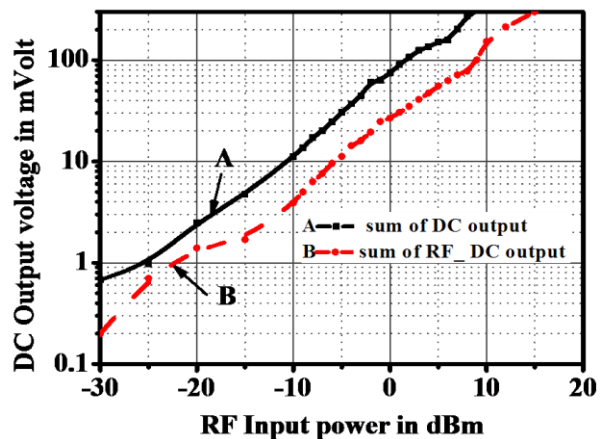
(b)

Fig.3.12. Experimental setups for single transmitter antenna with for 2 by 2 receiving WET arrays, (a) a single RF-to-DC (RF-combiner), (b) rectenna array (DC-combiner).

The proposed antenna design in this study provides coverage across the entire ISM band and achieves a gain of 14 dBi at the bore-sight. To evaluate the performance of the antenna configuration, measurements were conducted in an 8 by 8 anechoic chamber. For the RF source, a transmitting antenna with a gain of 9.7 dBi was used. The antenna transmitted a continuous wave signal at a frequency of 2.45 GHz, with the transmitted power varying from -20 dBm to 15 dBm. The transmitting antenna was positioned in the line of sight of the antenna array under investigation. The receiving antenna arrays were placed at different distances from each other, ranging from 10 cm to 120 cm. The DC output voltage was measured for both configurations of the 2 by 2 antenna array combinations, as shown in Fig. 3.13 (a). In Fig. 3.13 (b), the measured DC output voltage for two different rectenna arrays is presented. The measurements were performed at a fixed distance, and the input power levels were varied from -30 dBm to +20 dBm. These measurements provide insights into the performance of the rectenna arrays in terms of their ability to convert the received RF power into DC output voltage. The results demonstrate the relationship between the input power levels and the corresponding DC output voltage, providing valuable information for assessing the efficiency and effectiveness of the rectenna arrays in wireless energy transfer applications.



(a)



(b)

Fig.3.13. Simulation and experimental result for DC output voltages a) out voltage of 2 by 2 corporate feed rectenna array and b) Output DC voltage both configurations

The method for comparing the harvested RF power between the two rectenna topologies presented in Fig. 3.13 has been validated using a fabricated 2 by 2 antenna array with rectenna elements.

In the first topology, the RF signal from the antenna array is combined with a single rectifier. This configuration allows for harvesting more power near the main beam due to the higher power being fed to a single rectifier. By utilizing the diodes more efficiently, this topology offers advantages in power transfer efficiency in a point-to-point RF system with a narrow beam.

The second topology involves rectifying the received RF signal of each antenna element individually before combining them at the DC output. This configuration enables harvesting more power at angles away from the broadside. Each rectifier is connected to its respective antenna element, allowing it to respond to the broad pattern of that specific element. As a result, this topology is less sensitive to the incidence angle and can effectively capture power from a wider range of angles.

Comparisons of the RF signal from the antenna array to the single rectifier DC output voltages indicate that the second topology, which rectifies the signals from each antenna element individually, yields higher output voltages. This configuration is particularly suitable when dealing with large rectenna arrays because it avoids complex feeds and eliminates random polarization effects.

### 3.7 Conclusion

In this chapter, the focus is on the design and analysis of a suspended planar antenna and rectenna array for wireless energy transfer (WET) applications. The analysis includes different array configurations, such as  $2 \times 2$ ,  $4 \times 4$ , and  $8 \times 8$ , to evaluate the performance of the proposed antenna. The S-parameters of the antenna are verified to be within the bandwidth of the Industrial, Scientific, and Medical (ISM) band. Furthermore, a fabricated  $2 \times 2$  planar antenna array is tested and evaluated for its ability to receive wireless energy in WET applications. The study also investigates two different rectenna array configurations: (a) a DC output power by RF-combiner topology and (b) a DC output power by DC combiner topology. Comparisons are made between the RF signal from the antenna array and the DC output voltages of a single rectifier. It is found that the RF signal of each antenna element prior to combining it at the DC output

voltage yields higher output voltages compared to the RF signal combined with a single rectifier. Overall, the chapter presents the proposed suspended planar antenna and rectenna array, explores different array configurations, and compares the performance of the two rectenna configurations, highlighting their suitability for specific applications and scenarios.

## References:

- [1] C. A. Balanis, C. R. Birtcher, and D. K. Young, "Design of planar arrays for wireless power transfer," *IEEE Transactions on Antennas and Propagation*, vol. 60, no. 3, pp. 1537-1544, March 2012.
- [2] C. S. Lim, K. S. Oh, and T. Y. Yun, "Design of patch antenna array for wireless power transfer," *IEEE Transactions on Antennas and Propagation*, vol. 60, no. 3, pp. 1593-1602, March 2012.
- [3] J. Moon, J. Kim, and J. Kim, "Suspended planar patch antenna arrays for wireless power transfer," *IEEE Transactions on Antennas and Propagation*, vol. 60, no. 6, pp. 2969-2977, June 2012.
- [4] Y. Zhou, H. Zhang, and K. Huang, "A suspended planar patch antenna array for wireless power transfer," *IEEE Antennas and Wireless Propagation Letters*, vol. 14, pp. 383-386, 2015.
- [5] Y. Liu, R. Sun, and L. Deng, "Design of a corporate-fed planar patch antenna array for wireless power transfer," *Progress In Electromagnetics Research C*, vol. 45, pp. 109-117, 2013.
- [6] J. Y. Park and J. Kim, "A corporate-fed planar patch antenna array for wireless power transfer," *IEEE Transactions on Antennas and Propagation*, vol. 62, no. 8, pp. 4197-4202, August 2014.
- [7] C. A. Balanis, C. R. Birtcher, and D. K. Young, "Design of a corporate feed planar patch antenna array for wireless power transfer," in *Proceedings of the IEEE Antennas and Propagation Society International Symposium, Toronto, on, Canada*, July 2010, pp. 1-4.
- [8] Y. C. Wu, L. C. Kuo, and T. J. Huang, "A corporate-fed planar patch antenna array for wireless power transfer," *IEEE Antennas and Wireless Propagation Letters*, vol. 14, pp. 1714-1717, 2015.
- [9] W.C.Brown, "The history of power transmission by radio waves," *IEEE Trans. Microwave Theory Tech.*, vol. MTT-32, pp. 1230-1242, Sept. 1984
- [10] K. H. Kim, M. A. Qazi, and C. S. Kim, "Rectenna array design for wireless power transmission," *IEEE Transactions on Antennas and Propagation*, vol. 63, no. 7, pp. 3148-3155, July 2015.



- [11] D. M. Delin, R. D. McCarty, and G. D. Durgin, "The dipole rectenna: A broadband 2.45-GHz rectenna using reactive impedance surfaces," *IEEE Transactions on Microwave Theory and Techniques*, vol. 52, no. 4, pp. 1246-1253, April 2004.
- [12] B. R. Nezami, R. Maaskant, and A. G. Tijhuis, "A power combining approach for rectenna arrays for efficient wireless energy harvesting," *IEEE Transactions on Microwave Theory and Techniques*, vol. 65, no. 4, pp. 1339-1347, April 2017.
- [13] W. M. Su, J. R. Lin, and M. H. Weng, "A high-efficiency suspended planar patch antenna array for wireless power transfer systems," *IEEE Transactions on Antennas and Propagation*, vol. 64, no. 7, pp. 3143-3147, July 2016.
- [14] R. Sun, L. Deng, and Y. Liu, "Design of a suspended patch antenna array for wireless power transfer," *Journal of Electromagnetic Waves and Applications*, vol. 29, no. 16, pp. 2087-2098, 2015.
- [15] Y. Lee, S. Kwon, and J. Choi, "A suspended planar patch antenna array for wireless power transfer," in *Proceedings of the IEEE Antennas and Propagation Society International Symposium, San Diego, CA, USA*, July 2017, pp. 699-700.
- [16] A. M. Hoque, M. R. I. Faruque, and H. Tenhunen, "An RF energy harvesting system with a multi-input multi-output (MIMO) antenna and a 4-to-1 power combiner," *IEEE Transactions on Industrial Electronics*, vol. 61, no. 10, pp. 5508-5519, October 2014.
- [17] S. Huang, S. Yang, L. Zhang, and H. Zhai, "Design of a planar patch antenna array for wireless power transfer," *IEEE Transactions on Antennas and Propagation*, vol. 64, no. 7, pp. 3065-3074, July 2016.
- [18] Y. Wang, Z. Lai, X. Zhao, and C. Parini, "Design of planar patch antenna array for wireless energy transfer," *Electronics Letters*, vol. 50, no. 15, pp. 1108-1110, July 2014.
- [19] Y. Huang, X. Wu, W. Zhou, and X. Liu, "Design of a planar patch antenna array for wireless energy transfer," in *Proceedings of the 9th International Symposium on Antennas, Propagation and EM Theory (ISAPE), Tianjin, China*, October 2010, pp. 1250-1253.
- [20] H. Zhu, W. Ma, and L. Wang, "Design of a rectenna array for RF energy harvesting in wireless sensor networks," *IEEE Transactions on Antennas and Propagation*, vol. 62, no. 4, pp. 1811-1817, April 2014.
- [21] X. Wu, Y. Huang, and X. Liu, "Design of a planar patch antenna array for wireless power transfer," *IEEE Antennas and Wireless Propagation Letters*, vol. 10, pp. 44-47, 2011.

# Chapter 4

## Study on Broadband Planar Dual Fed Rectenna

### 4.1 Introduction

A rectangular microstrip antenna (RMSA) is one of the simplest planar antenna configurations which can be analyzed and designed very easily. It consists of a rectangular microstrip patch of length  $L$  and width  $W$  on a dielectric substrate backed by a metallic ground plane. RMSA with a coaxial probe feed and edge feed using microstrip line are shown in Figs 4.1 (a) and (b), respectively.

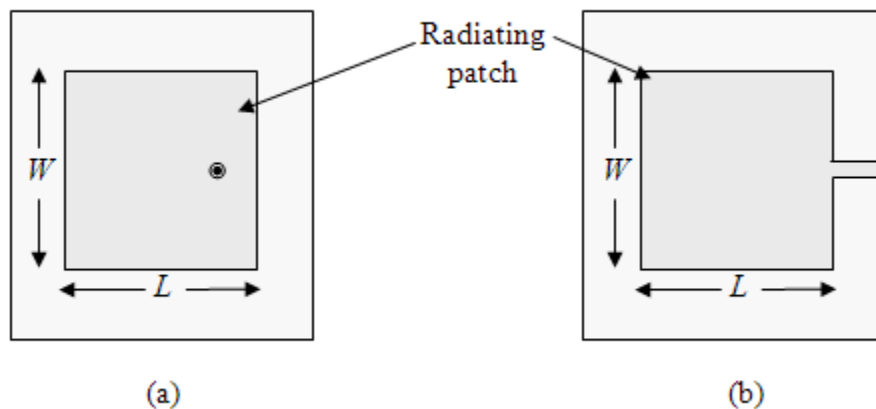


Fig.4.1 RMSA: (a) probe feed (b) edge feed

For the coaxial probe fed RMSA, the center conductor of co-axial feed is soldered to the radiating patch. The main advantage of these types of feeds is that they can be placed precisely at the desired location inside the patch to match with the required input impedances. On the other hand, microstrip line feed is advantageous when completely planar design is required. Both

coaxial fed and microstrip line fed antennas are very common for low bandwidth operations. Another thing is that these antennas are not suitable for full wave rectennas. In this chapter, dual feed RMSA are used to study broadband rectennas for full wave rectifications and various parametric studies have been carried out on dual feed rectennas.

## 4.2 Design Equations of RMSA

Various approximate design equations to construct RMSAs depend on operating frequency  $f_c$ , dielectric constant  $\epsilon_r$  and substrate height  $h$ . The approximate design equations are:

$$W = \frac{c}{2f_c} \sqrt{\frac{2}{\epsilon_r + 1}} \quad (4.1)$$

$$L = \frac{c}{2f_c \sqrt{\epsilon_e}} - 2 \Delta L \quad (4.2)$$

where,  $c$  is the velocity of light in free space ( $3 \times 10^{10}$  cm/sec),  $\epsilon_e$  is effective dielectric constant and  $\Delta L$  is the extension of the patch length due to fringing field effects. In general, the resonance frequency of the RMSA at any  $TM_{mn}$  mode is obtained using the following expression:

$$f_c = \frac{c}{2\sqrt{\epsilon_e}} \left[ \left( \frac{m}{L} \right)^2 + \left( \frac{n}{W} \right)^2 \right]^{\frac{1}{2}} \quad (4.3)$$

where,  $m$  and  $n$  are the modes along the  $L$  and  $W$ , respectively.

### 4.3 Dual Feed RMSA

Bandwidths of RMSAs with single feed ports are normally small and typically fall in the range of 1 to 10 %. By increasing the width of the rectangular patch or using thick substrate with low  $\epsilon_r$ , large bandwidth can be obtained. Another way to obtain larger bandwidth is to feed RMSA at two points located at the two opposite radiating edges. Contrary to RMSA with single feed, any dual feed configuration gives better BW when the rectangular patch width is smaller and the characteristic impedance of the patch approaches towards system impedance. But the directivity decreases with the decrease of the patch width and thus optimization of width is required. Some advantages of dual feed RMSAs are:

1. Large bandwidth when the patch width is small and its characteristic impedance tends to system impedance ( $50 \Omega$ ).
2. Since the length of the RMSA is  $\lambda/2$  for dual feed antenna, the input impedance at either of the port will be theoretically equal to system impedance ( $50 \Omega$ ) when other port is terminated with same impedance. As a result, theoretically a dual port RMSA is always matched at the centre frequency and it is not dependent upon the width of the patch.
3. The configuration is fully symmetrical and radiation pattern is in broadside direction at  $f_c$  (fundamental  $TM_{10}$  mode).
4. Normally at any point of time, induced voltages the two edges of dual feed antenna are of equal amplitude and opposite phases which makes it suitable for full wave rectenna using bridge rectifier circuit.
5. If the centre of dual feed antenna is shorted, then the antenna becomes suitable for full wave rectification with two diodes.

A typical dual feed suspended RMSA is shown in Fig. 4.2.

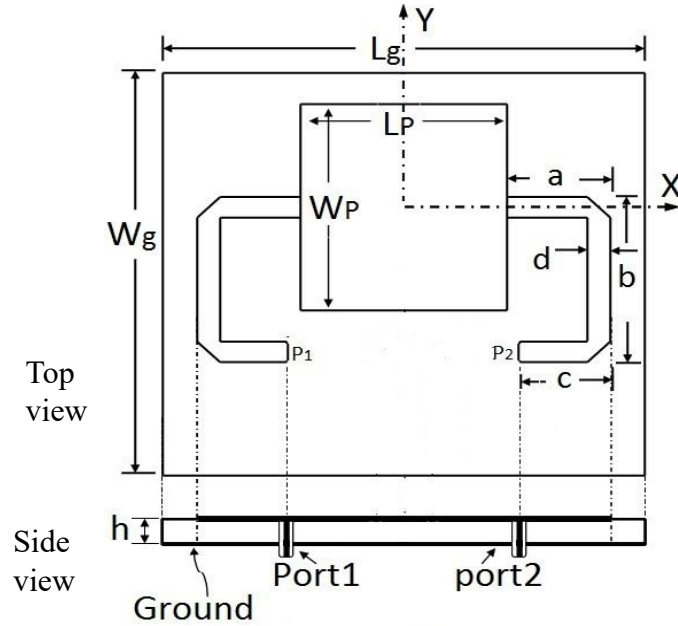


Fig. 4.2 Dual feed RMSA: (a) top and (b) side view

A broadband full wave rectenna can be constructed using a dual fed RMSA which are suitable for broadband wireless energy transfer at 2.45 GHz ISM band. The full wave rectenna structure is designed using a centre shorted dual edge feed microstrip patch antenna and two Schottky diodes. This antenna is inherently broadband in nature and can provide differential voltage at its two feed points. An optimized full wave rectenna is fabricated and tested. The proposed rectenna provides more conversion efficiency than a rectenna with similar antenna and conventional half wave rectifier.

A rectenna is a rectifying antenna system and it normally consists of single or multiple receiving antennas and rectifiers. Sometimes voltage multipliers are also included in rectenna systems to increase the voltage output [1]–[3]. The rectifier part of rectenna can be either half wave or full wave. The half wave rectifier is simple and can be constructed using single series or shunt diodes, but it can utilize only one half cycle of the AC signal. Several rectenna systems consist of half wave rectifier have been investigated so far [4]–[15]. On the other hand, full wave rectifier can take advantages of both half cycles of the AC signal. Rectenna with full-wave rectifier consist of two diodes or four diodes are also studied by researchers [16]–[22].

We focus on developing a rectenna system that utilizes full wave rectification to increase RF to DC conversion efficiency using differential voltage output from dual feed antennas. The

proposed rectenna system consists of dual edge feed broadband antenna and two-diode full wave rectifier. Dual feed antennas with differential voltage output are already reported for efficient rectenna with half wave rectifier [13] but here similar antenna is used for full wave rectifications. The working principle of the proposed configuration is similar to the traditional AC to DC conversion using a centre tapped transformer and full wave rectifier consists of two-diodes. The proposed system has been analyzed theoretically using commercially available IE3D and ADS software [23], [24]. An optimized rectenna system is fabricated for experimental verification and the measured results agree with the theoretical results.

#### 4.4 Centre Shorted Dual Edge Fed Broadband Microstrip

The proposed rectenna consists of a broadband dual edge fed microstrip antenna and full wave rectifier circuit. The broadband dual edge fed center shorted microstrip antenna geometry is shown in Fig 4.3. A dual edge fed center shorted antenna is optimized at 2.45 GHz considering low cost glass epoxy FR-4 substrate with dielectric constant  $\epsilon_r = 4.4$ , height  $h = 1.59$  mm and dielectric loss  $\tan \delta = 0.01$ . The dimensions of the optimized antenna geometry are: patch length  $L_p = 29.84$  mm, patch width  $W_p = 34$  mm, ground plane length  $L_g = 75$  mm and width  $W_g = 7$  mm. The width of  $50 \Omega$  microstrip feed line  $d$  is 3.036 mm, lengths  $a = 13.85$  mm,  $b = 31$  mm and  $c = 10.56$  mm, respectively.

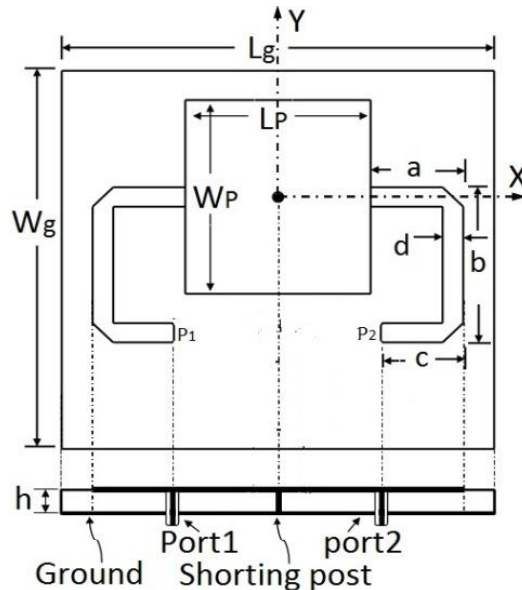


Fig. 4.3 The geometry of dual edge feed center shorted microstrip antenna top view and side view.

The antenna operates at the fundamental  $TM_{10}$  mode during power conversion and in this mode of operation; the voltage is maximum at the patch edges and minimum (zero) at the center of the patch. Two edge-fed microstrip lines are placed at two edges of the rectangular radiating patch where the voltages are maximum and out of phase with respect to each other. The center of the patch antenna is shorted to ground where the voltage is zero. The simulated variation of S-parameters with a frequency for the two edge feeds placed at optimized antenna edges are shown in Fig. 4.4 and corresponding Smith chart plot is shown in Fig 4.4. The value of  $S_{11}$  is close to -50 dB at 2.45 GHz and the antenna exhibits impedance bandwidth of 500 MHz (20%). This bandwidth is much larger than the bandwidth of a similar single feed microstrip antenna. Gain and efficiency of this antenna are 5.6 dBi and 46%, respectively. The value of  $S_{21}$  is -1.53 dB at resonating frequency.

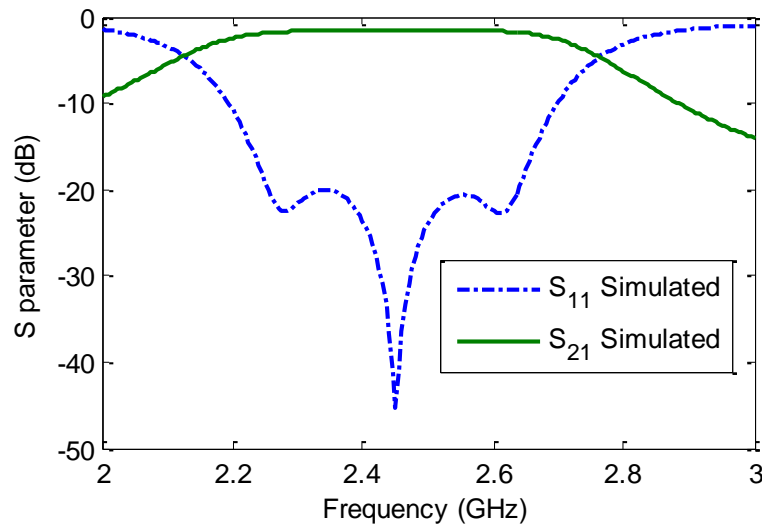


Fig. 4.4 Simulation of frequency v/s S-parameter results for broadband dual edge feed microstrip antenna.

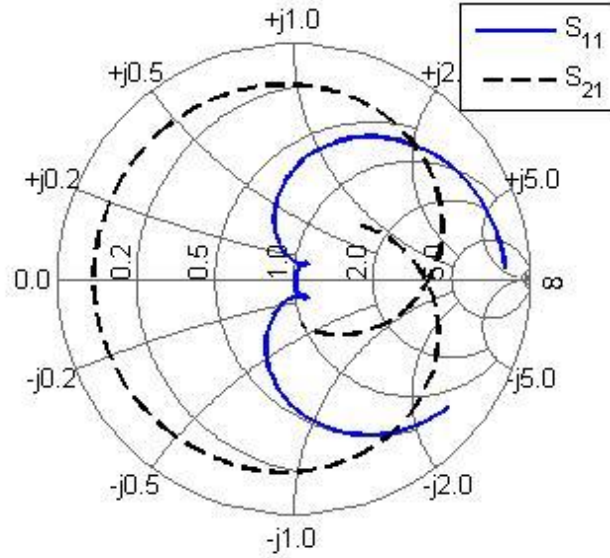


Fig. 4.5 Simulated input impedance of the broadband dual edge feed antenna on the smith chart.

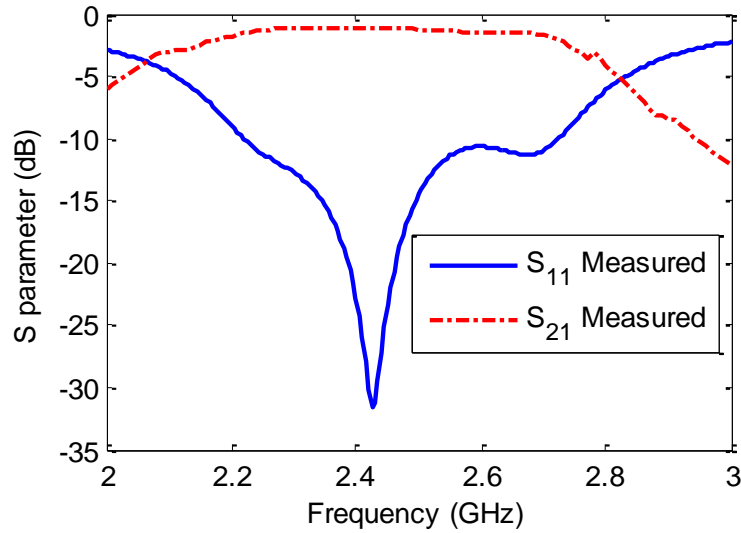


Fig. 4.6 The measured S-parameter of broadband dual edge feed microstrip antenna.

The optimized dual fed antenna is fabricated for measurement and the simulated and measured S-parameters of dual feed antenna as a function of frequency is shown in Fig. 4.6.  $S_{11}$  for the port 1 of the dual feed antenna is measured using a two port network analyzer (Agilent NA E5071B series) keeping another port matched with 50 Ohm. Since the antenna is symmetric,  $S_{11} = S_{22}$ . Hence, only  $S_{11}$  is measured. A little shift in the center frequency is observed, but the measured operating band ( $S_{11} < -10\text{dB}$ ) agrees with simulations.



### 4.5 Design of rectenna using full wave rectifier

The proposed full wave rectenna system consists of a center shorted dual edge fed microstrip antenna and two Schottky diodes are shown in Fig. 4.7. Two quarter wavelength impedance transformers are used for impedance matching. Edge feed ports P1 and P2 are used for connecting diodes and capacitors. During receiving mode this antenna acts like a center tap transformer and voltages induced at its two opposite feed locations are of equal amplitudes with 180 degree phase difference.

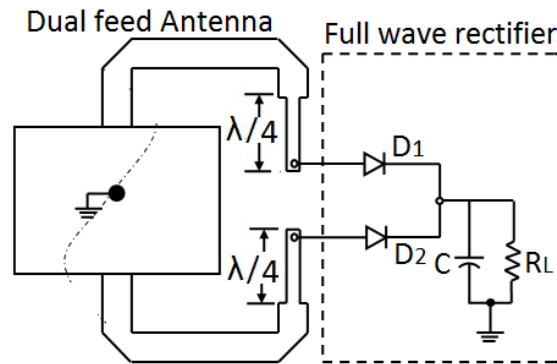


Fig. 4.7 Proposed full wave rectenna consists of dual feed center short microstrip antenna and full wave rectifier circuit.

For rectification two HSMS 2820 Schottky diodes are used. The generated rippled DC voltage is filtered using RC filter where the R is basically the load  $R_L = 50 \Omega$  and the value of the capacitor (C) is 1nF. The impedance matching quarter wavelength transformers is used to transform  $50 \Omega$  to  $100 \Omega$  such that at combining junction the impedance becomes  $50 \Omega$ .

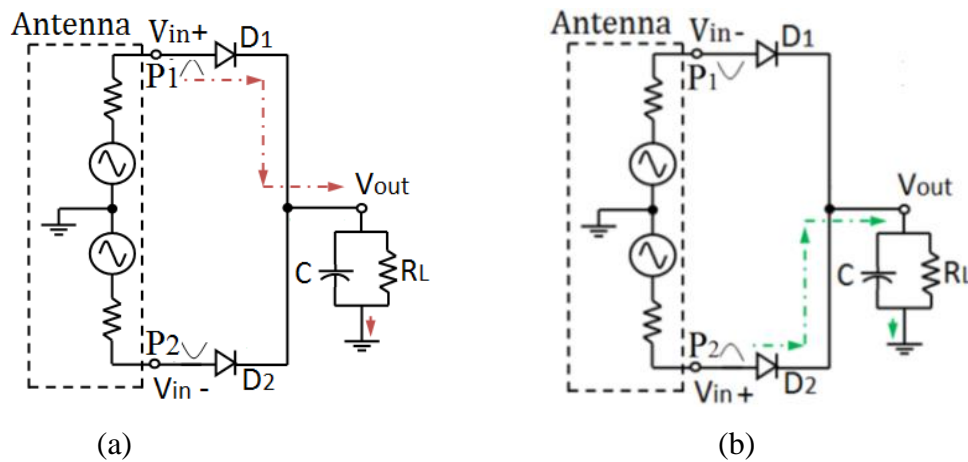


Fig. 4.8 Equivalent schematic of the proposed full wave rectenna showing the direction of the dc signal path (a) positive and (b) negative half cycles.

The rectenna shown in Fig.4.7 can be modeled like two-diode full wave rectifier connected to a dependent RF source as shown in Fig. 4.8. In the positive half cycle diode D1 conducts and D2 remains in OFF state as shown in Fig. 4.8 (a). During the negative half cycle, D2 conducts and D1 remains in OFF state as shown in Fig. 4.8(b).

#### 4.6 Simulation and Measurement of the Proposed Rectenna System

A complete EM and circuit co-simulation setup for RF energy harvesting is as shown in Fig. 4.9. ADS simulator is used for complete EM and circuit co-simulation. A suspended radiating patch antenna with 9.7 dBi gain (at 2.45 GHz) is considered as transmitter [16].

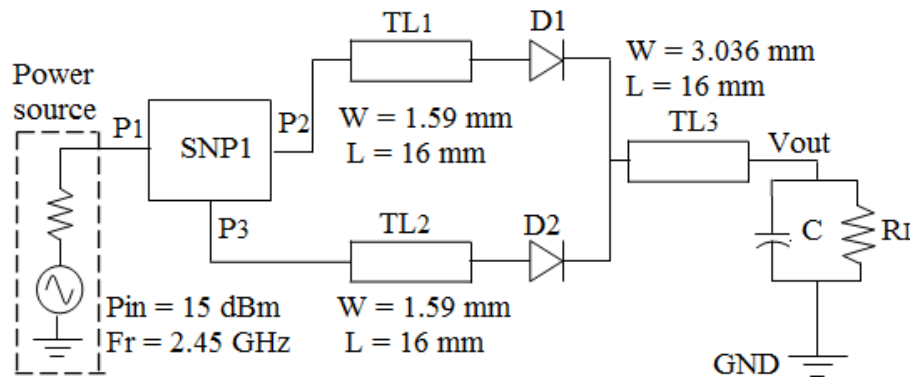


Fig. 4.9 EM and circuit co-simulation setup for the proposed full wave rectenna

The dual feed receiver antenna (Rx) is placed at 10 cm, 15 cm and 20 cm apart from transmitter (Tx) antenna for wireless RF energy transfer investigations. In the co-simulation setup, the three port model SNP1 represents the S-parameters in touchstone format generated from IE3D for single port Tx and two port Rx antennas placed at 10 cm to 20 cm apart from each other. The variable input power source is connected to transmitter antenna at port 1 and the ports 2 and 3 of dual fed receiver antenna are connected with full wave rectifier consists of Schottky diodes. The received power is observed across port 2 and port 3 of the Rx antenna and the DC output voltage ( $V_{out}$ ) is observed at the load for varying input power for various distances between transmitter and receiver antenna.

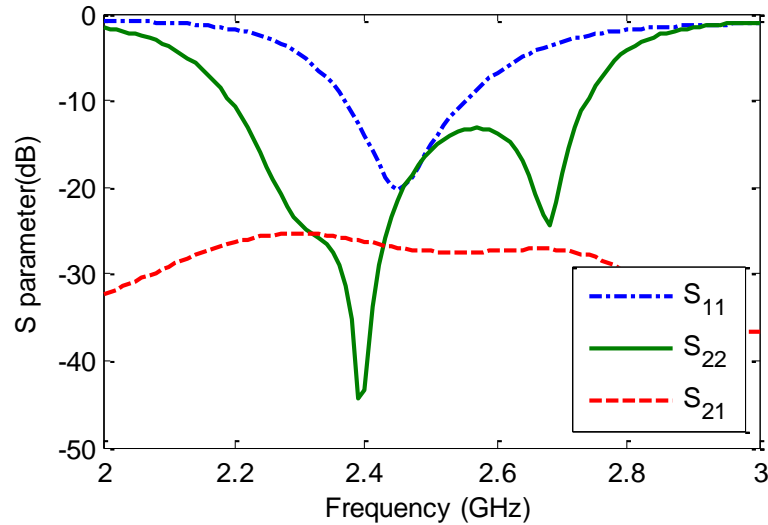


Fig. 4.10 The simulated S-parameters for the transmitter and receiver antennas placed at 15 cm apart.

The variation of S-parameters with frequency for the entire transmitter-receiver system for 15 cm distance between them is shown in Fig 4.10. It can be seen that in the presence of transmitter antenna the receiver antenna property is changed slightly. The value of  $S_{11}$  for transmitter antenna is -20 dB and  $S_{22}$  and  $S_{33}$  for receiver antenna are also close to -20 dB at 2.45 GHz. The mutual coupling between transmitter and receiver antenna is better than -27 dB at operating frequency. The receiver antenna bandwidth is still more than 500 MHz. The transmitter antenna shows a bandwidth of 140 MHz (2.381 GHz to 2.521 GHz).

The simulated gains of the transmitter and receiver antenna as a function of frequency are shown in Fig 4.11. From the Fig, the receiver dual feed antenna gain varies from 3.6 dBi to 4 dBi within frequency range from 2 to 3 GHz and the gain is 5.6 dBi at 2.45 GHz frequency. On the other hand, the transmitter antenna gain is 9.7 dBi at 2.45GHz.

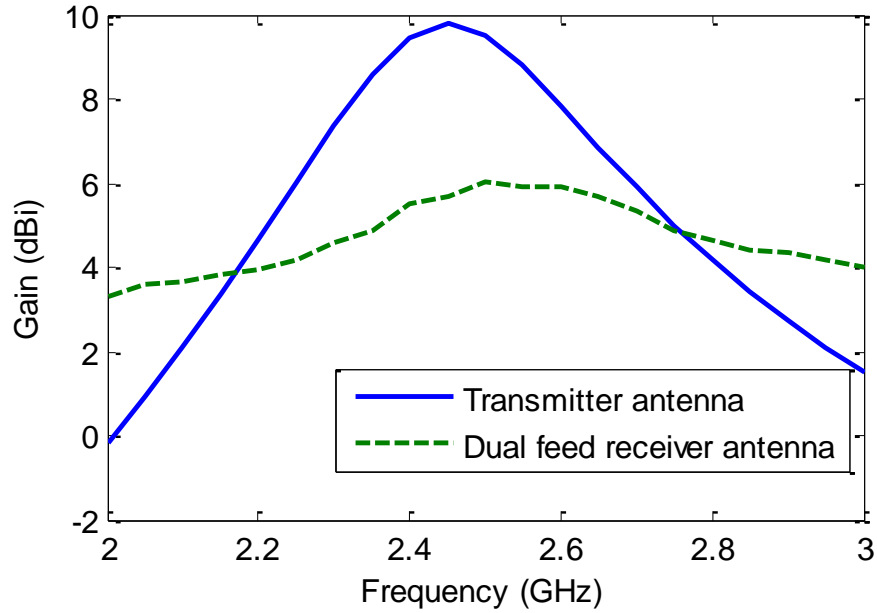


Fig. 4.11 Simulated gain with frequency of the transmitter and receiver antenna.

Table 4.1 comparing the parameters of transmitter antenna and receiving dual feed antenna

Performance characteristics	Tx_ Antenna RMSA	Rx_ Dual feed antenna	
		Simulated	Measured
Frequency(GHz)	2.45 GHz	2.45 GHz	2.436 GHz
$S_{11}$	-32 dB	-45 dB	-30 dB
VSWR	1.08	1.01	1.1
Impedance Band width (MHz)	(2.381 GHz to 2.521 GHz) 140 MHz	(2.2 to 2.7GHz) 500 MHz	(2.21 to 2.71 GHz) 500MHz
Impedance Band width efficiency(%)	5.71%	20%	20%
Gain in (dBi)	9.7 dBi	5.6 dBi	
Efficiency (%)	9.8%	46%	

A complete RF energy transfer system comprising of a center grounded dual feed antenna and Schottky diodes based full wave rectifier is designed and fabricated. The fabricated dual edge feed center short full-wave rectenna is shown in Fig 4.12.

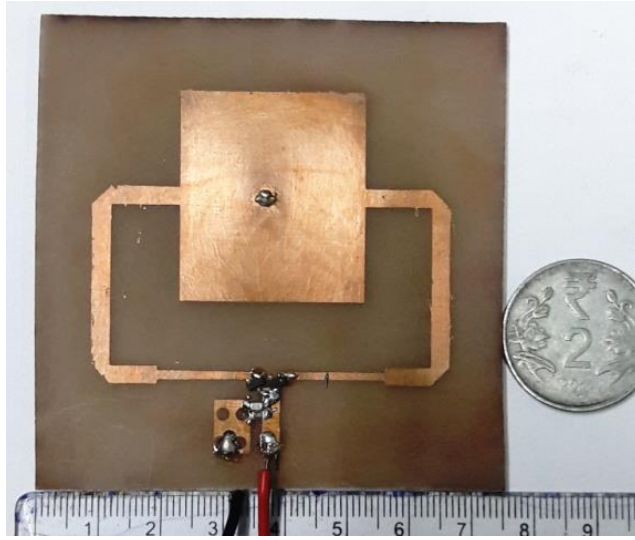


Fig. 4.12 The Fabricated broadband dual feed microstrip rectenna.

The measurement setup for RF wireless energy transfer is shown in Fig.4.13. The transmitter as a suspended patch antenna is fixed and receiver dual feed full wave rectenna are placed at a different distance of 10 cm, 15 cm and 20 cm apart respectively from each other for measurement of output DC voltage. A signal generator Rhode & Schwarz SMR20 was used as a source. Measurements are carried out for varying distances, incident power, and frequencies

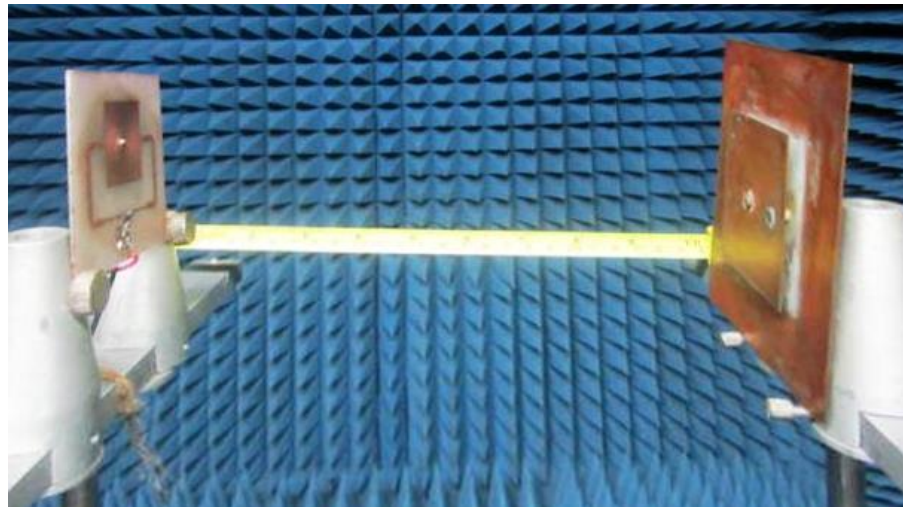


Fig. 4.13 Measurement setup for RF wireless energy transfer

When the transmitting and receiver antennas are placed at 10 cm, 15 cm, and 20 cm apart respectively from each other, the simulated and measured output DC voltages vary with variation of input transmitted power. The variation of output voltages for changing input power from -10 dBm to +15 dBm at 2.45 GHz is shown in Fig. 4.14.

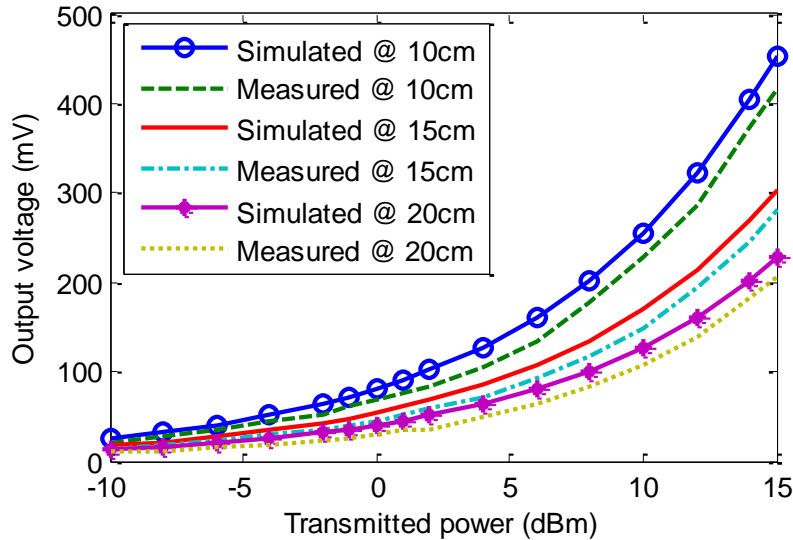


Fig. 4.14 Simulated and measured output voltage with transmitted power.

For 10 cm distance between transmitter and receiver, the simulated and measured output voltages vary from 25 mV to 451 mV and 20 mV to 406 mV, respectively. For 15 cm distance between transmitter and receiver, the simulated and measured output voltages vary from 17 mV to 277 mV and 14 mV to 251 mV, respectively. Similarly, for 20 cm distance, the measured and simulated output voltages vary from 12 mV to 206 mV, and 8 mV to 187 mV, respectively. The behaviors of measured and simulated output voltage curves are similar. But the measured voltage is always lower than the simulated result which is possibly due to some fabrication error and some extra losses from contacts.

The simulated and measured output voltages are studied for 2 GHz to 3 GHz frequency range, keeping 10 cm distance between the transmitter and receiver antennas and 15 dBm transmitted power. The variations of output voltages with the varying frequency are shown in Fig 4.15. Measured output voltages agree with the simulated results.

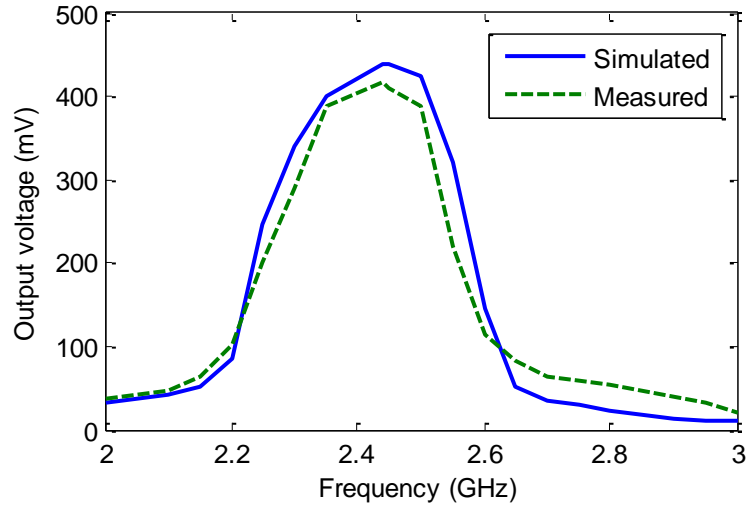


Fig. 4.15 The variation of simulated and measured output voltages with frequency

The simulated and measured maximum output voltages are 451 mV and 406 mV, respectively at 2.45 GHz. The graph shows that the simulated and measured output DC voltages follow cumulative effect of transmitter antenna gain and reflection coefficients. It is expected that this rectenna will be able to collect energy from any energy sources with narrower bandwidth which is covered by the rectenna bandwidth.

The received output voltages and efficiencies for the full wave rectenna system for 10 cm, 15 cm and 20 cm distances between transmitter and receiver are verified. Output DC voltages and efficiencies for 15 dBm transmitted power at 2.45 GHz are shown in Table. 4.2. The received output voltages from the receiver rectenna are obtained using EM and circuit co-simulations. The efficiency of the rectenna is calculated using equation (1).

$$\eta = \frac{\text{Power delivered to the load}}{\text{Power received by the antenna}} \quad (1)$$

When the transmitter and receiver are placed at 10 cm distance, the output simulated and measured voltages are 0.451 V and 0.406 V, respectively. For 15 cm distance, the output simulated and measured voltages are 0.277 V and 0.251 V, respectively. Similarly, for 20 cm distance, the output voltages are 0.206 V and 0.187 V, respectively. Thus, the simulated efficiencies for 10 cm, 15 cm and 20 cm distances are 24.7%, 21.8%, and 21.7%, respectively. Corresponding measured efficiencies are 20.00%, 17.92% and 17.89 %, respectively.

Table- 4.2: The simulated and measured results of the dual feed full wave rectenna at 2.45 GHz (Transmitted power = 15 dBm and load  $R_L = 50 \Omega$ ).

Distance (cm)	Simulated		Measured	Efficiency %	
	Received power (dBm)	Output voltage (V)	Output voltage (V)	Simulated (%)	Measured (%)
10	12.17	0.451	0.406	24.7	20.00
15	8.47	0.277	0.251	21.8	17.92
20	5.92	0.206	0.187	21.7	17.89

The output voltages and efficiencies of the proposed full wave rectenna is also compared theoretically with conventional half wave rectenna constructed using the same antenna as shown in Table 4.3. It is observed that simulated output voltages for the full wave rectenna are always higher than output voltages for half wave rectenna. Simulated full wave rectenna efficiencies for 10 cm, 15 cm and 20 cm distances between transmitter and receiver antennas are 24.7 %, 21.8% and 21.7 %, respectively. Similarly, half wave rectenna efficiencies are 17.3 %, 16.7 % and 15.8 %, respectively. Thus, the full wave dual feed rectenna efficiency is better than half wave dual feed rectenna.

Table-4.3: Comparison between full wave rectenna with half wave rectenna simulation results at 2.45 GHz (Transmitted power = 15 dBm and load  $R_L = 50 \Omega$ ).

Distance (cm)	Simulated			Efficiency %	
	Received power (dBm)	Full wave Output voltage (V)	Half wave Output voltage (V)	Full wave (%)	Half wave (%)
10	12.17	0.451	0.378	24.7	17.3
15	8.47	0.277	0.242	21.8	16.7
20	5.92	0.206	0.176	21.7	15.8



## 4.7. Broadband Rectenna with Full-Wave Rectification

A broadband full-wave rectifying-antenna (rectenna) is studied which utilizes both half cycles for RF wireless energy transfer. The proposed full-wave rectenna configuration is designed using a broadband dual edge-feed microstrip antenna and a bridge rectifier. This antenna is inherently broadband in nature and can provide differential voltages at its two edges with respect to its centre at  $TM_{01}$  mode. Various output properties for the proposed rectenna configuration are also studied. An optimized rectenna is finally fabricated for experimental verification and measured results agree with the theoretical results.

A rectenna system is proposed that utilizes differential voltages from a broadband dual-feed antenna and bridge rectifier to achieve broadband and efficient RF to DC conversion. The working principle of the proposed configuration is similar to the traditional AC to DC conversion using a transformer and bridge rectifier. The proposed system has been analyzed theoretically using commercially available IE3D and ADS software [23], [24]. An optimized rectenna system is fabricated for experimental verification and the measured results agree with the theoretical results.

## 4.8. Dual edge-fed broadband microstrip antenna

The proposed full-wave rectenna consists of a broadband dual edge fed microstrip antenna and bridge rectifier circuit. The broadband dual edge-fed microstrip antenna geometry and fabricated antenna is shown in Fig 4.16 (a) and (b), respectively. A dual edge-fed microstrip antenna is optimized at 2.45 GHz considering glass epoxy FR-4 substrate with dielectric constant  $\epsilon_r = 4.4$ , height  $h = 1.59$  mm and dielectric loss  $\tan\delta = 0.01$ . The dimensions of the optimized antenna geometry are: patch length  $L_p = 29.84$  mm, patch width  $W_p = 34$  mm, ground plane length  $L_g = 75$ mm and width  $W_g = 73$ mm. The width of  $50 \Omega$  microstrip feed line  $d$  is 3.036 mm, lengths  $a = 13.85$  mm,  $b = 31$  mm and  $c = 10.56$  mm, respectively.

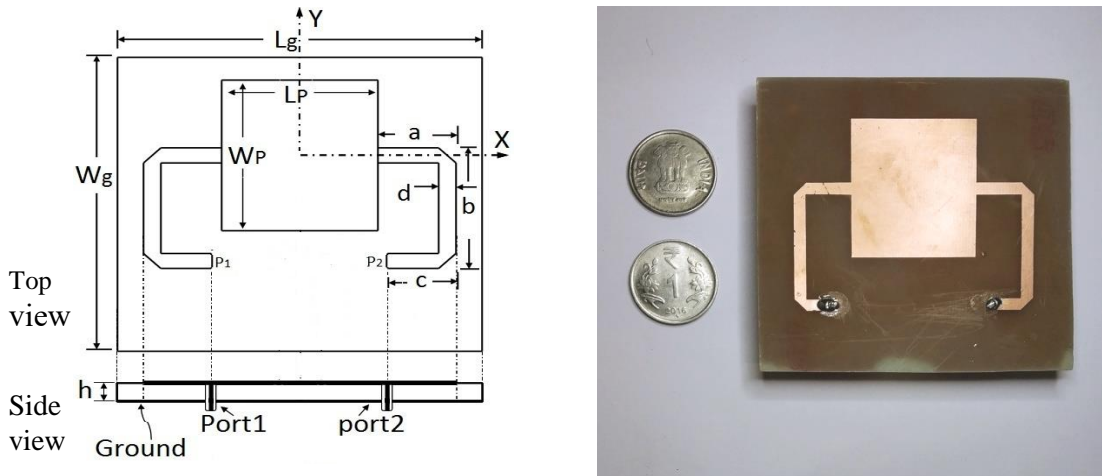


Fig.4.16. The dual edge-feed broadband microstrip antenna (a) geometry top view and side view (b) top view fabricated antenna

The antenna operates at the fundamental  $TM_{10}$  mode during power conversion and in this mode of operation the voltage is maximum at the patch edges and minimum (zero) at the centre of the radiating patch. Two microstrip feed lines are placed at two edges of the rectangular radiating patch where the peak voltages are maximum and out of phase with respect to each other.

A dual edge-fed rectangular microstrip antenna is optimized using IE3D software at 2.45 GHz and then an optimized configuration is fabricated for experimental verifications. The simulated and measured variations of S-parameters with frequencies for the dual edge-fed antenna are shown in Fig 4.17. Since, the configuration is symmetric,  $S_{11} = S_{22}$ , and return loss for only one port and is observed. The simulated value of  $S_{11}$  is close to  $-45$  dB at 2.45 GHz and the antenna exhibits impedance bandwidth of 500 MHz (20%) for  $S_{11} < -10$ dB. It can be observed that the bandwidth of this antenna is larger than the bandwidth of a similar microstrip antenna with same width and single feed. Simulated gain and efficiency of this antenna are 5.6 dBi and 46%, respectively.

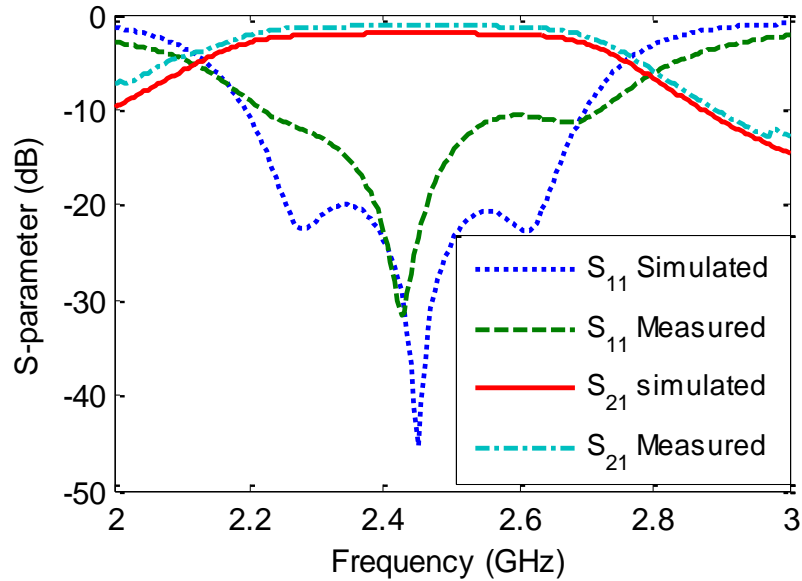


Fig. 4.17 Simulated and measured S-parameter of dual edge-feed microstrip antenna

A little shift in the centre frequency is observed for the measured centre frequency, but the measured operating band ( $S_{11} < -10$  dB) agrees with simulations. At 2.45 GHz the value of simulated and measured  $S_{21}$  are  $-1.63$  dB and  $-1.34$  dB respectively.

#### 4.9 Design of Rectenna Using Bridge Rectifier

The proposed full-wave bridge rectenna system consists of a dual edge fed microstrip antenna and four Schottky diodes are shown in Fig4.18. Two quarter wavelength impedance transformers are used for impedance matching. Edge-feed ports P1 and P2 are used for connecting diodes, capacitor and load resistor. During receiving mode this antenna acts like a transformer and voltages induced at its two opposite feed locations are of equal amplitudes with  $180^\circ$  degree phase difference with respect to its center position. For rectification four HSMS-2820 Schottky diodes are used. The generated rippled DC voltage is filtered using RC filter where the R is basically the load  $R_L = 50 \Omega$  and the value of the capacitor (C) is 1.3 pF. The impedance matching quarter wavelength transformers is optimized using EM software.

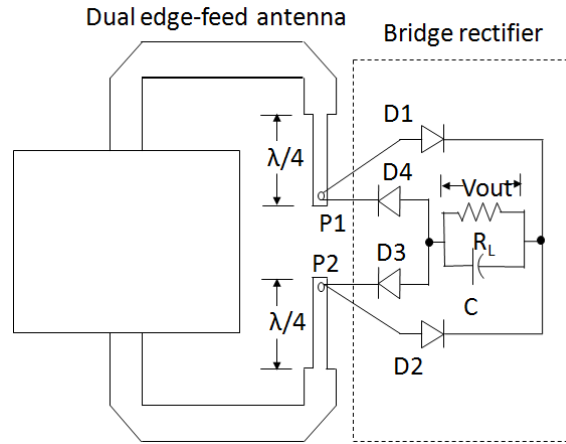


Fig. 4.18 Proposed bridge rectenna consists of dual edge-feed microstrip antenna and bridge rectifier circuit.

The rectenna shown in Fig 4.18 can be modeled like bridge full wave rectifier connected to a dependent RF source as shown in Fig 4.19. In the positive half cycle diode D1 and D3 conduction state as shown in Fig 4.19 (a). During the negative half cycle, D2 and D4 conduction state as shown in Fig 4.19 (b).

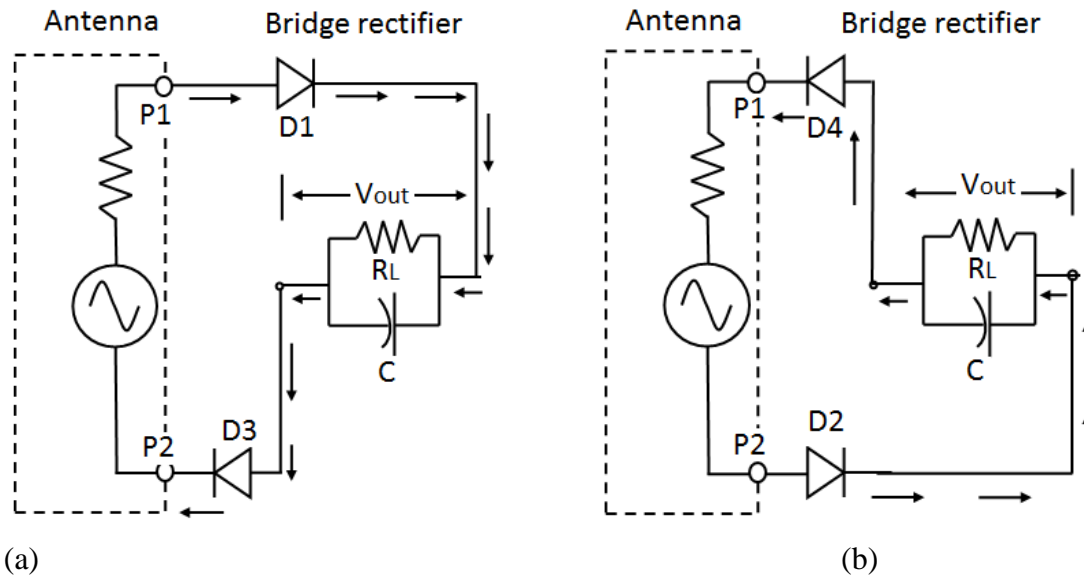


Fig 4.19 Equivalent schematic of the proposed full wave rectenna showing the direction of the dc signal path (a) positive and (b) negative half cycles

#### 4.10 Simulation and measurement of the proposed rectenna system

A complete EM and circuit co-simulation setup for RF wireless power transfer is shown in Fig 4.20. ADS simulator is used to complete the circuit co-simulation where IE3D simulated EM results are included. A suspended radiating patch antenna with 9.7 dBi gain (at 2.45 GHz) is considered as transmitter. The dual feed receiver antenna ( $R_x$ ) is placed at 10 cm, 15 cm and 20 cm apart from transmitter ( $T_x$ ) antenna for the present wireless RF energy transfer investigations. In the co-simulation setup, the three port model SNP1 represents the S-parameters of the transceiver system in touchstone format generated using IE3D simulator. Among the three ports of SNP1, port P1 represents the transmitter and other two ports P2 and P3 represents dual edge-ports of receiver antenna placed at 10 cm to 20 cm apart. The variable input power source is connected to transmitter antenna at P1 and the P2 and P3 of dual edge-fed receiver antenna are connected with bridge rectifier and RC filter. The received power is observed across P2 and P3 of the receiver antenna and the DC output voltage ( $V_{out}$ ) is observed at the load for varying input power for various distances between transmitter and receiver antennas.

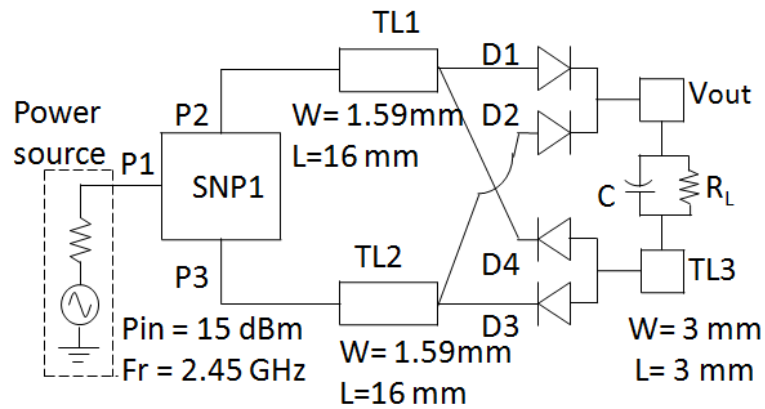


Fig 4.20 EM and circuit co-simulation setup for the proposed full wave rectenna

The variation of S-parameters with frequency for the entire transmitter-receiver system for 15 cm distance between them is shown in Fig 4.21. It can be seen that in presence of transmitter antenna the receiver antenna property is changed slightly. The value of  $S_{11}$  for transmitter antenna is  $-20$  dB and the values of  $S_{22}$  and  $S_{33}$  for receiver antenna are also close to  $-20$  dB at 2.45 GHz. The mutual coupling between transmitter and receiver antenna is more than  $-27$  dB at

the operating frequency. The receiver antenna bandwidth is still more than 500 MHz. The transmitter antenna shows a bandwidth of 140 MHz (2.381 GHz to 2.521 GHz).

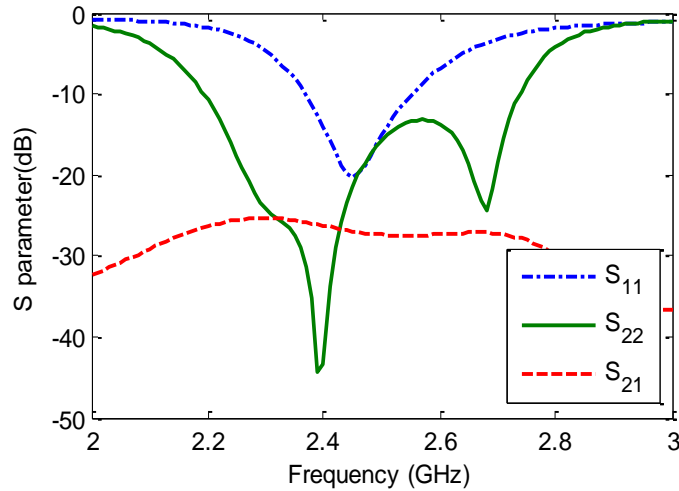


Fig 4.21 Simulated S-parameters for the transmitter and receiver antennas placed at 15 cm apart

The simulated gains of the transmitter and receiver antenna as a function of frequency are shown in Fig 4.22. From the Fig, the receiver dual feed antenna gain varies from 3.6 dBi to 4 dBi within frequency range from 2 to 3 GHz and the gain is 5.6 dBi at 2.45 GHz frequency. On the other hand, the transmitter antenna gain is 9.7 dBi at 2.45GHz.

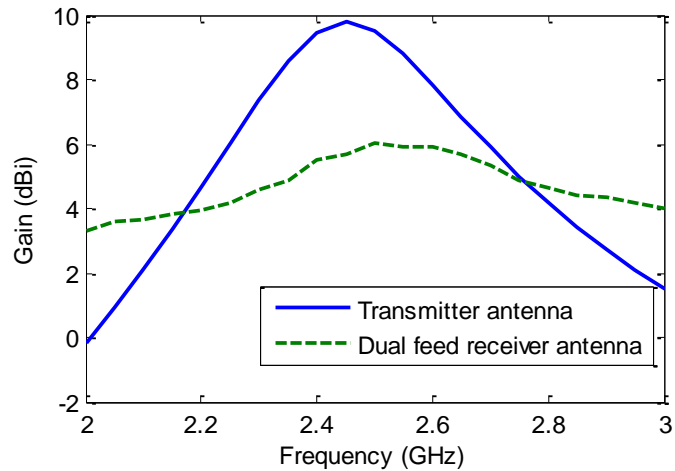


Fig 4.22 Simulated gain with variable frequency of the transmitter and receiver antenna

A complete RF energy transfer system comprising of a dual feed antenna and Schottky diodes based bridge rectifier is finally fabricated for experimental verifications. The fabricated dual edge-feed bridge rectenna is shown in Fig 4.23.

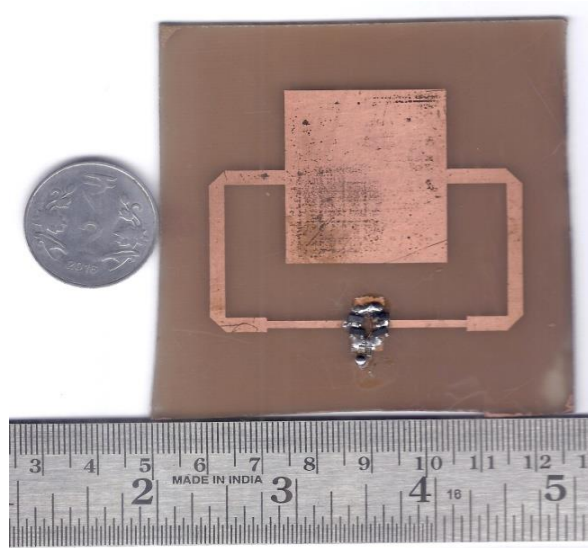


Fig 4.23 Fabricated dual edge-feed microstrip bridge rectenna

The measurement setup for RF wireless energy transfer is shown in Fig 4.24. During measurements, the transmitter antenna position is kept fixed and the position of the receiver dual edge-fed full-wave rectenna is varied to keep distances between these two antennas equal to 10 cm, 15 cm or 20 cm, respectively. A signal generator Rhode & Schwarz SMR20 was used as a RF source. Different parametric studies are carried out for varying distances, incident power, and frequencies.

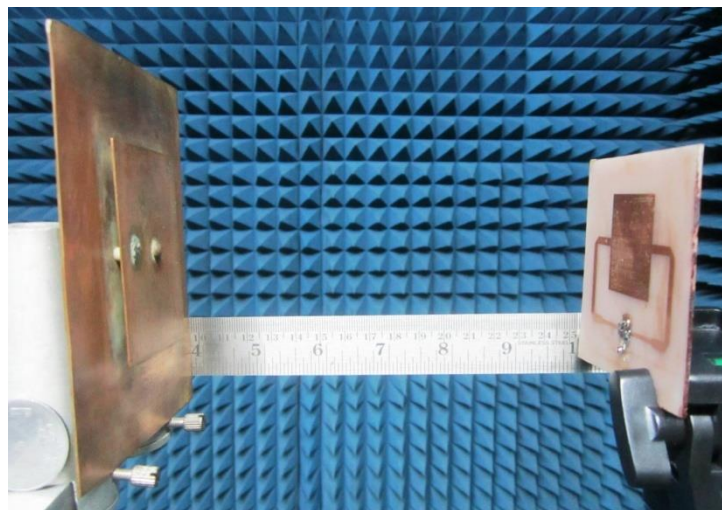


Fig 4.24 Experimental setup for RF wireless energy transfer.

When the transmitting and receiver antennas are placed at 10 cm, 15 cm, and 20 cm apart respectively from each other, the simulated and measured output DC voltages vary with variation of distance between antennas and input transmitted power. The variation of output voltages for changing input power from -10 dBm to +15 dBm at 2.45 GHz is shown in Fig 4.25. For 10 cm distance between transmitter and receiver, the simulated and measured output voltages vary from 30 mV to 515 mV and 28 mV to 482 mV, respectively. For 15 cm distance between transmitter and receiver, the simulated and measured output voltages vary from 18 mV to 326 mV and 15 mV to 305 mV, respectively. Similarly, for 20 cm distance, the measured and simulated output voltages vary from 13 mV to 0.240 mV, and 9 mV to 218 mV, respectively. The behaviours of measured and simulated output voltage curves are similar. But the measured voltage is always lower than the simulated result which is possibly due to some fabrication error and some extra losses from contacts.

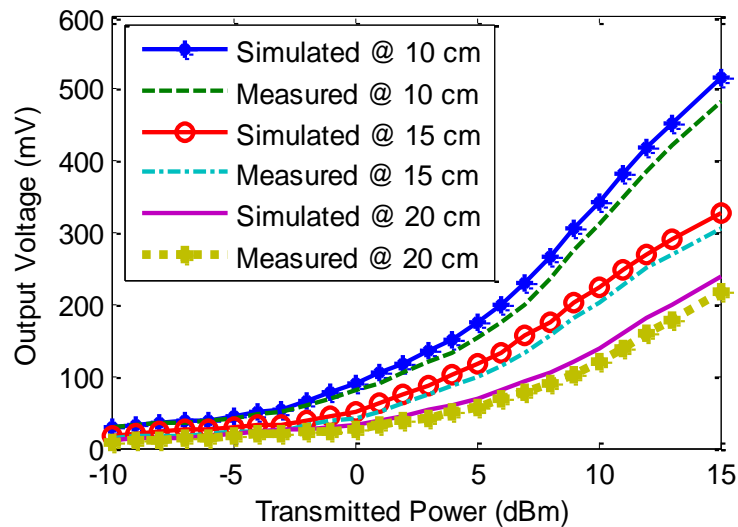


Fig 4.25 Simulated and measured output voltages with variable transmitted power

The simulated and measured output voltages are investigated for 2 GHz to 3 GHz frequency range, keeping 10 cm distance between the transmitter and receiver antennas and 15 dBm transmitted power. The variations of output voltages with varying frequencies are shown in Fig 4.26. In this Fig compared the single feed and dual feed transmitter antennas with dual feed receiver full-wave rectenna output voltages. The single feed transmitter with dual feed receiver



full-wave rectenna measured output voltages closely agree with the simulated results. The simulated and measured maximum output voltages are 515 mV and 482 mV, respectively at 2.45 GHz. Simulated and measured output DC voltages follow cumulative effect of transmitter antenna gain and reflection coefficients. Similarly, in Fig 10 shows the simulated output voltages of dual feed antenna used as transmitter and receiver full-wave rectenna, the voltage is very with frequency from 2 GHz to 3 GHz. The output voltage is 480 mV maximum at 2.45 GHz resonance frequency and nature of graph shows broadband as compared to proposed setup. It observed that both transceiver are broadband then output voltage curve is broadband or either transmitter are receiver is narrow band then the output voltages curve is narrow band.

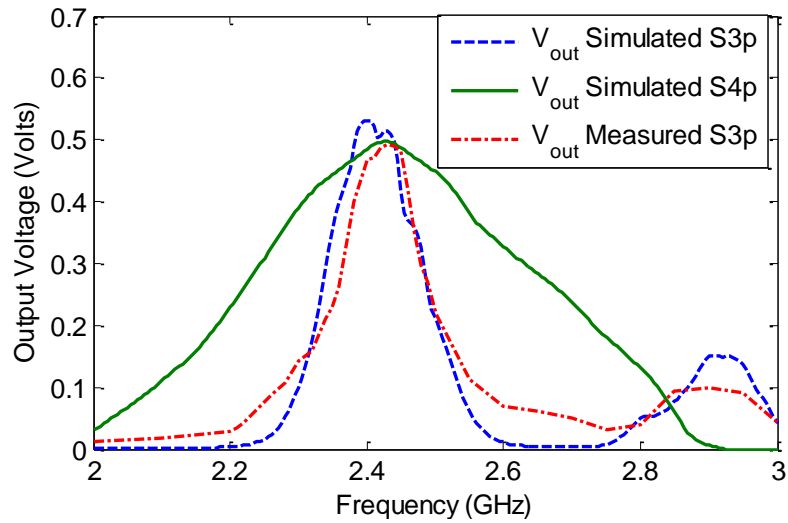


Fig 4.26 Variation of simulated and measured output voltages with variable frequencies compared with broadband dual fed transceiver

The received output voltages and efficiencies for the full-wave rectenna system at 10 cm, 15 cm and 20 cm distances between transmitter and receiver antennas are also verified. Output DC voltages and efficiencies for 15 dBm transmitted power at 2.45 GHz for different distances between transmitter and receiver antenna are shown in Table 4.4. The received output voltages from the receiver rectenna are obtained using EM and circuit co-simulations. The efficiency of the rectenna is calculated using equation (1).

$$\eta = \frac{\text{Power delivered to the load}}{\text{Power received by the antenna}} \quad (1)$$

When the transmitter and receiver antennas are placed at 10 cm distance, the simulated and measured output voltages are 515 mV and 482 mV, respectively. For 15 cm distance, the simulated and measured output voltages are 326 mV and 305 mV, respectively. Similarly, for 20 cm distance, the voltages are 240 mV and 218 mV, respectively. Thus, the simulated efficiencies for 10 cm, 15 cm and 20 cm distances are 32.2%, 30.3%, and 29.5%, respectively and corresponding measured efficiencies are 28.2%, 26.3% and 24.3%, respectively.

Table.4.4. Simulated and measured results of the microstrip full-wave bridge rectenna at 2.45 GHz. (load resistor = 50 Ω)

Distance in (cm)	Simulated		Measured	Efficiency ( $\eta$ )	
	Received Power (dBm)	Output voltage (mV)	Output voltage (mV)	Simulated (%)	Measured (%)
10	12.17	515	482	32.2	28.2
15	8.47	326	326	30.3	26.5
20	5.92	240	218	29.5	24.3

#### 4.11 Conclusion

A full-wave broadband rectenna is proposed for RF wireless energy transfer at 2.45 GHz. The proposed configuration consists of a dual feed broadband antenna with 500MHz bandwidth and a bridge rectifier. Parametric studies are carried out on the full-wave rectenna to investigate its different output properties for changing frequencies and different distances between transmitter and receiver antennas. A full-wave optimized rectenna system is fabricated for experimental verification and the measured results agree with the theoretical results. The simulated and measured efficiencies obtained for the optimized full-wave bridge rectenna for 20 cm distance between transmitter and receiver antenna are 29.5%, and 24.3%, respectively. A broadband dual feed full wave rectenna. This rectenna can be useful for broadband wireless energy transfer for ISM band. The proposed full wave rectenna configuration provides better efficiency than conventional half wave rectenna constructed using same antenna. An optimized rectenna system is fabricated for experimental verification and the measured results agree with the theoretical results. It is expected that this rectenna will be able to collect energy from any single or multiple

narrow band energy sources where individual source bands are covered by the rectenna bandwidth.

## References

- [1] Ito M, et al. (2014), “High efficient bridge rectifiers in 100MHz and 2.4GHz bands”, *IEEE Wireless Power Transfer Conference*, Jeju, pp. 64-67.
- [2] Saen T, et al. (2011), “Fundamentals of the bridge RF rectifier with an impedance transformer”, *IEEE MTT-S International Microwave Workshop Series on Innovative Kyoto*. pp. 255-258.
- [3] Brown W. C. (1984), “The history of power transmission by radio waves”, *IEEE Trans. Microwave Theory & Tech.* Vol. 32, pp. 1230-1242.
- [4] Mattsson M, Kolitsidas C I, and Jonsson B L G. (2018), “Dual-band dual-polarized full-wave rectenna based on differential field sampling”, *IEEE Antennas and Wireless Propagation Letters*. Vol.17, No. 6, pp. 956-959.
- [5] Imai S, Tamaru S, Fujimori K, Sanagi M, and Nogi S, (2011), “Efficiency and harmonics generation in microwave to DC conversion circuits of half-wave and full-wave rectifier types”, *IEEE MTT-S International Microwave Workshop Series Uji*, Kyoto. pp.15-18.
- [6] Pham BL. and Pham A.( 2013), “Triple bands antenna and high efficiency rectifier design for RF energy harvesting at 900, 1900 and 2400 MHz”, *IEEE MTT-S International Microwave Symposium Digest (MTT)*, Seattle, WA. pp.1-3.
- [7] Marian V, Allard B, Vollaire C, and Verdier J.( 2012), “Strategy for microwave energy harvesting from ambient field or a feeding source”, *IEEE Transactions on Power Electronics*. Vol. 27, No. 11, pp. 4481-4491.
- [8] Erkmén F, Almoneef T S, and Ramahi O M,( 2017), “Electromagnetic energy harvesting using full-wave rectification”, *IEEE Transactions on Microwave Theory and Techniques*, Vol. 65, No. 5, pp. 1843-1851.
- [9] Yamamoto T, Fujimori K, Sanagi M and Nogi S,( 2007), “The design of mw-class RF-DC conversion circuit using the full-wave rectification”, *European Microwave Conference, Munich.*, pp. 905-908.
- [10] Sun H, and Xu G.( 2015), “A differentially-driven rectifier for enhanced RF power harvesting”, *IEEE MTT-S International Microwave Workshop Series (IMWS-AMP)*, Suzhou. pp. 1-3.
- [11] Imai S, Tamaru S, Fujimori K, Sanagi M and Nogi S,( 2011), “Efficiency and harmonics generation in microwave to DC conversion circuits of half-wave and full-wave rectifier types”, *IEEE MTT-S International Microwave Workshop Series Uji*, Kyoto. pp. 15-18.
- [12] Zhang Y P, Wang J J “Theory and analysis of differentially-driven microstrip antennas”, *IEEE Transactions on Antennas and Propagation*, Vol. 54, No. 4, pp. 1092-1099. 2016.

- [13] Sun H “An enhanced rectenna using differentially fed rectifier for wireless power transmission”, *IEEE Antennas and Wireless Propagation Letters*. Vol. 15, pp. 32-35.
- [14] Ray S, Kumar G. “Broadband suspended dual-feed microstrip antenna with feed network”, *Proc. SPIE 5445, Microwave Opt Technol Lett*. pp. 458-461 (2004).
- [15] Reza Ashtari, Michael Baginski and Robert Dean “A 2.45-GHz frequency-selective rectenna for wireless energy harvesting”, *Microwave Opt Technol Lett*. Vol. 58, pp. 2508– 2512, ( 2016).
- [16] Qijuan He and Changjun Liu, “An enhanced microwave rectifying circuit using HSMS-282”, *Microwave Opt Technol Lett*. Vol. 51, pp. 1151–1153, ( 2009).
- [17] Su CH, Huang SI.( 2017), “Wireless power collection using radio frequency identification system”, *Microw Opt Technol Lett*. Vol. 59, pp. 2855–2861
- [18] Erkmén F, Almoneef TS and Ramahi OM.( 2017), “Electromagnetic Energy Harvesting Using Full-Wave Rectification”, *IEEE Transactions on Microwave Theory and Techniques*. Vol. 65, No. 5, pp. 1843-1851.
- [19] Itoh K.( 2015), “RF bridge rectifier and its good possibility for wireless power transmission systems”, *IEEE International Symposium on Radio-Frequency Integration Technology (RFIT)*, Sendai. pp. 226-228.
- [20] Shi Y, Jing J, Fan Y, Yang L, Pang J, Wang M.( 2018), “Efficient RF energy harvest with a novel broadband Vivaldi rectenna”, *Microw Opt Technol Lett*. Vol. 60, pp. 2420–2425.
- [21] Q. Xue, X. Y. Zhang, and C. K. Chin,( 2006), “A novel differential-fed patch antenna”, *IEEE Antennas Wireless Propag. Lett*. Vol. 5, pp. 471–474.
- [22] Arrawatia, Baghini MS and Kumar G.( 2015), “Differential microstrip antenna for RF energy harvesting”, *IEEE Transactions on Antennas and Propagation*. Vol. 63, No. 4, pp. 1581-1588.
- [23] IE3D 12.0, Zeland Software Inc., Fremont, CA, USA.
- [24] Agilent Advanced Design System, 2009, Agilent Technologies, USA.

## Chapter 5

# Study on Planar Broadband Small Signal Sensor for Microwave Imaging

### 5.1 Introduction

In microwave, a DC bias circuit can be employed to operate the detector diode above the cut-in voltage. In this chapter a planar biasing network is proposed for detection of low power. This network is suitable for microwave imaging.

### 5.2. RF Low Power Detection Using A DC Bias Circuit

RF low power detection using a DC bias circuit is a technique commonly used to detect and measure weak RF signals while providing a stable and bias voltage for the detection circuitry [1]-[4]. The DC bias circuit ensures proper operation of the detection circuit and enhances its sensitivity. Here's an overview of how it works:

**DC Bias Circuit:** The DC bias circuit is responsible for providing a stable DC voltage to the detection circuitry. It typically consists of passive components such as resistors, capacitors, and sometimes inductors. The circuit is designed to establish a bias voltage that ensures the detection circuit operates within its linear and sensitive range. **Bias Point:** The DC bias circuit sets a bias point for the detection circuit, which establishes the operating conditions for optimal detection sensitivity. The bias point is typically chosen to be in the linear region of the detection circuit's transfer characteristics.

**RF Signal Coupling:** The weak RF signal to be detected is coupled into the detection circuitry while maintaining the DC bias established by the bias circuit. This coupling is achieved using techniques such as capacitive coupling or inductive coupling, depending on the specific circuit design and application requirements. **Detection:** The RF signal, combined with the DC bias, is then processed in the detection circuitry. This circuitry may include filters, and detectors, depending on the specific detection requirements. The amplification stage boosts the weak RF

signal to a measurable level, while the detection stage extracts the desired information from the RF signal.

**Signal Conditioning:** The detected signal may undergo further conditioning, such as filtering or amplification, to improve its quality and prepare it for subsequent processing or measurement. This conditioning stage may include additional active or passive components depending on the specific application. **Output and Measurement:** The final output of the detection circuit is typically a voltage or current signal proportional to the detected RF signal strength. This output can be further rectified from AC to DC, processed, or measured using instruments such as oscilloscopes, spectrum analyzers, or data acquisition systems to quantify the detected RF power or extract specific information from the signal.

Designing an RF small signal detector circuit for the Industrial, Scientific, and Medical (ISM) band frequency [5]-[10]. A detector is a nonlinear device used to achieve frequency conversion from an input RF signal to a output DC voltage. This device is also known as the virtual battery and is commonly used for the extraction of DC power from free-space power transmissions, allowing other devices to receive power and exchange information. For this detector, a Schottky diode HSMS-2820 is selected due to its great advantage in comparison to the PN junctions in offering low-forward voltage drop and fast switching speed. Today, detector circuits are of great popularity in power scavenging and RF-ID tag applications by offering long lifetime, low cost, and small size [11]-[20]. In this work a detector circuit is realized from simulation and fabricated into a prototype model for because they offer a measurement. The results from this experimental demonstrate good detection or DC rectification by the diode, proving, how important it is to have an optimal matching network for the system so that maximum power is transfer and less is reflected.

### 5.3. A 2.45 GHz RF Small Signal Detector

The proposed RF small signal detector is presented in Fig. 5.1(a), illustrating its geometry. The detector is fabricated on an FR4 substrate and incorporates various components such as radial stubs, a blocking capacitor ( $C_{in}$ ), an input impedance matching strip line, a  $\lambda/4$  microstrip line serving as an equivalent inductance, a matching impedance between the DC blocking capacitor and Schottky diode, a rectifier, and a filter. These components are carefully designed and arranged to ensure efficient detection of RF signals. Fig. 5.1(b) shows the fabrication process

of the RF small signal detector. The detector is constructed using the HSMS-282x Schottky diode, known for its excellent performance in RF applications. The entire circuit is fabricated on the FR4 substrate, which provides a suitable platform for high-frequency circuits. The design and fabrication process of the detector are crucial in achieving its desired performance characteristics.

Overall, the design and fabrication of the RF small signal detector are critical in achieving efficient and reliable RF signal detection. The components and layout of the detector are optimized to ensure optimal performance at the desired operating frequency of 2.45 GHz.

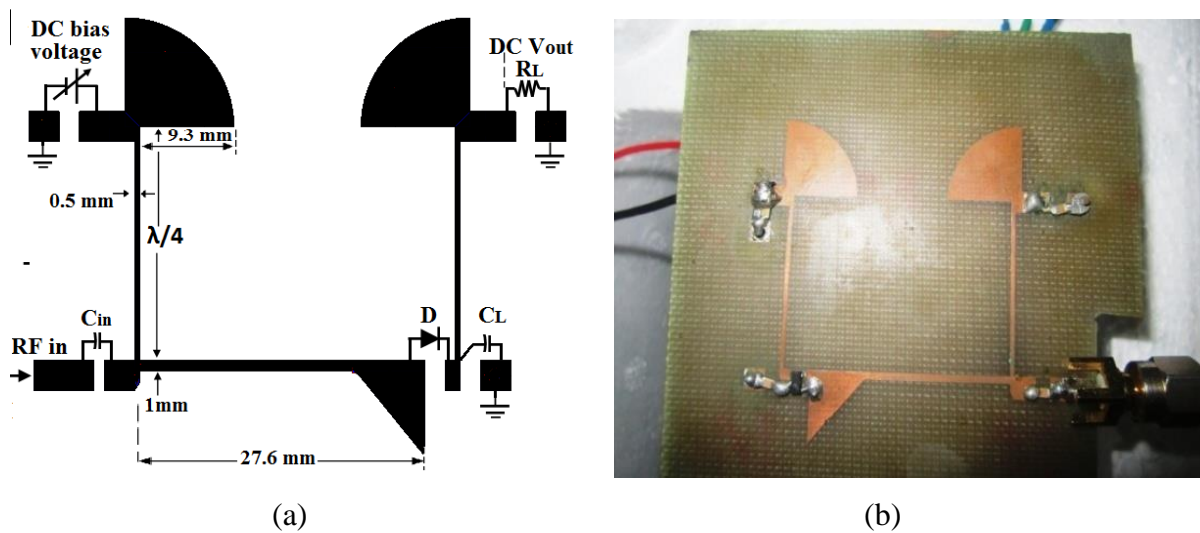


Fig.5.1 (a) Geometry of RF small signal detector, (b) fabricated planar small signal detector sensor for RF to DC.

The simulated and measured S-parameters of the small signal detector and rectifier are shown in Fig. 5.2 (a) and (b) respectively. The simulated S-parameter provides a different load resistance of -37.5 dB at a 2.45 GHz resonant frequency and a bandwidth of 2.25 to 2.65 GHz. The fabricated detector provides an S-parameter of -17 dB at 2.45 GHz resonant frequency, and the impedance band width is 2.38 GHz to 2.5 GHz.

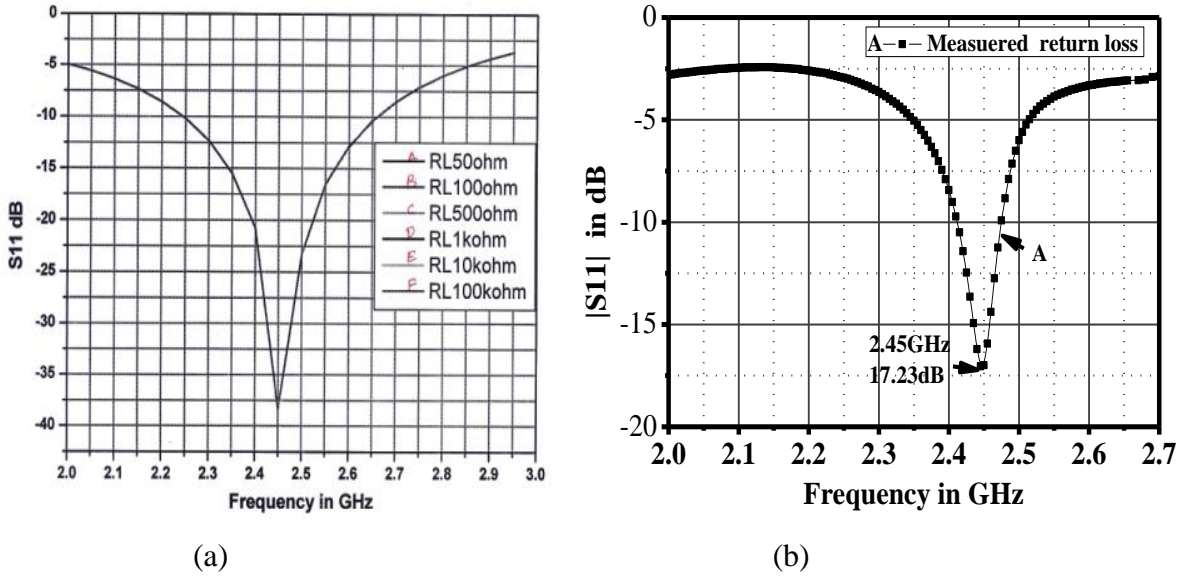


Fig. 5.2 S-parameter results for planar small signal detector sensor for RF to DC (a) simulated S-parameter with different load (b) Fabricated power detector measured S-parameter

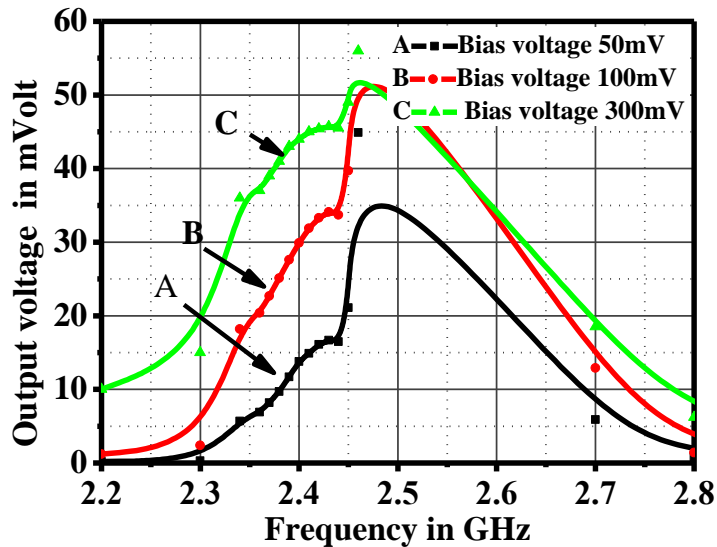


Fig. 5.3 Measured output DC voltage with different fixed DC bias voltages

The DC output voltages of a small RF signal detector were measured at different DC bias input voltages of 50 mV, 100 mV, and 300 mV. The measurements were conducted to evaluate the performance of the detector at the resonant frequency of 2.45 GHz. The measured DC output voltages were found to be 35 mV, 50 mV, and 55 mV, respectively, corresponding to the



different bias input voltages. These results are shown in Fig. 5.3(a) and (b), illustrating the relationship between the bias input voltage and the resulting DC output voltage at the resonant frequency.

### 5.3 Conclusion

The RF small signal detector and rectifier are proposed for microwave imaging sensors and wireless energy harvesting. It detects the very low RF signals from biasing inputs, and output data are collected for reconstructing the microwave images.

### References

- [1] J. L. Dawson, "A study of small-signal RF detection," *IEEE Transactions on Microwave Theory and Techniques*, vol. 45, no. 8, pp. 1234-1239, August 1997.
- [2] M. A. Ali, M. A. Abdel-Rahman, and Y. M. M. Antar, "A small-signal RF detection technique using planar antennas for microwave imaging applications," *IEEE Transactions on Antennas and Propagation*, vol. 61, no. 1, pp. 62-70, January 2013.
- [3] S. Rommel et al., "Ultra wideband signal detection with a Schottky diode based envelope detector," *Progress in Electromagnetic Research Symposium (PIERS), Shanghai, 2016*, pp. 5054-5054
- [4] P. Hallbjörner, "A broadband detector diode for use in planar circuits," *IEEE Transactions on Microwave Theory and Techniques*, vol. 28, no. 12, pp. 1362-1365, December 1980.
- [5] G. Gosnzalez-Valenzuela, A. Ceballos, and F. C. Martinez-Tarifa, "Design and characterization of a single-diode RF power detector for low-power applications," *IEEE Transactions on Microwave Theory and Techniques*, vol. 61, no. 11, pp. 4051-4058, November 2013.
- [6] S. D. Alley and K. A. Zaki, "A low-power RF-to-DC converter using a single diode for energy harvesting applications," *IEEE Transactions on Circuits and Systems II: Express Briefs*, vol. 57, no. 5, pp. 346-350, May 2010.
- [7] Y. J. Jang and W. S. Park, "Design of a low-power single-diode RF energy harvester with high power conversion efficiency," *IEEE Transactions on Microwave Theory and Techniques*, vol. 62, no. 10, pp. 2438-2446, October 2014.
- [8] M. Liu, Y. Zhao, and C. Liang, "Small-signal RF power detection using a diode connected MOS transistor in deep sub-micron CMOS process," in *Proceedings of the 13th International Conference on Solid-State and Integrated Circuit Technology, Hangzhou, China*, November 2016, pp. 954-956.
- [9] M. Nikolic, F. Giuppi, D. M. Filic, and D. Maksimovic, "A 2.45-GHz RF energy harvester with a -19 dBm sensitivity and a 41% efficiency for IoT applications," *IEEE Journal of Solid-State Circuits*, vol. 53, no. 3, pp. 900-912, March 2018.

- [10] S. Liu, X. Chen, K. K. Tsang, and Y. Huang, "A highly efficient RF-to-DC converter with self-adjusted CMOS rectifier for RF energy harvesting," *IEEE Journal of Solid-State Circuits*, vol. 47, no. 9, pp. 2223-2234, September 2012.
- [11] H. W. Wang, W. C. Lee, and Y. J. Yang, "A 2.45-GHz RF energy-harvesting circuit with a low-power bias generator," *IEEE Transactions on Circuits and Systems II: Express Briefs*, vol. 62, no. 12, pp. 1179-1183, December 2015.
- [12] Y. Li, L. Li, and R. Sarpeshkar, "A 2.45-GHz self-sustaining RF energy-harvesting system for universal low-power wireless sensor nodes," *IEEE Transactions on Circuits and Systems II: Express Briefs*, vol. 64, no. 5, pp. 494-498, May 2017.
- [13] X. Wu, H. W. Wang, and Y. J. Yang, "A 2.45-GHz rectifier with backscattering suppression for RF energy harvesting," *IEEE Transactions on Circuits and Systems II: Express Briefs*, vol. 62, no. 3, pp. 250-254, March 2015.
- [14] A. M. Shaar, D. Hamid, and H. Tenhunen, "Small-signal RF detection in wideband transceivers using MOS capacitors," in *Proceedings of the 26th Norchip Conference, Copenhagen, Denmark*, November 2008, pp. 173-176.
- [15] Y. Li, K. Huang, X. Liu, and K. J. Chen, "An RF power detector with low voltage and small-signal response for cognitive radio systems," *IEEE Transactions on Microwave Theory and Techniques*, vol. 60, no. 10, pp. 3301-3309, October 2012.
- [16] B. Mohebpour, H. Abdipour, and J. Laskar, "Wideband small-signal RF detection using diode-connected MOS transistors in a 0.18- $\mu\text{m}$  CMOS process," *IEEE Transactions on Microwave Theory and Techniques*, vol. 61, no. 3, pp. 1349-1358, March 2013.
- [17] W. K. Li, T. S. Ng, S. P. Yang, and W. C. Siu, "Broadband low-power RF power detector with wide dynamic range," *Electronics Letters*, vol. 43, no. 16, pp. 875-876, August 2007.
- [18] M. S. Khan and M. J. Deen, "A wideband linear envelope detector for RF power detection with an improved dynamic range," *IEEE Transactions on Circuits and Systems II: Express Briefs*, vol. 65, no. 6, pp. 707-711, June 2018.
- [19] T. C. Lei, "A broadband RF energy harvesting system with integrated RF-to-DC converter for wireless sensor networks," *IEEE Transactions on Circuits and Systems II: Express Briefs*, vol. 58, no. 12, pp. 904-908, December 2011.
- [20] A. Afifi and M. S. El-Ghazaly, "A high-efficiency RF energy harvesting system for wireless sensor networks," *IEEE Transactions on Circuits and Systems II: Express Briefs*, vol. 60, no. 9, pp. 594-598, September 2013.

# Chapter 6

## Study on Microwave Near Field Imaging Using Planar Rectenna Array

### 6.1. Introduction

Microwave techniques suitable for imaging metallic objects are studied theoretically using electromagnetic and circuit co-simulations and then verified experimentally at 2.45 GHz. Objects of various shapes are kept in the near field of both the transmitter and receiver antennas without any focusing elements. Objects are illuminated by a movable radiating antenna and scattered signals from the objects are captured by an array of rectennas to construct multiple almost unusable unfocused images. The final images are constructed by averaging multiple unfocused images. Experimental results are in agreement with the simulations.

Imaging techniques based on non-ionizing electromagnetic (EM) signals are now popular for various applications. Imaging techniques using a microwave, millimeter waves or terahertz waves [1-6] have been studied by several researchers for non-destructive testing (NDT) [7-9], radar imaging [10-12], and biomedical imaging [13-17]. In these techniques attenuated, diffused or scattered EM signals from actively or passively illuminated objects are captured, analyzed and processed using signal processing techniques to construct the images [18-23].

A two dimensional microwave imaging system is investigated theoretically using EM and circuit co-simulation techniques and then the system is experimentally verified at 2.45 GHz. The proposed method uses a movable radiating antenna and a non movable array of receiver rectennas and utilizes principle of both scanning and raster imaging techniques and two images of different resolutions are obtained simultaneously after each scanning. Metallic objects are placed in the near field of both transmitter and receiver antennas. Objects under analysis are continuously illuminated by a movable transmitter antenna and the forward scattered signals from the objects are captured by a non movable rectenna array. Finally, images have been constructed using voltages captured at receiver rectennas. Focusing elements like lens or

reflectors are not used in this study. In such near field situation normally direct one shot ray-tracing cannot provide faithful images. So, in this study, the final images have been constructed by averaging multiple almost unusable unfocused ray-traced images. EM and circuit co-simulations are performed by commercially available software CST Microwave Studio® and Advanced Design Software [24, 25]. Images are constructed and averaged using MATLAB [26].

## 6.2. Proposed Imaging System

The setup for proposed 2D microwave imaging system is shown in Fig. 6.1. The near field microwave imaging setup consists of a movable transmitter ( $T_x$ ) antenna, which moves along the XY plane. The receiver ( $R_x$ ) side consists of an array of antennas, which are located behind the imaging object and kept stationary.

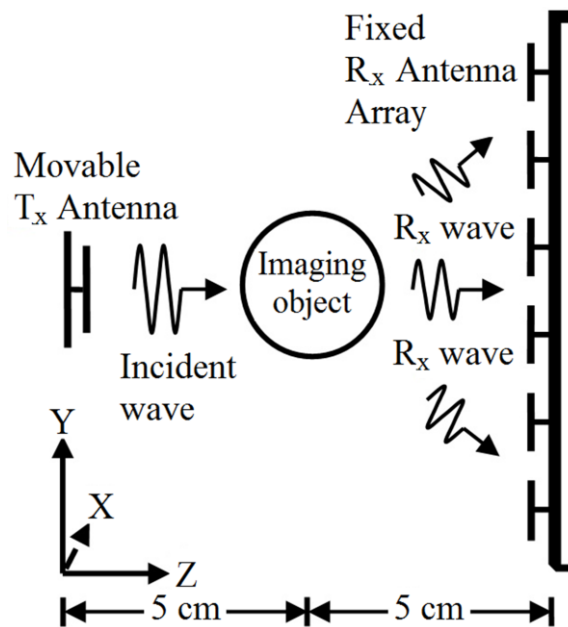


Fig. 6.1. Proposed setup for 2D microwave near field imaging.

Receiver antennas are then connected with rectifying Schottky diodes, impedance matching transformers and low-pass filters to form the detecting rectenna system. Transmitter antenna and receiver rectenna array are kept 10 cm apart from each other and the stationary imaging object is placed in between. The transmitter antenna transmits 2.45 GHz continuous sinusoidal signal. The transmitted signal is then attenuated, diffracted and scattered by the imaging object and finally received by rectenna array. The received voltages at rectenna are captured in a matrix form for the construction of the images.

### 6.2.1 Transmitter Antenna

A planar suspended patch antenna designed at 2.45 GHz is used as the transmitter antenna. To achieve large gain, an air dielectric is chosen. The geometry of the suspended patch antenna is shown in Fig. 6.2. (a). The spacing between the radiating patch and the ground plane is chosen as 5 mm. A shorting and supporting post is used at the centre of the radiating patch, where the voltage is ideally zero for a rectangular patch resonating at  $TM_{10}$  mode. The optimized dimensions of the suspended planar patch antenna operating at 2.45 GHz are as follows: patch length ( $L_p$ ) is 5.492 cm, patch width ( $W_p$ ) is 6.296 cm, ground length ( $L_g$ ) is 8.492 cm and ground width ( $W_g$ ) is 9.296 cm. A 50  $\Omega$  SMA connector is placed 1.505 cm away from the centre of the patch. Simulated S-parameter with frequency for  $T_x$  antenna is shown in Fig. 6.2 (b). The antenna resonates at 2.45 GHz and exhibits impedance bandwidth of 140 MHz. It can be noted that at 2.45 GHz frequency, the near field distance is approximately 11.7 cm, which is more than the distance between the transmitter and receiver antennas. The simulated gain of the antenna is 9.78 dBi at the operating frequency.

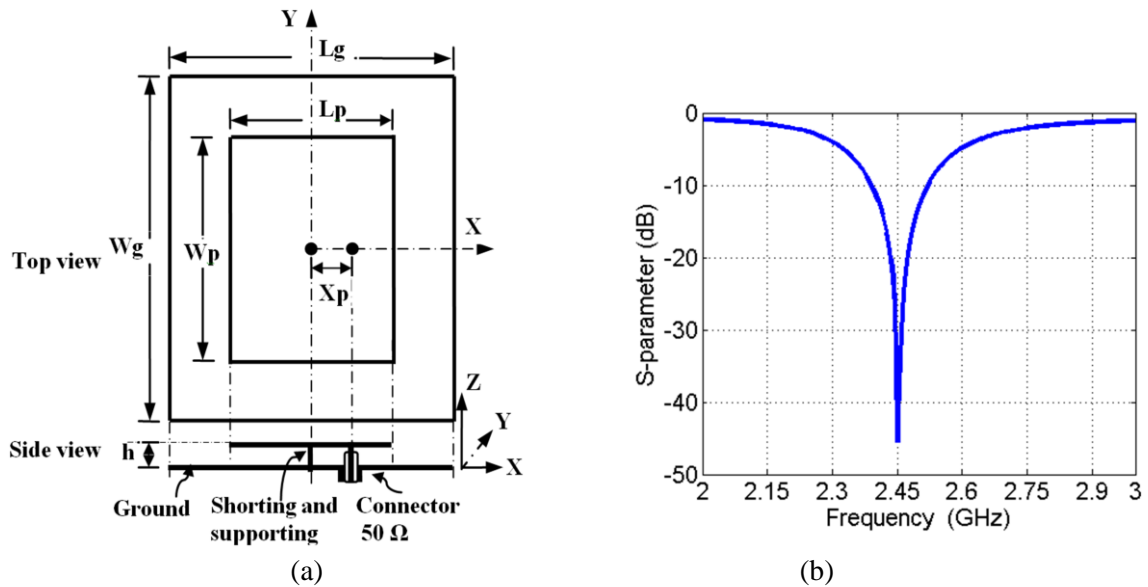


Fig. 6.2. (a) Geometry of transmitter antenna and (b) Simulated S-parameters v/s frequency curves.

### 6.2.2. Receiving Rectenna Array

The receiving rectenna array consists of an array of  $6 \times 6$  suspended antennas and suitable RF to DC converters. The top and side views of the receiver planar array of  $6 \times 6$  antennas are shown in Fig.6.3 (a). Here, a 45 cm  $\times$  52 cm glass epoxy FR4 substrate with single sided copper

clad is taken. The copper clad of the substrate is used as a common ground for all suspended antenna elements. The substrate used here helps to avoid unwanted shorting of feed probes during connection with RF to DC converters. Radiating patches are kept suspended in the air, above the glass epoxy substrate layer using shorting posts placed at the middle of the patches. Here air substrate thickness ( $h_1$ ) is 5 mm and thickness of dielectric ( $h_2$ ) is 1.59 mm. All antennas used for the rectenna arrays are optimized for 2.45 GHz. For optimized receiver antennas,  $L_a$  is 5.43 cm,  $W_a$  is 6.86 cm and coaxial probe feeds with a characteristic impedance of  $50 \Omega$  are placed 1.70 cm away from the centers of the radiating patches. Inter element spacing between antennas in X and Y directions are  $d_x = 0.62\lambda$  and  $d_y = 0.61\lambda$ , respectively.

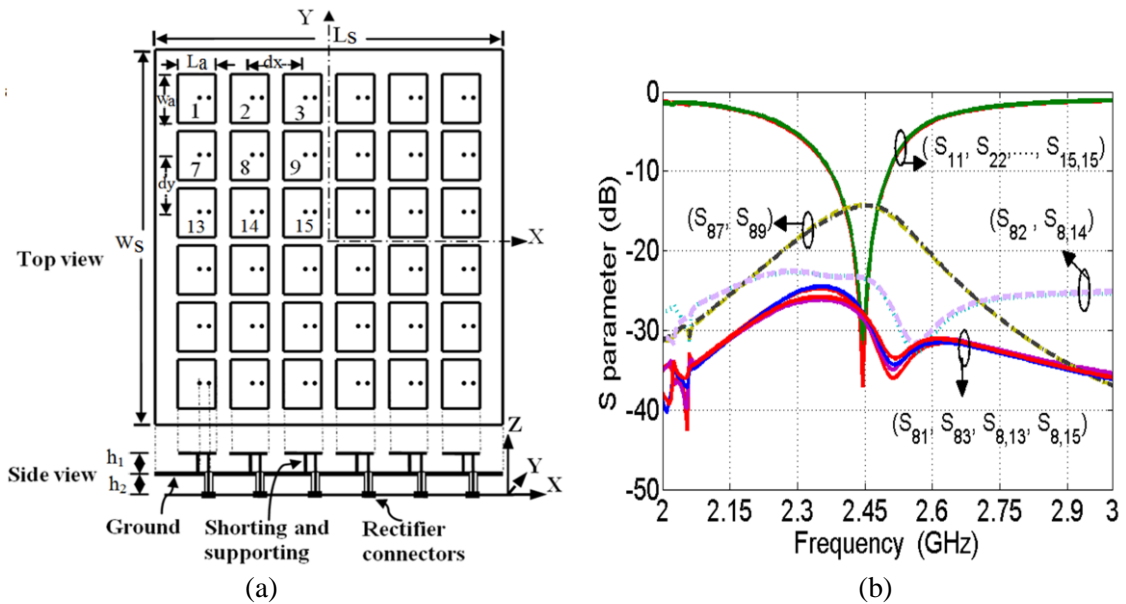


Fig.6.3. (a) Geometry of  $6 \times 6$  receiver antenna array and (b) Simulated S-parameters v/s frequency curves.

Further, feed locations of each antenna were slightly tuned to operate them at 2.45 GHz with the almost same bandwidth. The variations of S-parameters with frequency for array elements are shown in Fig. 6.3 (b). All antenna elements resonate at 2.45 GHz and exhibit impedance bandwidth of 134 MHz. The isolations between the antennas are below  $-14$  dB for all elements. The isolations between the individual components are lesser in the case of two consecutive horizontally placed elements compared to the isolation between two consecutive vertically placed elements.

### 6.2.3. RF to DC converter

Each RF to DC converter consists of an impedance matching circuit for delivering the maximum power, a Schottky diode to perform rectification and a low pass filter for smoothing the ripple of the output DC. Surface mount Schottky diode HSMS 2820 is chosen for this

operation because it has a fast reverse recovery time, low forward voltage drop and high cutoff frequency. The RF to DC circuit has been optimized using commercially available Advance Design System (ADS) software.

### 6.3. Simulation Model for Obtaining 2D Microwave Images

EM and circuit co-simulation setup for the proposed imaging system is shown in Fig. 6.4 (a) - (c). The EM simulation of a complete transceiver along with object as shown in Fig. 6.4 (a) is simulated using CST studio and the network shown in Fig. 6.4 (b) is simulated using ADS. The rectifier network is shown in Fig. 6.4 (c). A scanning area of 40 cm  $\times$  44 cm is considered for the detection of the metallic object. The scanning of the object is performed by moving the transmitter antenna on the scanning area which is divided into an array of grid points. In figure 15  $\times$  15 grid points ( $P_1, P_2 \dots P_{225}$ ) are shown. In EM and circuit co-simulation process S-parameters are generated for the transceiver system along with imaging objects using EM simulator and then power source, impedance matched rectifier circuit blocks are added in the circuit simulator. All the 36 receiver antennas are connected to 36 impedance matched rectifier.  $T_x$  antenna transmits CW input signal with power  $P_{in}$  at different grid positions and each receiver antennas receive signals and finally the output voltages ( $V_{o1}, V_{o2} \dots V_{o36}$ ) are captured at output ports. When  $T_x$  antenna is placed at  $P_1$ , the voltages generated at rectennas for varying input power (-15 dBm to 10 dBm) are shown in Fig. 6.4 (d). It can be seen that all curves are not fully linear and  $V_{o1}$  is higher than other output voltages because transmitting antenna is placed closer to receiver antenna 1. During scanning,  $T_x$  antenna starts its movement from  $P_1$  and approaches towards  $P_{15}$  along the X direction and after completion of the first row it moves to  $P_{16}$  of the second row and the process continues till it reaches  $P_{225}$ . For this study, the transmitter input power of 10 dBm is considered for generation of all images. So during scanning, the  $T_x$  antenna moves at 15  $\times$  15 grid points to complete the scanning of an entire area of the imaging object

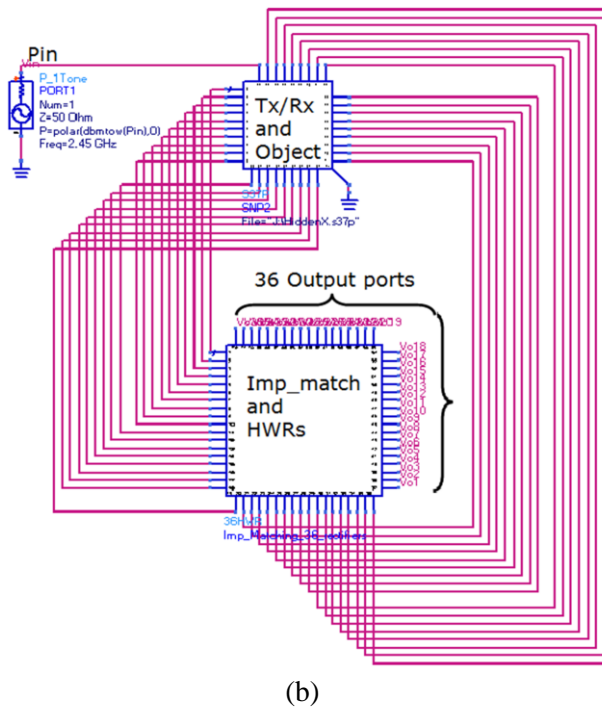
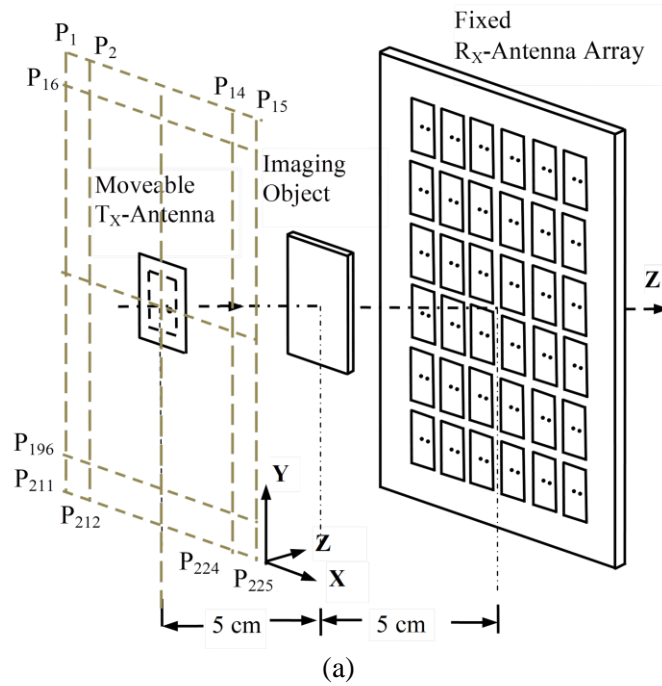
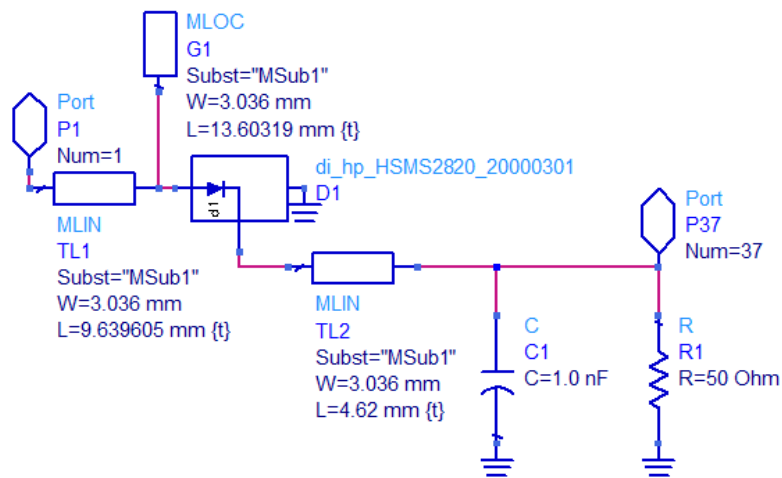


Fig.6.4. (a) EM simulation setup for microwave imaging using  $6 \times 6$  rectenna array, (b) The circuit co-simulation setup

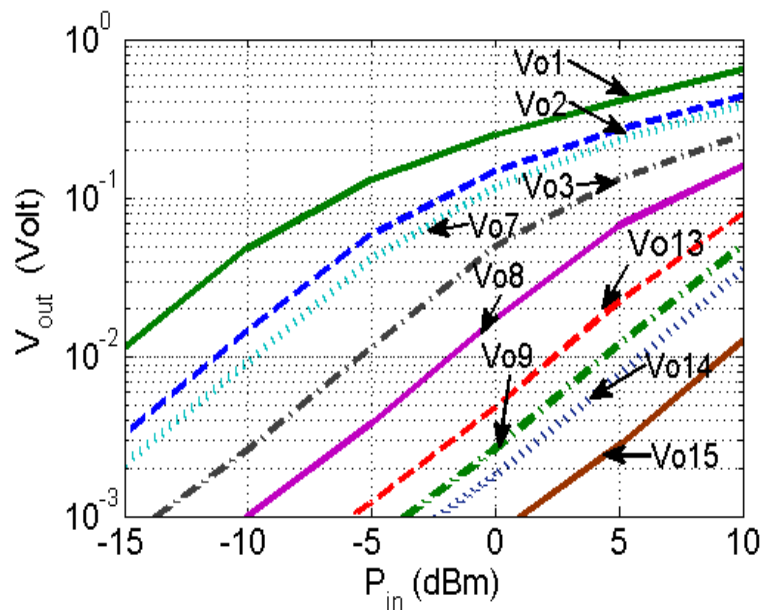
During the scanning process, for each grid points, the received signals are captured and stored power by the  $6 \times 6$  receiving elements. Thus, the captured data contains  $36 \times 225$  pixel information. Rearranging these data, a  $15 \times 15$  pixel image can be constructed for each of the receiver elements from 225 scanning points of  $T_x$  antenna. During a single scanning process, 36 images of  $15 \times 15$  pixels are constructed for all 36 receiver elements. Due to the changes in view



angles, these images hold different information and can finally be added to obtain a single image. A single RF to DC



(a)



(b)

Fig.6.5. (a) A single RF to DC block and (b) Output voltages at different rectenna v/s input power

The RF to DC circuit has been optimized using commercially available Advance Design System (ADS) software as shown in Fig. 6.5 (a). The received DC output voltages for different rectenna array are shown in Fig. 6.5 (b). All the RF to DC circuit for 6 by 6 rectenna arrays is simulated using ADS as shown in Fig. 6.6.



## 6.4. Construction of Images

For image construction, voltages are captured in array format from receiver rectenna array. The captured voltage data array is first normalized by dividing all individual array elements by the maximum received voltage, then raw images have been constructed from the normalized array using MATLAB command 'imagesc' which displays data in an array using predefined color map. Thus, the images constructed in this study are color mapped monochromatic in nature. Averaged images are constructed from multiple images by adding intensity for a particular pixel position and then dividing by the number of images. Finally, for smoothing of images, array data have been interpolated to achieve images with four times resolution using MATLAB function 'interp'. No complex filtering techniques have been used in this study; however, filtering techniques can be used to improve the images further.

## 6.5 Simulated 2D Microwave Images

### i) Simulation 2D Image for Rectangular Metallic Object

Initially, a  $20\text{ cm} \times 17\text{ cm}$  rectangular metallic sheet of 1 mm thickness is considered using continuous RF signals. In the first case,  $15 \times 15$  pixel images are constructed for  $T_x$  antenna placed at 225 different scanning points and a fixed receiver element. The image constructed for the first receiver element is shown in Fig. 6.7 (a). It is observed that in absence of obstruction, when an image is constructed for a single receiver element, then the received power at that element is maximum for the  $T_x$  antenna positioned at the closest grid point and the received power decreases significantly when the distance between the  $T_x$  antenna position and the receiver element increases. When there is an object placed between the  $T_x$  and  $R_x$  antennas, then the received power for nearest grid points may not be maximum. In fact, the received power from  $T_x$  antenna placed at different grid points will change due to the signal perturbation from the object. Sometimes, power received from the  $T_x$  antenna placed at the furthest grid positions provides insignificant image information. So, these ray-traced unfocused images do not provide complete information regarding the object shapes or positions and almost unusable in nature. All similar 36 images for 36 individual  $R_x$  elements are shown in Fig 6.7 (b).

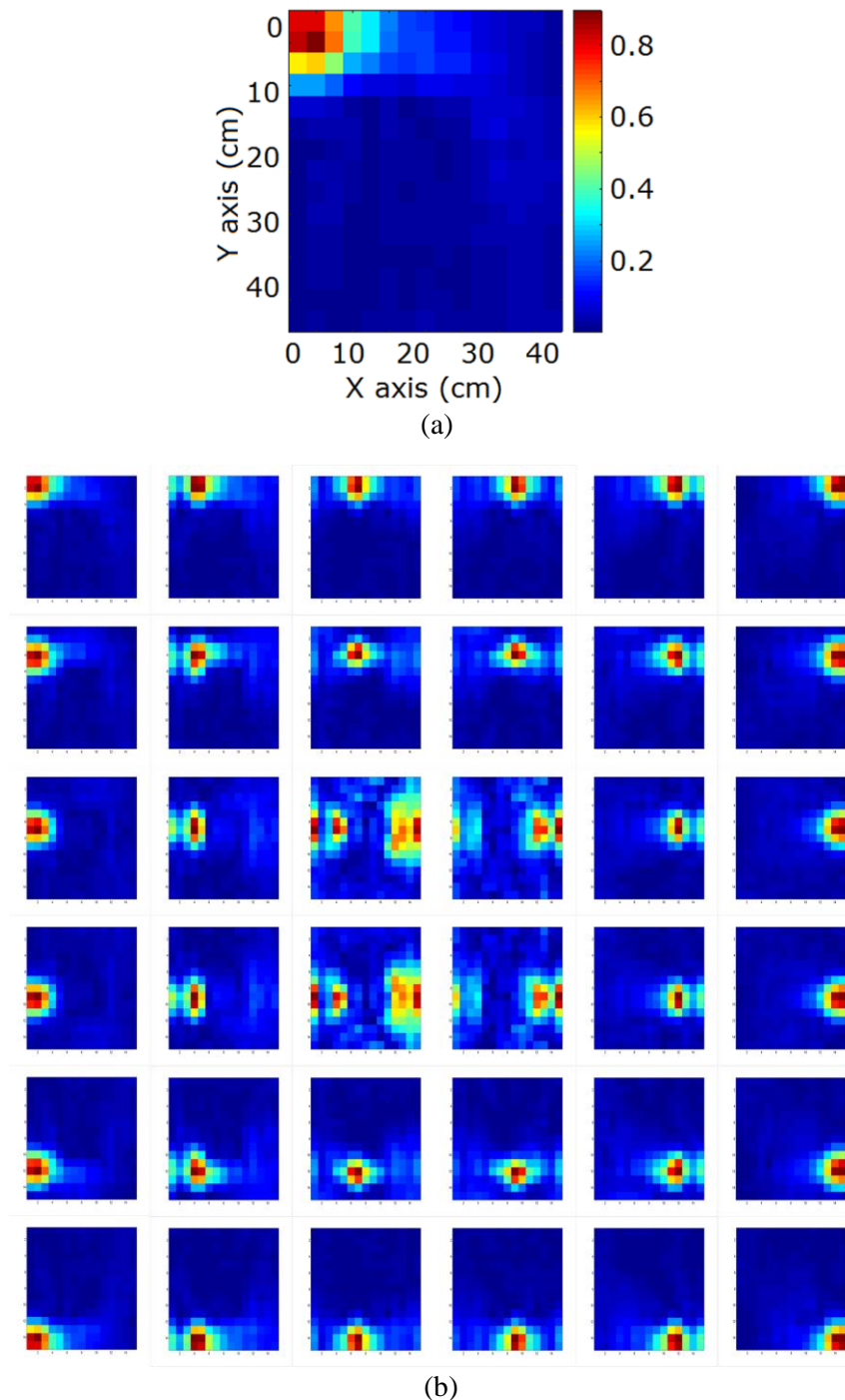


Fig. 6.7. (a)  $15 \times 15$  pixel image of rectangular object for the first receiver element, (b) All similar 36 images constructed by  $6 \times 6$  receiver elements.

When  $T_x$  antenna is placed at outer grid positions, only one bright spot is observed but when it moves at central grid positions, the signal is perturbed due to the presence of the object and spreading of maximum power can be observed. These 36 images are finally averaged to obtain a final  $15 \times 15$  pixel image which is shown in Fig. 6.8 (a). Now the shape of the object is visible from the image. This image is further improved by means of interpolation and an

interpolated image with a clearly visible rectangular object is shown in Fig. 6.8(b).

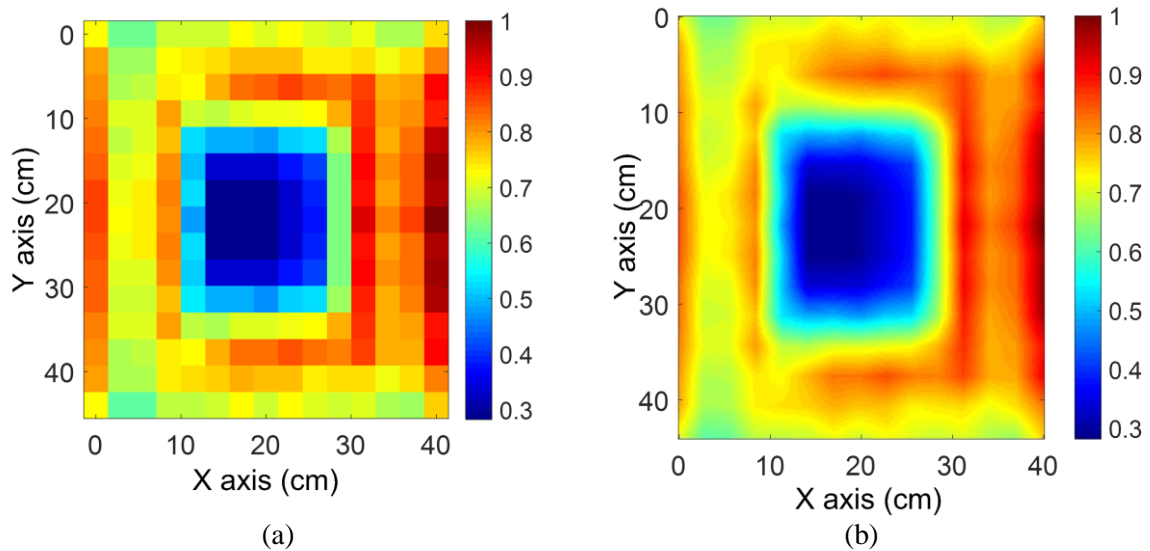
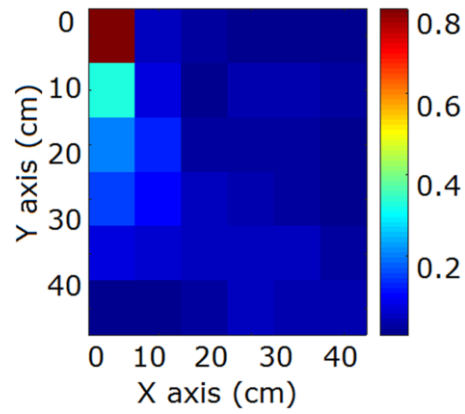


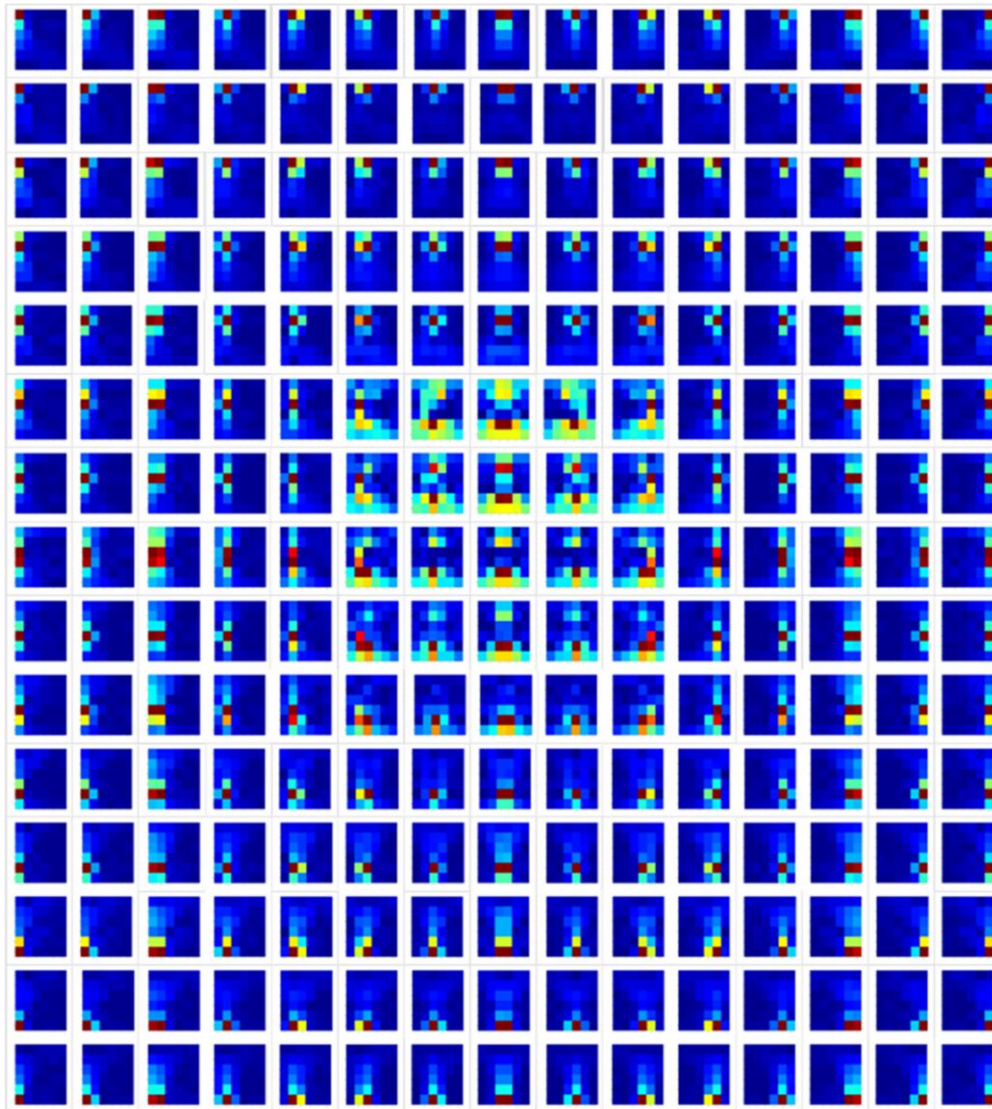
Fig. 6.8 (a)  $15 \times 15$  pixel image of the rectangular object obtained by averaging 36 images, and (b) An interpolated image for the same object.

In the second case,  $6 \times 6$  pixel images are constructed for 36 receiver elements when the  $T_x$  antenna is placed at a fixed scanning point. An image constructed for  $T_x$  antenna located at the first grid point is shown in Fig.6.9 (a). It is observed that in the absence of an object, received power at closest receiver element remains maximum just like earlier case.

The  $T_x$  antenna scan the imaging object using roster scanning process at 225 different scanning points and a fixed receiver element transmit. These unfocused images do not provide complete information regarding the object shapes or positions and almost unusable in nature. All similar 6 by 6 images for 225 individual Rx elements are shown in Fig. 6.9 (b).



(a)



(b)

Fig. 6.9.(a)  $6 \times 6$  pixel image constructed from 36 receiver elements for transmitter at grid position  $P_1$ , (b) Similar 225 images for transmitter placed at individual grid positions.



Like the earlier case, these images give some information about the shape of the image object but none of individually them provide clear information regarding the shape of the object. When  $T_x$  antenna moves at central grid positions, the signal is perturbed due to the presence of the object and spreading of maximum power is observed. These 225 images are finally averaged to obtain a  $6 \times 6$  pixel image as shown in Fig. 6.10 (a). In this image, the shape and position of the object is visible. This image is further improved by means of interpolation and an interpolated image is shown in Fig.6.10 (b).

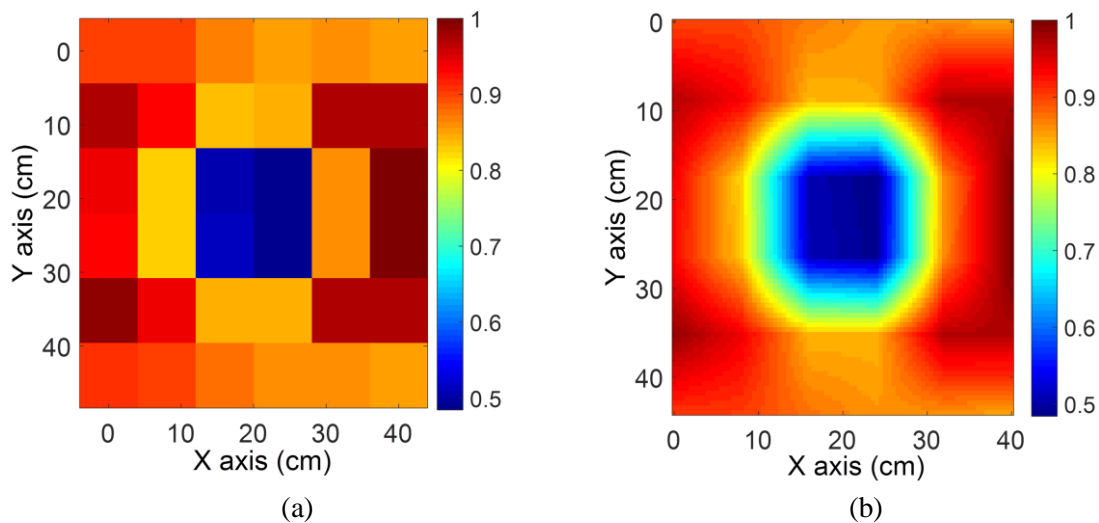


Fig. 6.10. (a) Averaged  $6 \times 6$  pixel image of the rectangular object obtained by averaging 225 images (b) image of same object after interpolation.

Among these two cases, in the first case, a  $15 \times 15$  pixel image is obtained, which has more resolution and clearly shows the position and size of a rectangular image object. For the second case, a  $6 \times 6$  pixel image is obtained which have a comparatively lesser resolution but has less sensitivity towards different noises than the previous because it averages the number of images. One more thing can be observed in this figure that an almost square shaped image is obtained for a rectangular object, which can be rectified if aspect ratios of pixels are considered.

## ii) Simulation of 2D image for circular metallic object.

Similar to rectangular simulation process in this case circular metal is placed a 20 cm diameter metallic sheet of 1 mm thickness. EM and circuit co-simulation setup for the proposed imaging system is shown in Fig. 6.4 (a) - (c). The EM simulation of a complete transceiver along with object as shown in Fig. 6.4 (a) is simulated using CST studio and the network shown in Fig. 6.4 (b) is simulated using ADS. The rectifier network is shown in Fig. 6.4 (c). A scanning area

of  $40 \text{ cm} \times 44 \text{ cm}$  is considered for the detection of the circular metallic object. The scanning of the object is performed by moving the transmitter antenna on the scanning area which is divided into an array of grid points. In Fig.  $15 \times 15$  grid points (P1, P2 ... P225).

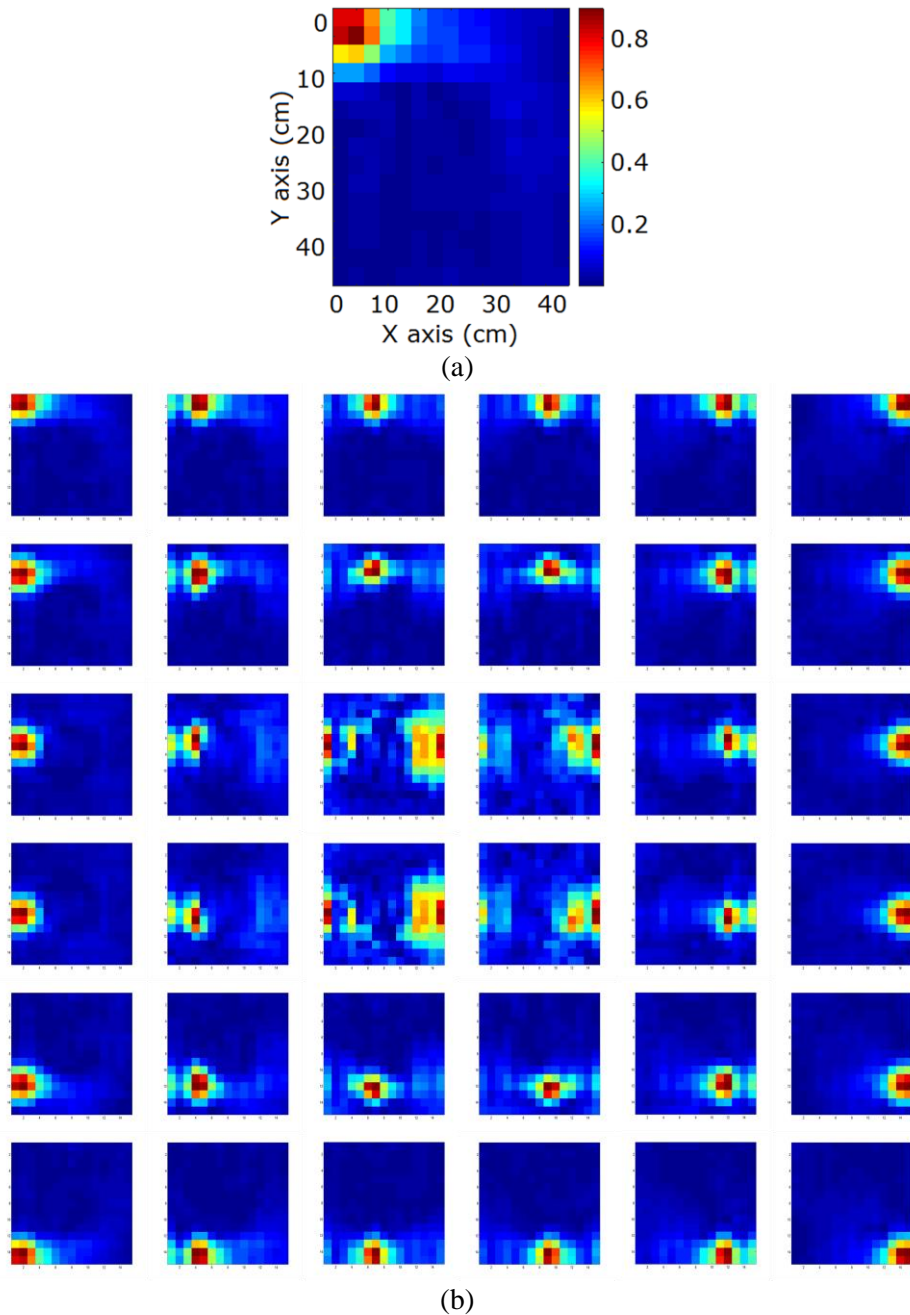


Fig. 6.11. (a)  $15 \times 15$  pixel image of circular object for the first receiver element, (b) All similar 36 images constructed by  $6 \times 6$  receiver elements.

In the first case,  $15 \times 15$  pixel images are constructed for Tx antenna placed at 225 different scanning points and a fixed receiver element. The image constructed for the first receiver element is shown in Fig. 6.11 (a). It is observed that in absence of obstruction, when an



image is constructed for a single receiver element. So, these ray-traced unfocused images do not provide complete information regarding the object shapes or positions and almost unusable in nature. All similar 36 images for 36 individual Rx elements are shown in Fig. 6.11 (b).

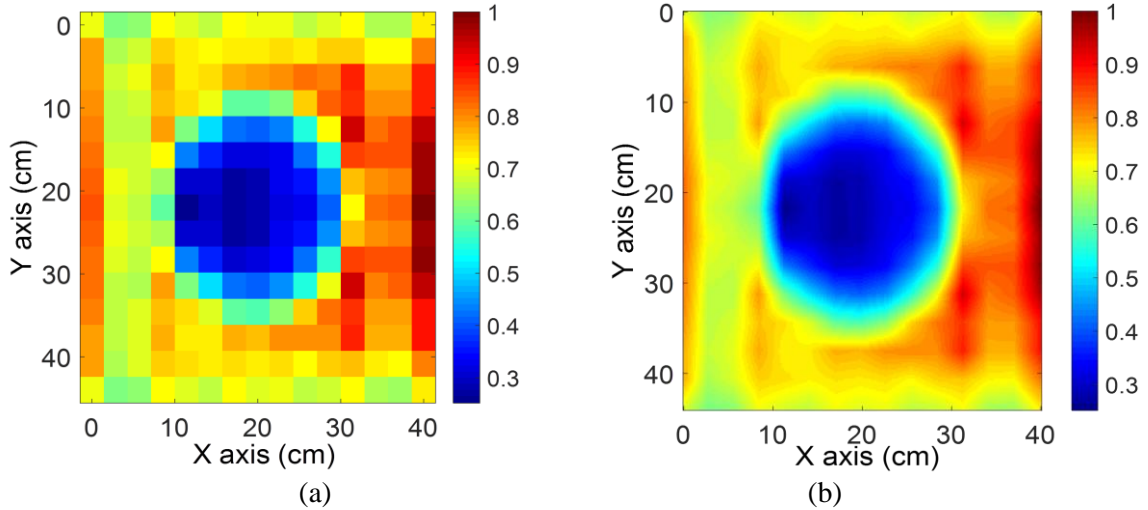


Fig.6.12. Images for circular object: (a)  $15 \times 15$  pixel image obtained by averaging 36 images, (b) interpolated image constructed from  $15 \times 15$  pixel image,

The averaged  $15 \times 15$  pixel image created from 36 images is shown in Fig. 6.12 (a) and now the 2D image shape of the circular object is visible from the image. This image is further improved by means of interpolation and an interpolated image with a clearly visible circular object is shown in Fig.6.12 (b).

In the second case:  $6 \times 6$  pixel images are constructed for 36 receiver elements when the Tx antenna is placed at a fixed scanning point. An image constructed for Tx antenna located at the first grid point is shown in Fig.6.13 (a). It is observed that in the absence of an object, received power at closest receiver element remains maximum just like earlier case.

The Tx antenna scan the imaging object using roster scanning process at 225 different scanning points and a fixed receiver elements, these unfocused images do not provide complete information regarding the object shapes or positions and almost unusable in nature. All similar  $6 \times 6$  images for 225 individual Rx elements are shown in Fig. 6.13 (b).

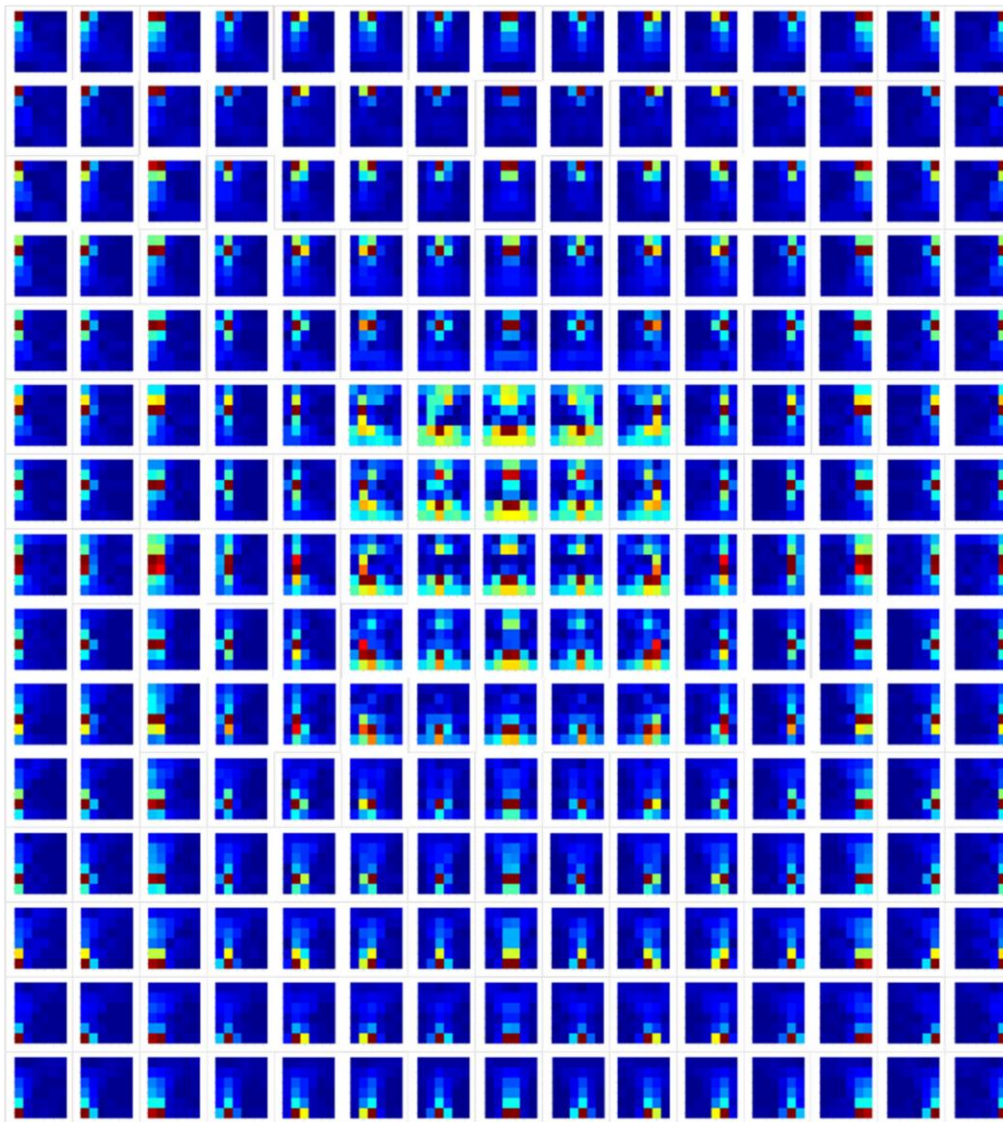
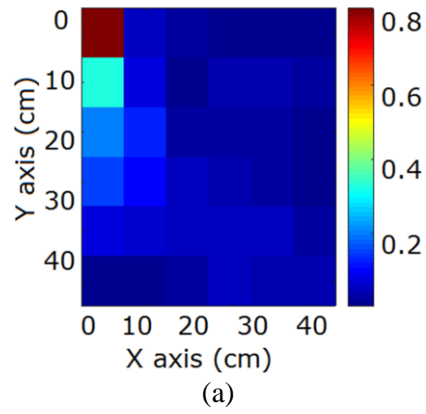


Fig. 6.13 (a)  $6 \times 6$  pixel image constructed from 36 receiver elements for transmitter at grid position P1, (b) Similar 225 images for transmitter placed at individual grid positions.

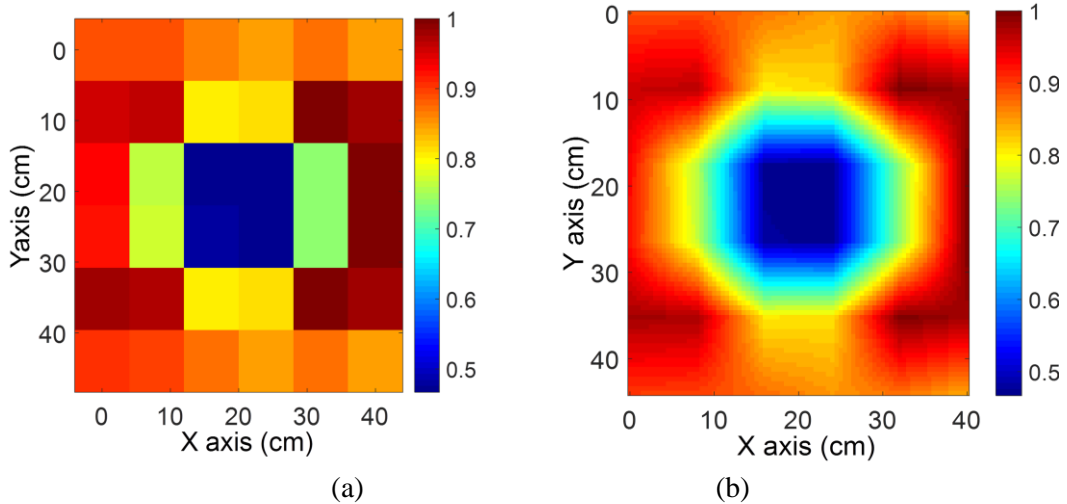


Fig.6.14. Images for circular object: (c) Averaged  $6 \times 6$  pixel image obtained by averaging 225 images and (d) interpolated image constructed from the  $6 \times 6$  pixel image.

Similarly, the average  $6 \times 6$  pixel image of the circular object constructed from 225 scanning points is shown in Fig.6.14 (a) and an interpolated version of the same is shown in Fig.16.14 (b). Since the resolution of this image is very low, it is difficult to distinguish between object shapes from the constructed  $6 \times 6$  pixel image.

Among these two cases, in the first case, a  $15 \times 15$  pixel 2D circular image is obtained from Fig. 6.12 (b) which has more resolution and clearly shows the position and size of a 2D circular image object. For the second case, a  $6 \times 6$  pixel image is obtained from Fig. 6.14 (b) which have a comparatively lesser resolution but has less sensitivity towards different noises than the previous because it averages the number of images. One more thing can be observed in this figure that an almost square shaped image is obtained for a circular object, which can be rectified if aspect ratios of pixels are considered.

## 6.6. Experimental 2D microwave images

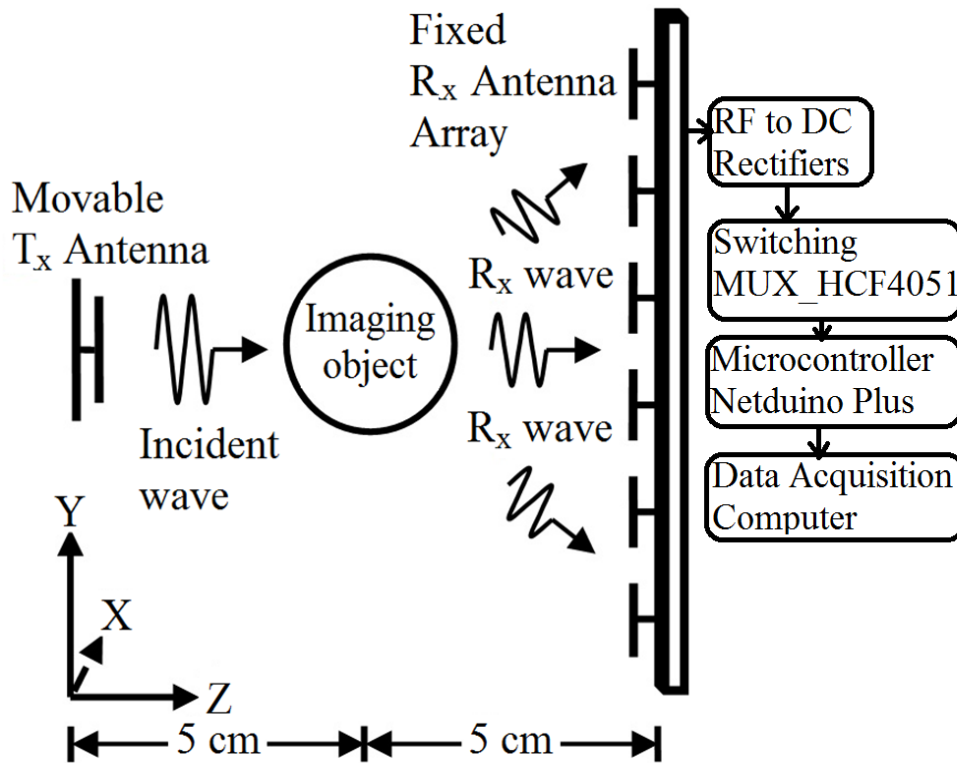


Fig 6.15. Proposed Experimental setup for the complete imaging system

The imaging techniques described earlier are finally verified experimentally. Here, other than the number of scanning position, all other parameters are kept unchanged. The numbers of scanning points are reduced to  $8 \times 8$  for simplicity. So, here, the  $T_x$  antenna moves at  $8 \times 8$  grid points to complete the scanning of an entire area of the imaging object and the new distances between two consecutive grid points along the X-axis are 5 cm and Y-axis are 5.5 cm. Just like simulations, during the scanning process, for each grid points, the received signal powers at  $6 \times 6$  receiving rectenna elements are captured and stored. Thus, the captured data contains  $36 \times 64 = 2304$  numbers of pixel information. Rearranging these data,  $8 \times 8$  pixel images are constructed for each of the receiver elements from 64 scanning points of  $T_x$  antenna. So, during the scanning process, 36 images of  $8 \times 8$  pixel are constructed for all 36 receiver elements. Due to the change in view angles, these images provide different information and can finally be averaged to obtain a single  $8 \times 8$  pixel image. Similarly, rearranging the same data,  $6 \times 6$  pixel images are constructed for each of the 64  $T_x$  antenna positions and  $6 \times 6$  receiver elements. So, 64 images of  $6 \times 6$  pixels are constructed for all 64 grid points. As discussed previous case, due to the change

in view angles, all these images hold different information and finally these are averaged to obtain a single  $6 \times 6$  pixel average image.

A fabricated transmitter antenna is shown in Fig. 6.16 (a) and the fabricated  $6 \times 6$  receiver antenna array is shown in Fig. 6.16 (b). Receiver antenna elements are connected to RF to DC circuits which are separately fabricated on PCBs and connected at the bottom of the ground plane. A fabricated rectifier circuit developed using microstrip lines is shown in Fig. 6.16 (c).

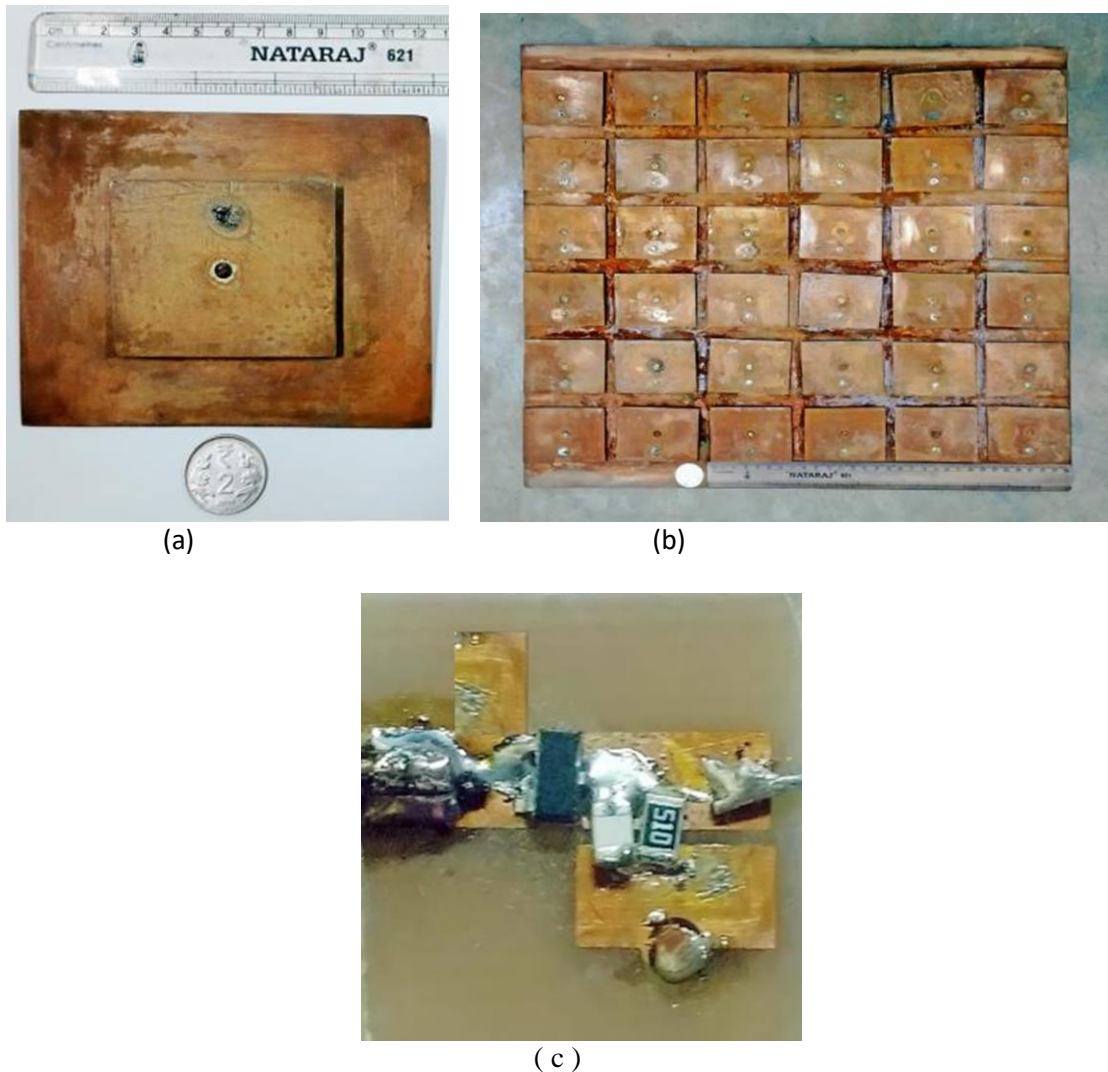


Fig. 6.16.(a) Fabricated transmitter antenna,(b) Fabricated  $6 \times 6$  receiver antenna array and (c) RF to DC rectifier

Experimental setup for the complete imaging system is shown in Fig. 6.17. For mechanical support Styrofoam blocks with dielectric constant of 1.03 are used. A  $20 \text{ cm} \times 17 \text{ cm}$  rectangular object, a circular object with  $20 \text{ cm}$  diameter and another 'X' shaped object with  $20 \text{ cm}$  arms and  $5 \text{ cm}$  arm thickness made of Aluminum metal sheets are shown in the inset of Fig. 6.17.





Fig. 6.17. The complete experimental setup for 2D microwave imaging system

Output voltages from rectennas are collected using Netduino and analog multiplexers. The complete experimental setup is shown in Fig. 6.17. The transmitter antenna is moved manually at different scanning positions.

### 6.6.1 The switching and interfacing system

In this thesis, we have designed a sub-system of microwave imaging technology which implements the data acquisition functionality for reconstruction of the image. This subsystem is controlled by a microcontroller, an analog switching circuit and the computer. As the microcontroller, we have used Netduino plus, a recently developed ATMEL-based microcontroller board with in-built A/D converter. On the other hand, we have used CMOS logic based 4051 Analog Multiplexer IC for switching purpose. In our scheme, data has to read out from an  $m \times n$  array of antenna. The higher the values of  $m$  and  $n$  are, the higher resolution is achieved. Since the micro-controller, NETDUINO is voltage-driven, it is necessary to represent the pixel value of the pixel elements of the object image by a voltage level, which is usually very small, of the order of millivolts. Small voltage is a challenge as far as accurate measurement system of the voltage level is concerned. Moreover, since there are many different voltage levels

to be measured, it is difficult to read then simultaneously and reconstruct the image. Due to limited number of input ports, the scanning of the image elements have to be done in a hybrid manner-both serial and parallel scanning is employed. To illustrate this, let us take an example of a 6x6 array, as shown in the fig, which we have implemented in our experiment. Here there are 36 elements altogether in the array, arranged in 6 rows and 6 columns. Now, using the proposed technique, 6 elements are scanned at a time. This is the parallel aspect of the scanning system. Then again, after a certain time-span, 6 other elements are scanned. In this way, it takes 6 clock pulses to cover all 36 elements once. The later constitutes the serial aspect of the scanning scheme. To keep the imaging system running, this process has to be carried out repeatedly, a complete dataset being generated in every 6 six clock pulses.

We can categorize the scanning techniques in two ways row-major and column-major.

In the first technique, n elements of each row are read out simultaneously. So, at each step being executed, a horizontal strip of the image is reconstructed. A row of the m x n matrix corresponds to a horizontal strip of the image. Since there are 'm' number of rows, it takes m clock pulses to obtain the complete image. This can be termed as row-major technique.

On the other hand, the other method requires m elements of each column to be read out simultaneously. So, at each step being executed, a vertical strip of the image is reconstructed. A column of the m x n matrix corresponds to a vertical strip of the image. Since there are 'n' number of columns, it takes n clock pulses to obtain the complete image.

Here we have taken the time gap between two sets of voltage read out to be 3 seconds. However, this adjustable and we can reduce the time gap until and unless it is greater than the time required for analog to digital conversion of the input voltages. Considering the time gap between two clock pulses to be 3 seconds, 18 seconds time is required to complete a full scan of the image. The synchronization is controlled by the Netduino microcontroller. The digital I/O ports of the microcontroller have been configured as output lines and pulses have been transmitted using them in such a manner that those lines collectively represent a MOD 6 counter. The sequences generated by the counter are 000->001->010->011->100->101->000 and so on. Each of these sequences can be designated as a state and each state corresponds to the parallel readout of voltages from 6 pins. Since there are 6 states, it justifies the requirement of 6 time spans for the completion of a full scan. The encoded sequences as mentioned are used to perform the switching operation of the analog multiplexer (MUX) circuit. As we have used 8:1 multiplexer IC units, we require 3 select lines to control them, i.e. to select which data input line is to be connected to the output. For example, if the sequence is 000, input line 0 of all the multiplexers will be selected. After a 3 second gap, the sequence will become 001 and then input

line 1 of the multiplexers will be chosen. In this way, by using 6 different sequences (states), 6 input lines of each multiplexer are used. The complete functional block diagram of our set up is shown below Fig. 6.18.

### Microwave Imaging Block Diagram

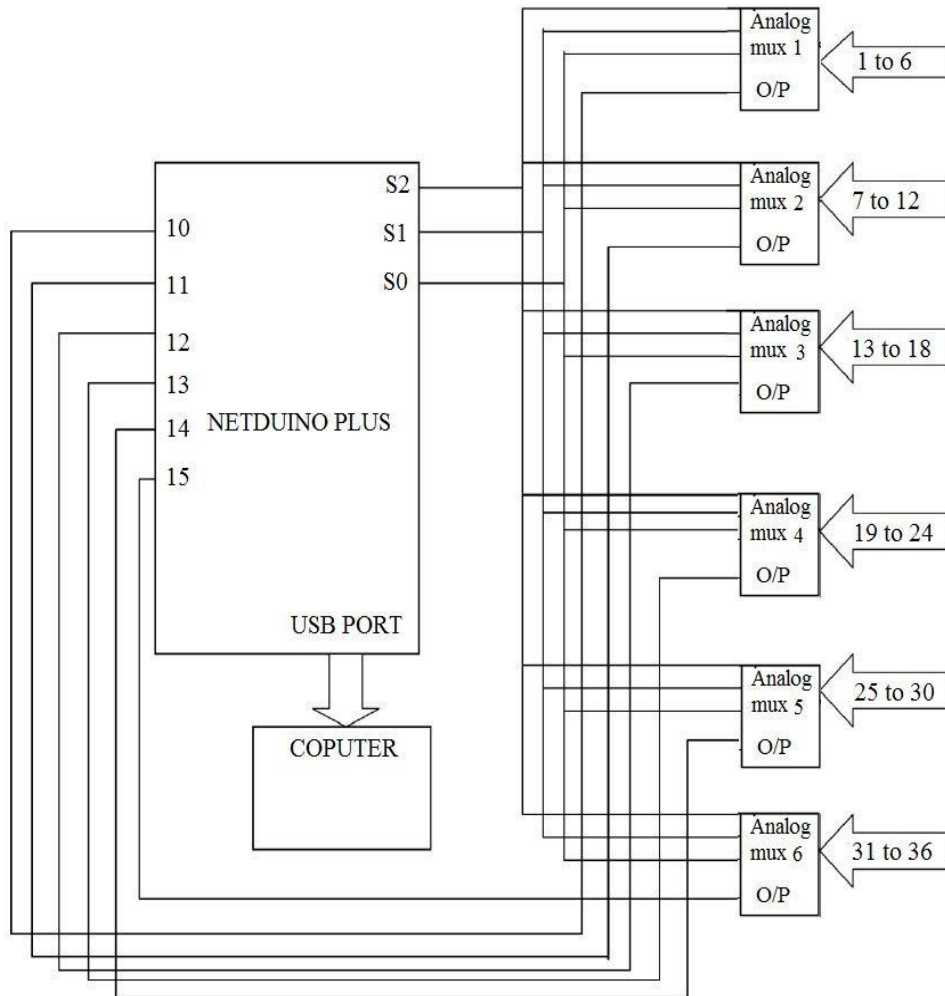


Fig. 6.18. Microwave imaging Block diagram



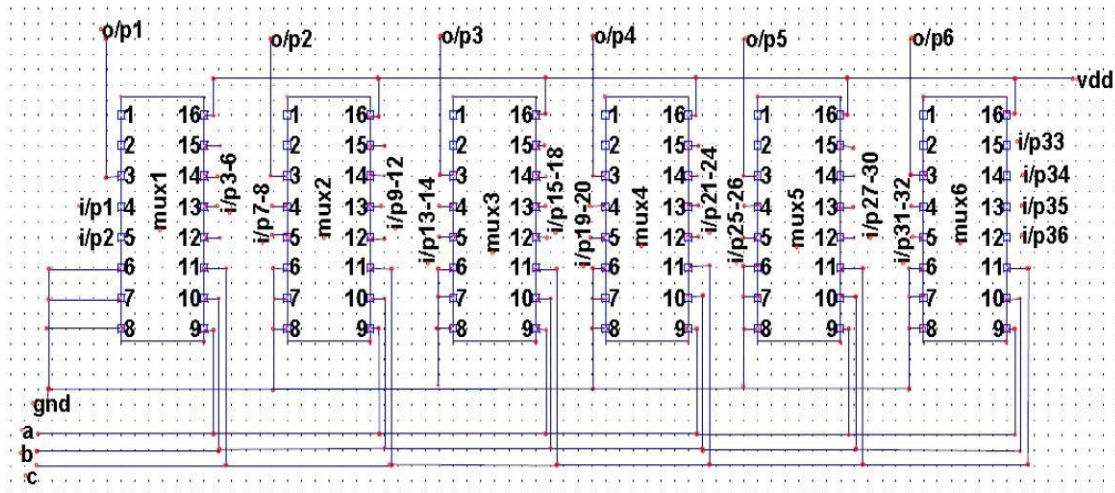


Fig.6.19 Microwave imaging switching circuit system

The HF 4051 analog multiplexer/demultiplexer as shown in Fig. 6.20(a) is a digitally controlled analog switch having low ON impedance and very low OFF leakage current. This multiplexer circuit dissipates extremely low quiescent power over the full VDD - Vss supply voltage range independent of the logic state of the control signals. When logic ‘1’ is present at inhibit input terminal all channel are off. This device is a single 8-channel multiplexer having three binary control input. A, B and C, and an inhibit input. The three binary signals select 1 to 8 channels to be turned on, and connect one of the 8 inputs to the output.

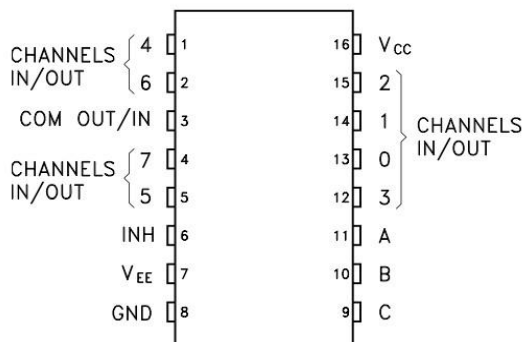


Fig.6.20. (a) HCF 4051-Single 8-channel analog multiplexer/demultiplexer, (b) Netduino Plus2

We have connected Vcc of the 4051 IC to 5 volt supply available from the Netduino plus board, VSS and VEE are shorted and connected to ground. We have taken 6 inputs from pin no 4,5,12,13,14,15 for each six ICs. And the outputs are taken from pin no 3 for each six ICs. The output from each IC is fed to the six analog inputs of the Netduino plus sdk board.

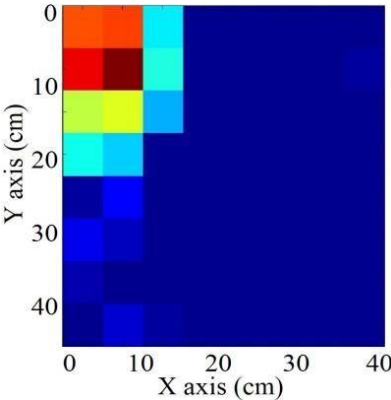
Here Mux A, Mux B and Mux C are used as three control lines from which control bits are sent to the select line of muxes used in our project. At first, by setting Mux A ,Mux B ,Mux C

000 we have activated first input line of all the six Muxes and took input from the six lines and showed it in the output screen. We have repeated the above procedure for next five times. Each time we have given a delay of 3 sec before taking next 6 input values. So total scanning of the 6 by 6 array requires a time span of 18 seconds. In the above program (Appendix), var voltagePort0 - var voltagePort5 are declared as variables to store the input analog values initially. Then "double value0 to double value35" are the actual analog values which are read by the analog input ports in one run. These values are converted to strings to show in the output screen by the command value0.ToString("f3") (Appendix),. To show the output in the screen we have used the command Debug.Print (Appendix).

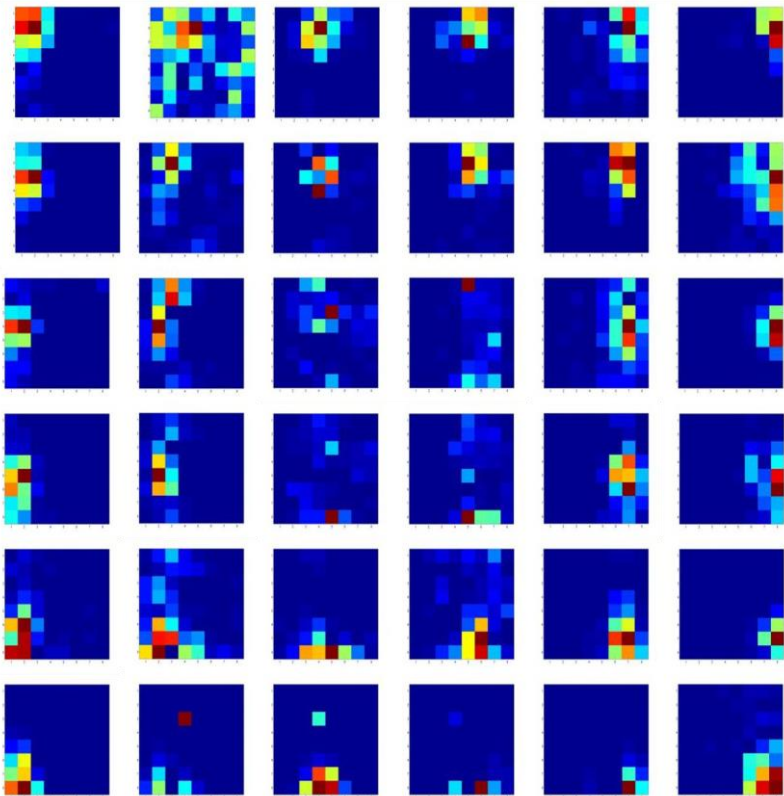
Once the data is stored in the computer with the help of the microcontroller and the switching circuit, the data analysis part can be done using MATLAB. By the use of colormap of 'pcolor' function of MATLAB, a graphical representation is obtain in form of a 6x6 colored grid which is basically the pixel representation of the image of the object to be reconstructed. The data collected by the sensors are used to plot the reconstructed image as a interpolated surface pixel plot with 6x6 data elements using pcolor function of MATLAB.

#### i) Measured 2D Image for Rectangular Metallic Object.

Initially, a rectangular metallic object placed between the Tx and Rx antennas considered using continuous RF signals. In the first case,  $8 \times 8$  pixel images are constructed for Tx antenna placed at 64 different scanning points and a fixed receiver element. The image constructed for the first receiver element is shown in Fig. 6.22 (a). It is observed that in absence of obstruction, when an image is constructed for a single receiver element, then the received power at that element is maximum for the Tx antenna positioned at the closest grid point and the received power decreases significantly when the distance between the Tx antenna position and the receiver element increases. In fact, the received power from Tx antenna placed at different grid points will change due to the signal perturbation from the object. Sometimes, power received from the Tx antenna placed at the furthest grid positions provides insignificant image information. So, these ray-traced unfocused images do not provide complete information regarding the object shapes or positions and almost unusable in nature. All similar 36 images for 36 individual Rx elements are shown in Fig. 6.22 (b).



(a)



(b)

Fig.6.22. a)  $8 \times 8$  pixel image of rectangular object for the first receiver element, (b) All similar 36 images constructed by  $6 \times 6$  receiver elements.

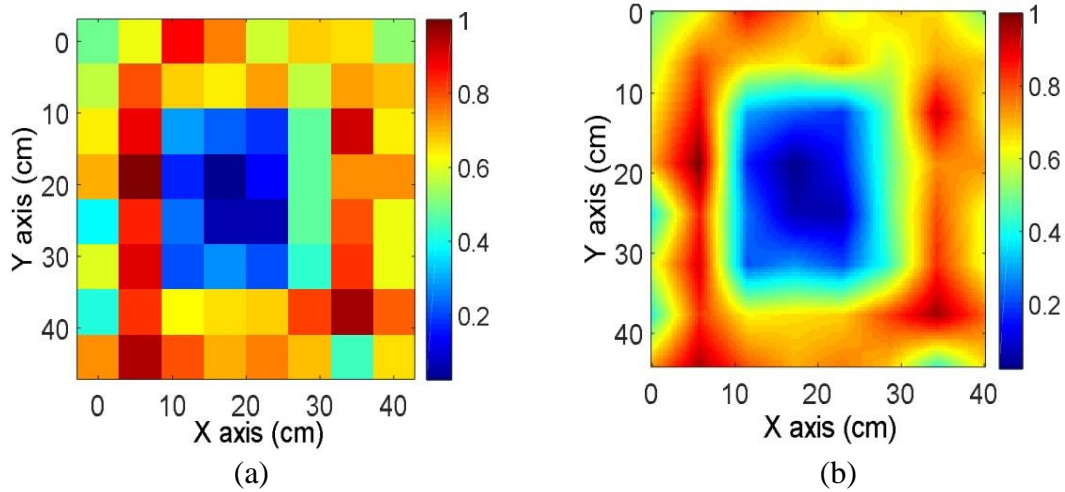


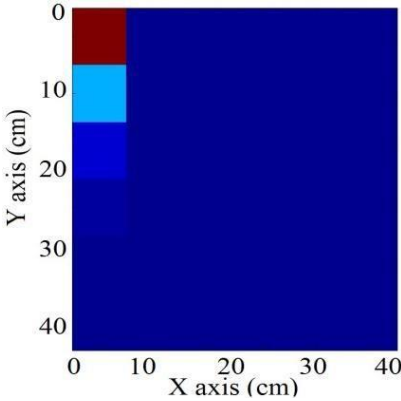
Fig. 6.23. Images for rectangular object: (a) Averaged  $8 \times 8$  pixel image constructed from 36 images (b) Interpolated image constructed from  $8 \times 8$  pixel image

The experimental averaged and normalized  $8 \times 8$  pixel image constructed from 36 images for the rectangular object is shown in Fig. 6.23(a). Like the simulated cases, the shape and position of the rectangular object are visible from the images. These images are further improved by means of interpolation and interpolated images are shown in Fig. 6.23 (b).

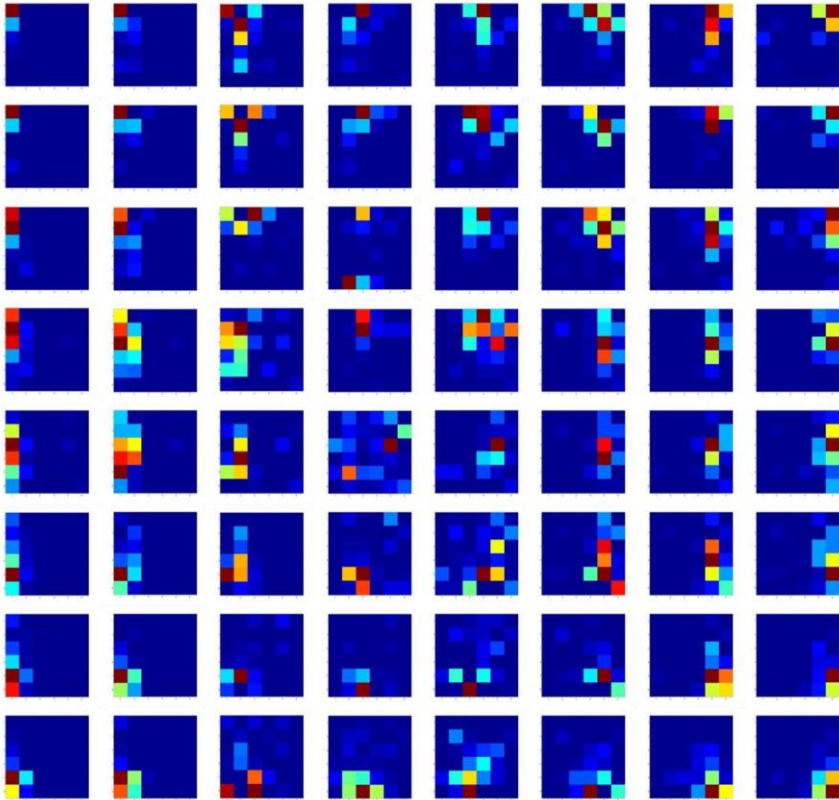
In the second case:  $6 \times 6$  pixel images are constructed for 36 receiver elements when the  $T_x$  antenna is placed at a fixed scanning point. An image constructed for  $T_x$  antenna located at the first grid point is shown in Fig.6.24 (a). It is observed that in the absence of an object, received power at closest receiver element remains maximum just like earlier case.

The  $T_x$  antenna scan the imaging object using roster scanning process at 64 different scanning points and a fixed receiver element and transmit. These unfocused images do not provide complete information regarding the object shapes or positions and almost unusable in nature. All similar 6 by 6 images for 64 individual Rx elements are shown in Fig. 6.24(b).

Like the earlier case, these images give some information about the shape of the image object but none of individually them provide clear information regarding the shape of the object. When  $T_x$  antenna moves at central grid positions, the signal is perturbed due to the presence of the object and spreading of maximum power is observed. These 64 images are finally averaged to obtain a  $6 \times 6$  pixel image as shown in Fig. 6.25(a). In this image, the shape is not clear but position of the object is visible. This image is further improved by means of interpolation and an interpolated image is shown in Fig.6.25 (b).



(a)



(b)

Fig. 6.24. (a)  $6 \times 6$  pixel image constructed from 36 receiver elements for transmitter at grid position  $P_1$ , (b) Similar 64 images for transmitter placed at individual grid positions.



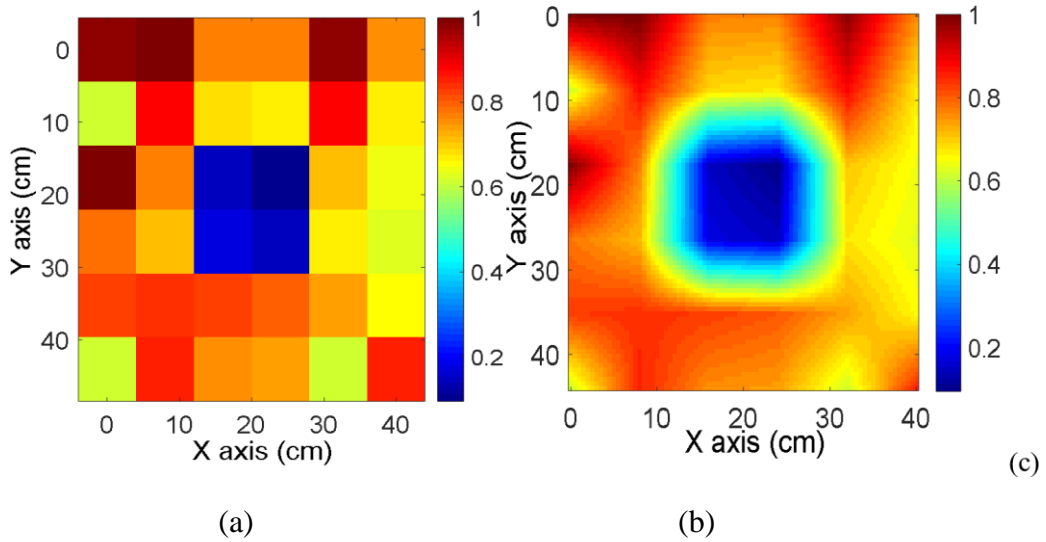
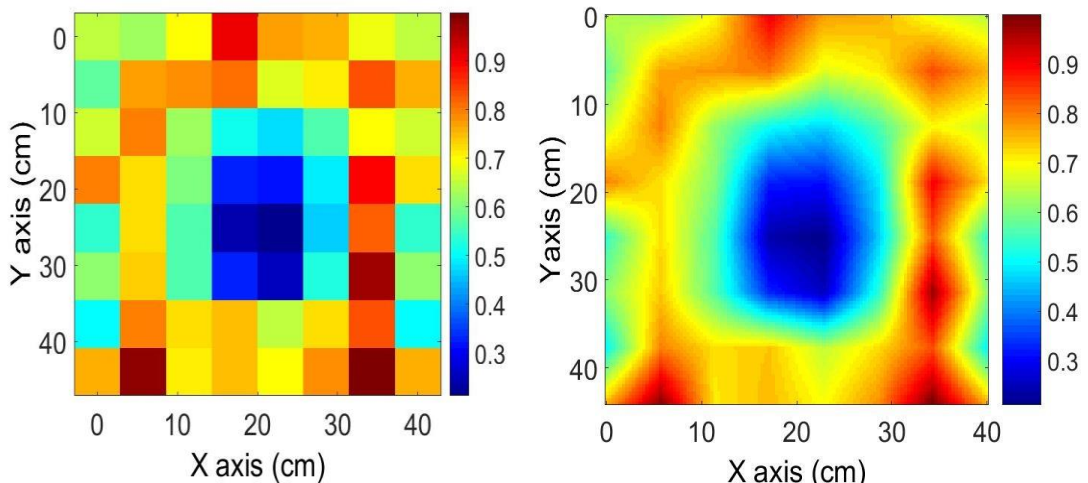


Fig.6.25. Images for rectangular object: (a) Averaged  $6 \times 6$  pixel image constructed from 64 images, (b) interpolated image constructed from  $6 \times 6$  pixel image.

### ii) Measured 2D Image for Circular Metallic Object

A similar experiment is carried out for a circular metallic imaging object. First case; The averaged  $8 \times 8$  pixel image created from 36 images is shown in Fig. 6.26 (a) and the interpolated version is shown in Fig. 6.26 (b). On the second case, another averaged  $6 \times 6$  pixel image of the circular object constructed from 64 scanning points is shown in Fig. 6.26 (c) and an interpolated version of the same is shown in Fig. 6.26 (d).



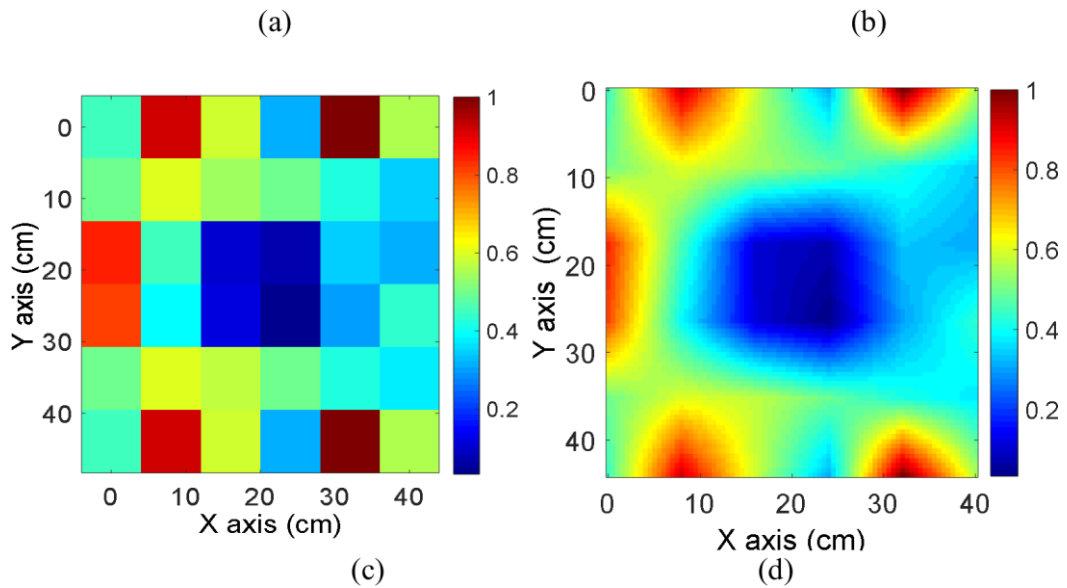

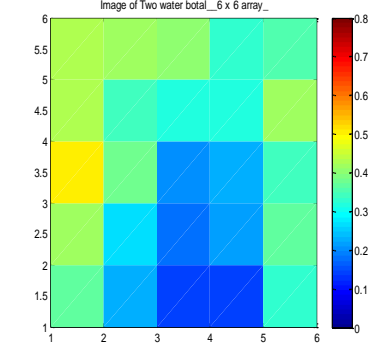
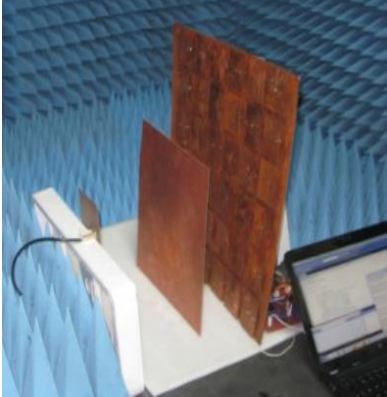
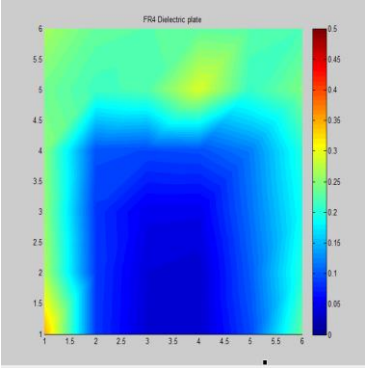
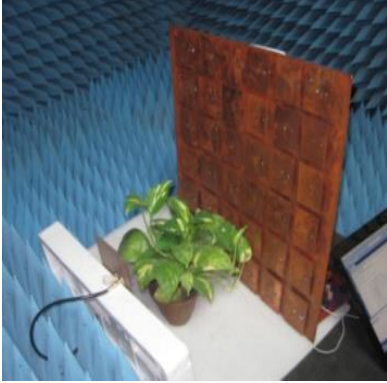
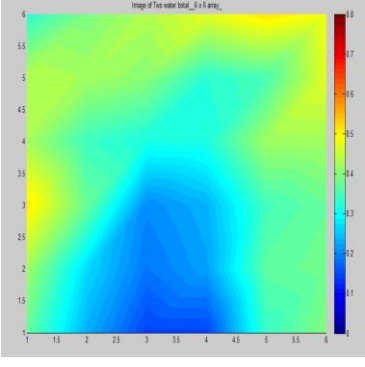


Fig.6.26. Experimental Images for circular object: (a) Averaged  $8 \times 8$  pixel image constructed from 36 images (b) Interpolated image constructed from  $8 \times 8$  pixel image, (c) Averaged  $6 \times 6$  pixel image constructed from 64 images, (d) interpolated image constructed from  $6 \times 6$  pixel image.

Among these two cases, in the first case, a  $8 \times 8$  pixel 2D circular image is obtained from Fig. 6.26 (b) which has more resolution and clearly shows the position and size of a 2D circular image object. For the second case, a  $6 \times 6$  pixel image is obtained from Fig. 6.26 (c) which have a comparatively lesser resolution but has less sensitivity towards different noises than the previous because it averages the number of images.

## 6.7 Experimental Setup Different Microwave Images for Water Boatel, FR4 Substrate and Money Plant.

For different objects are placed in between Tx antenna and Rx antenna array for microwave imaging. The experimental results agree with the imaging results as shown below Table. But since the resolutions of these images are low, for some cases it is difficult to distinguish exact shapes from the constructed images.

Experiment setups	2D planar images
1. setup for water boatel and 2D image	
	
2. Setup for rectangle FR4 substrata and its 2D image	
	
.3 Setup for money plant and its 2D image	
	



## 6.8 Experimental Moving Objects Microwave Images for Water Boatel and FR4 Substrate

Experimental conduction of different objects placed in between Tx and Rx antenna for microwave imaging. Conducted the experiment on real-time based the output power obtained from 36 elements Rx-rectenna array, initially no input for 5sec the output obtained -47dBm, a 1 water bottle fixed for 9sec the output is -37dBm, for 2 bottles are fixed 15sec the output is -40dBm. If water bottle is moving the out power all so fluctuating and lastly FR4 substrate standing and moving in between Tx and Rx antenna the output is fixed and fluctuated these are show in Fig. 6.27. The average output power graph as shown in fig. 6.28.

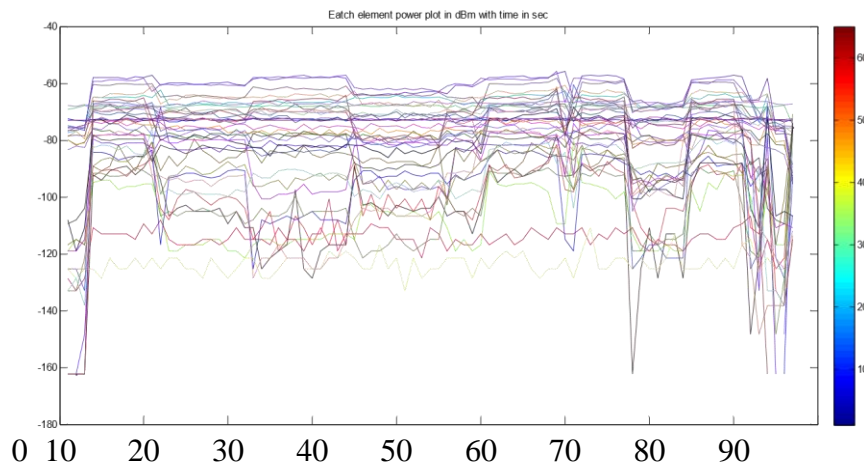


Fig. 6.27. Real time verse output power for 36 sensors different moving objects

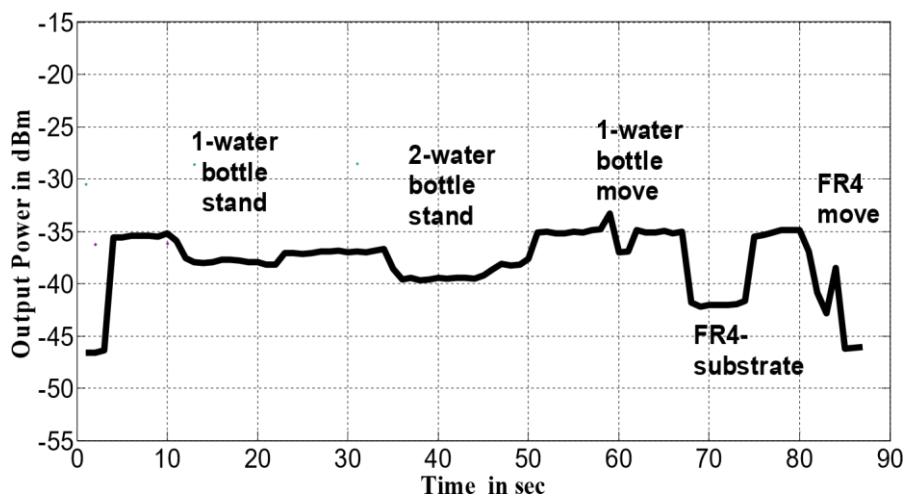


Fig. 6.28. Real time verse output power for sum 36 sensors different moving objects

## 6.8 Microwave imaging for hidden metallic object detection

The proposed Microwave imaging for hidden 'X' metallic object in wooden box detection system is shown in Fig. 6.29. The EM simulation of a complete transceiver along with hidden 'X' object as shown in Fig. 6.29 4 is simulated using CST studio and circuit simulation using ADS. A scanning area of  $40\text{ cm} \times 44\text{ cm}$  is considered for the detection of the metallic object in the wooden box. The scanning of the object is performed by moving the transmitter antenna on the scanning area which is divided into an array of grid points. In Fig.  $15 \times 15$  grid points (P1, P2 ... P625) are shown.

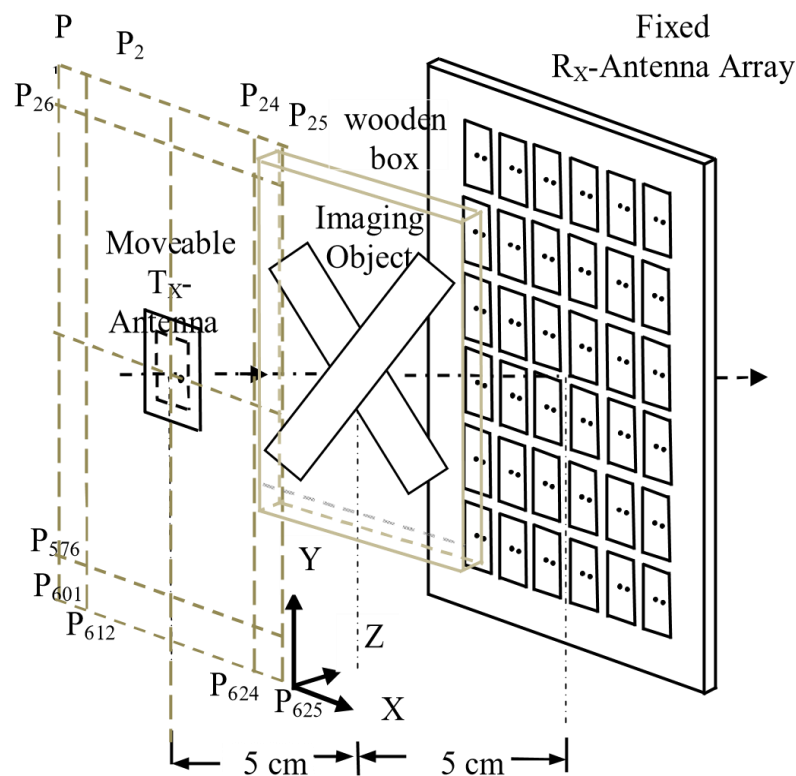


Fig. 6.29. (a) Simulation setup for hidden "X" object in wooden box microwave imaging using  $6 \times 6$  rectenna array.

In EM and circuit co-simulation process S-parameters are generated for the transceiver system along with imaging objects using EM simulator and then power source, impedance matched rectifier circuit blocks are added in the circuit simulator. All the 36 receiver antennas are connected to 36 impedance matched rectifier. Tx antenna transmits CW input signal with power  $P_{in}$  at different grid positions and each receiver antennas receive signals and finally the output voltages ( $V_{o1}, V_{o2} \dots V_{o36}$ ) are captured at output ports. When Tx antenna is placed at

P1, the voltages generated at rectennas for varying input power (–15 dBm to 10 dBm). During scanning, Tx antenna starts its movement from P1 and approaches towards P25 along the X direction and after completion of the first row it moves to P26 of the second row and the process continues till it reaches P625. For this study, the transmitter input power of 10 dBm is considered for generation of all images. So during scanning, the Tx antenna moves at  $25 \times 25$  grid points to complete the scanning of an entire area of the imaging object. During the raster scanning process, for each grid points, the received signals are captured and stored power by the  $6 \times 6$  receiving elements. Thus, the captured data contains  $36 \times 625$  pixel information. Rearranging these data, a  $25 \times 25$  pixel image can be constructed for each of the receiver elements from 625 scanning points of Tx antenna. During a single scanning process, 36 images of  $25 \times 25$  pixels are constructed for all 36 receiver elements. Due to the changes in view angles, these images hold different information and can finally be added to obtain a single image.

## 6.9 Simulated 2D microwave images for hidden objects

### i) "X" Shape Metallic Object 2D Image

Initially, a  $20 \text{ cm} \times 5 \text{ cm}$ , two "X" metallic sheet of 1 mm thickness is hidden in  $35 \text{ cm} \times 30 \text{ cm}$  wooden box considered using continuous RF signals. In the first case,  $25 \times 25$  pixel images are constructed for  $T_x$  antenna placed at 625 different scanning points and a fixed receiver element. The image constructed for the first receiver element is shown in Fig. 6.30 (a). It is observed that in absence of obstruction, when an image is constructed for a single receiver element, then the received power at that element is maximum for the  $T_x$  antenna positioned at the closest grid point and the received power decreases significantly when the distance between the  $T_x$  antenna position and the receiver element increases.

When there is a wooden box with "X" object placed between the  $T_x$  and  $R_x$  antennas, then the received power for nearest grid points may not be maximum. In fact, the received power from  $T_x$  antenna placed at different grid points will change due to the signal perturbation from the object. Sometimes, power received from the  $T_x$  antenna placed at the furthest grid positions provides insignificant image information. So, these ray-traced unfocused images do not provide complete information regarding the object shapes or positions and almost unusable in nature. All similar 36 images for 36 individual Rx elements are shown in Fig.6.30 (b).

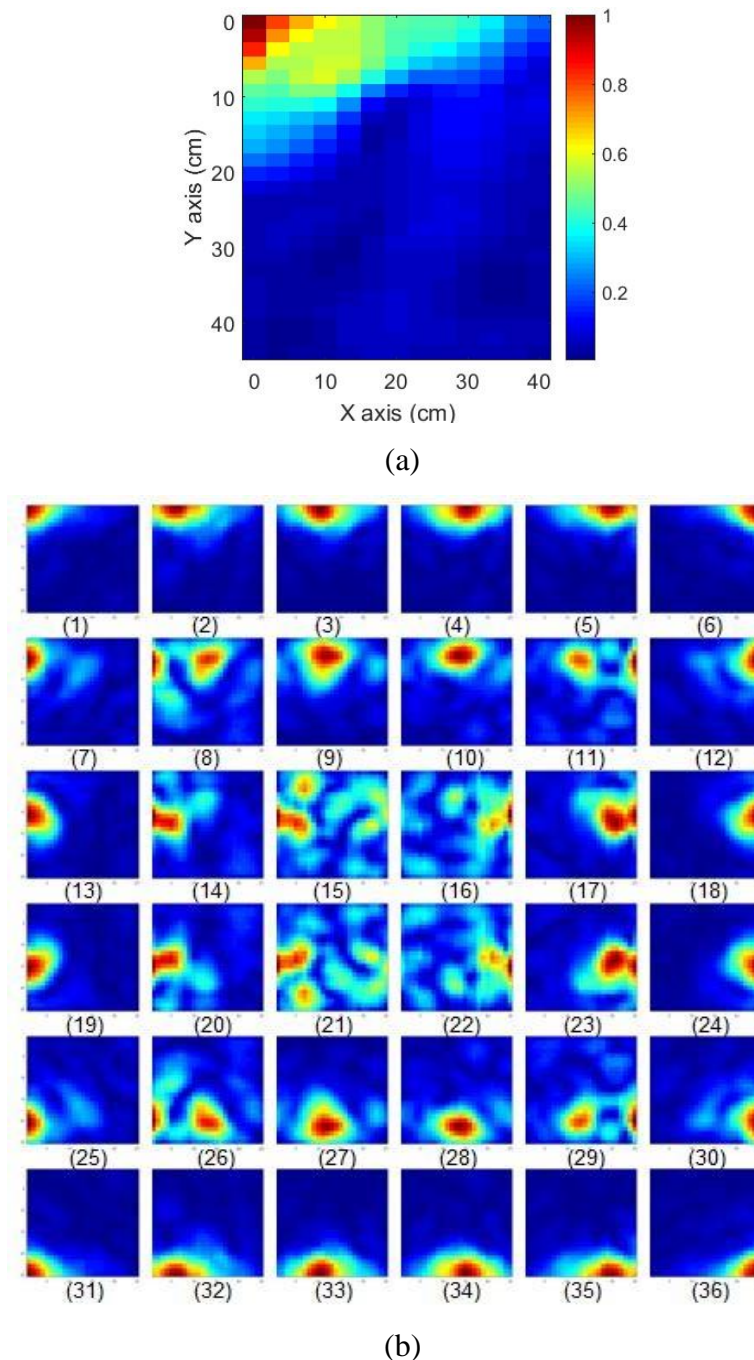


Fig. 6.30. (a)  $25 \times 25$  pixel image of rectangular object for the first receiver element, (b) All similar 36 images constructed by  $6 \times 6$  receiver elements.

When  $T_x$  antenna is placed at outer grid positions, only one bright spot is observed but when it moves at central grid positions, the signal is perturbed due to the presence of the object and spreading of maximum power can be observed. These 36 images are finally averaged to obtain a final  $25 \times 25$  pixel 'X' image which is shown in Fig. 6.31 (a). Now the shape of the 'X' object is visible from the image. This image is further improved by means of interpolation and

an interpolated image with a clearly visible ‘X’ object is shown in Fig. 6.31 (b). Simulations for hidden object in wooden box are carried out for ‘X’ shaped metallic object.

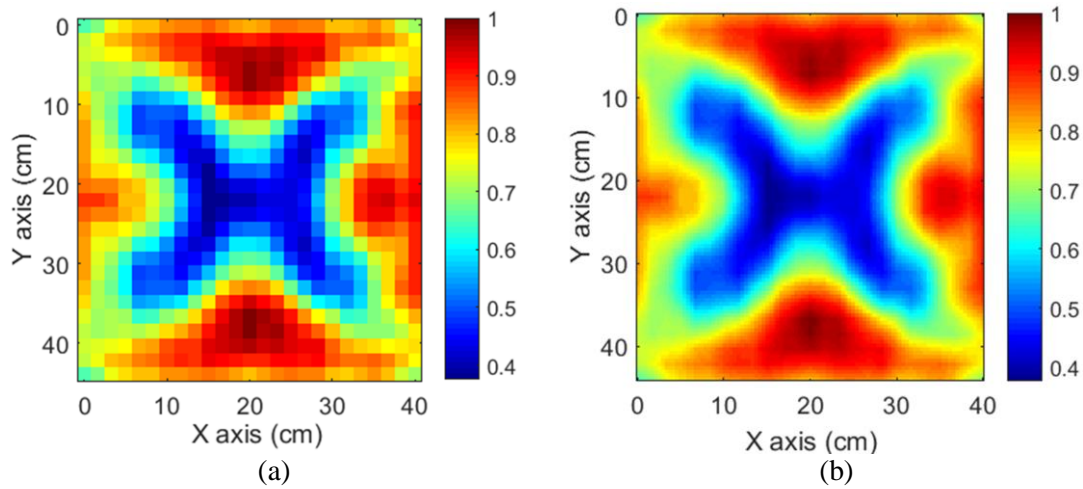
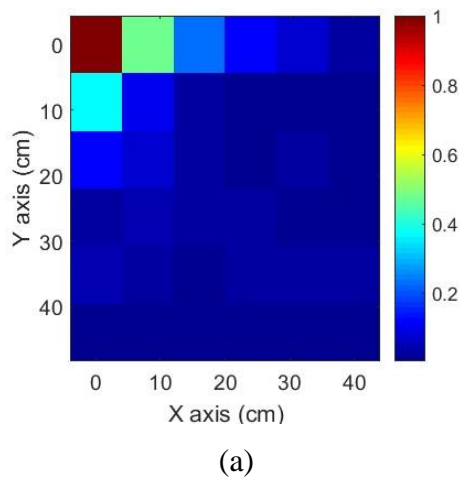


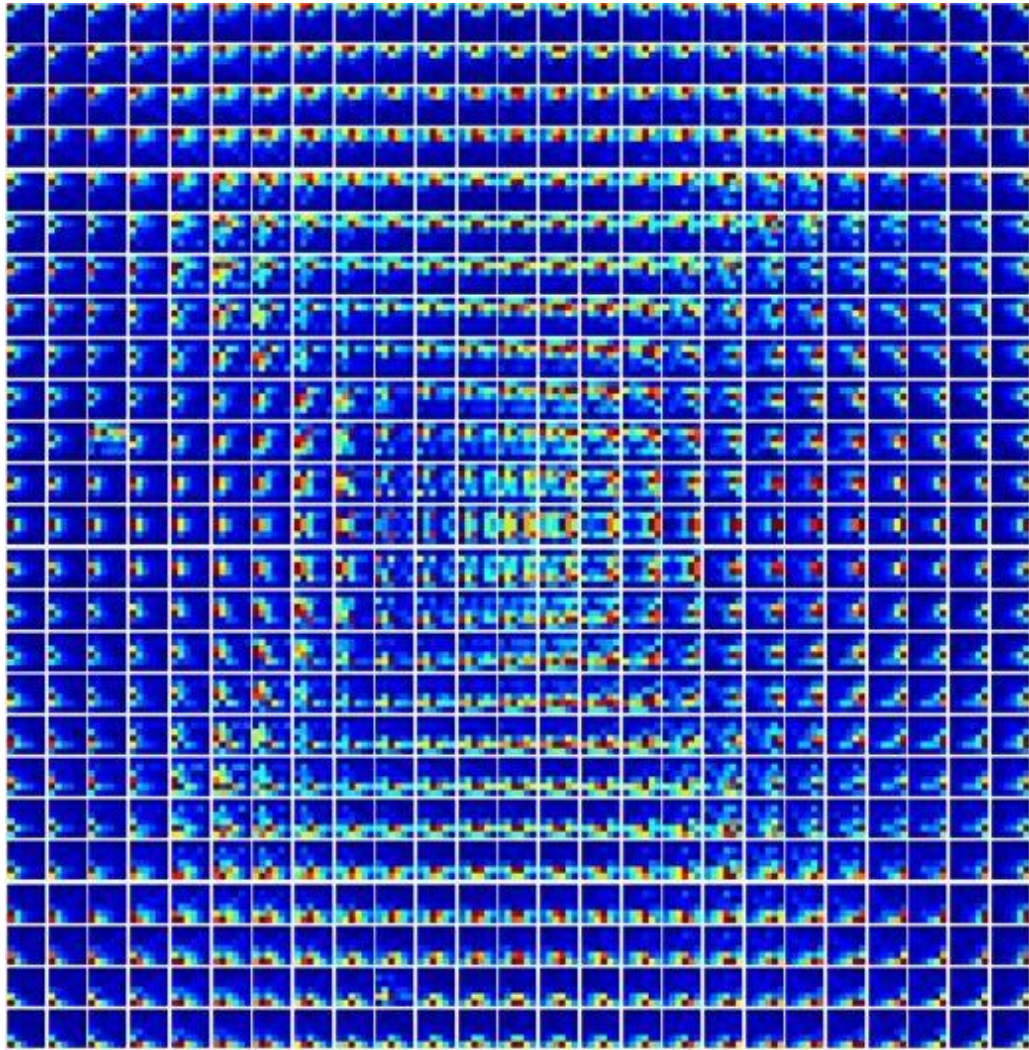
Fig. 6.31. simulated images for ‘X’ shaped object is hidden in wooden box:

(a) Averaged  $25 \times 25$  pixel image, (b) interpolated image constructed from  $25 \times 25$  pixel

In the second case,  $6 \times 6$  pixel images are constructed for 36 receiver elements when the Tx antenna is placed at a fixed scanning point. An image constructed for Tx antenna located at the first grid point is shown in Fig6.32 (a). It is observed that in the absence of an object, received power at closest receiver element remains maximum just like earlier case. All received 625 images from individual grid positions are shown in Fig.6.32 (b).







(b)

Fig. 6.32. (a)  $6 \times 6$  pixel image constructed from 36 receiver elements for transmitter at grid position  $P_1$ , (b) Similar 625 images for transmitter placed at individual grid positions ( $P_1$  to  $P_{625}$ )

Average  $6 \times 6$  pixel image of the 'X' shaped object constructed from 625 scanning points is shown in Fig.6.33 (a) and an interpolated version of the same object as shown in Fig.6.33 (d). Hidden 'X' Object shape can easily be detected from  $25 \times 25$  pixel image but it is difficult to distinguish the shape of an object from the constructed  $6 \times 6$  pixel image.

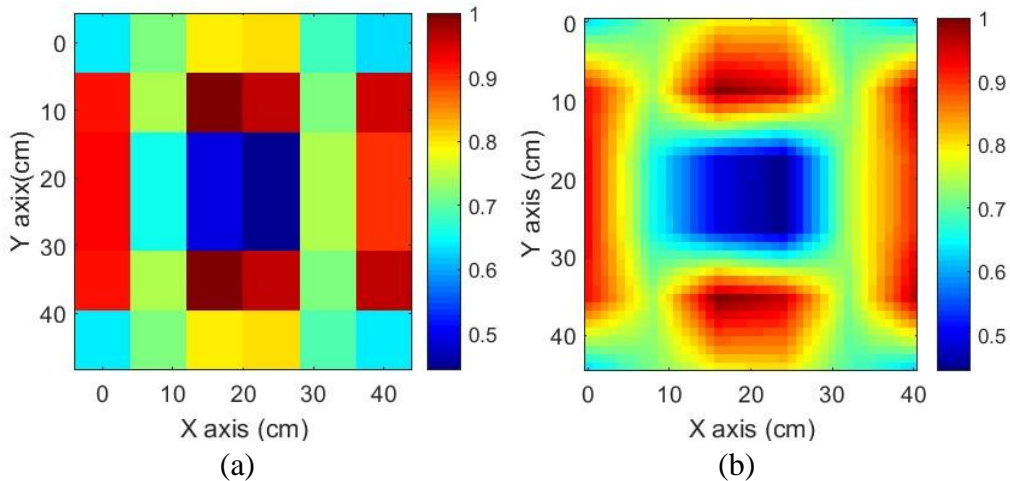


Fig.6.33. Images for ‘X’ shaped object: (c) Averaged  $6 \times 6$  pixel image and (d) interpolated image constructed from  $6 \times 6$  pixel image.

ii) Simulated 2D Image for Triangle Metallic Object.

A similar hidden object experiment is carried out for a triangle metallic imaging object. The averaged  $15 \times 15$  pixel image created from 36 images is shown in Fig. 6.34(a) and the interpolated version is shown in Fig. 6.34 (b). On the second case, another averaged  $6 \times 6$  pixel image of the circular object constructed from 64 scanning points is shown in Fig. 16.34 ( c ) and an interpolated version of the same is shown in Fig. 6.34 (d).

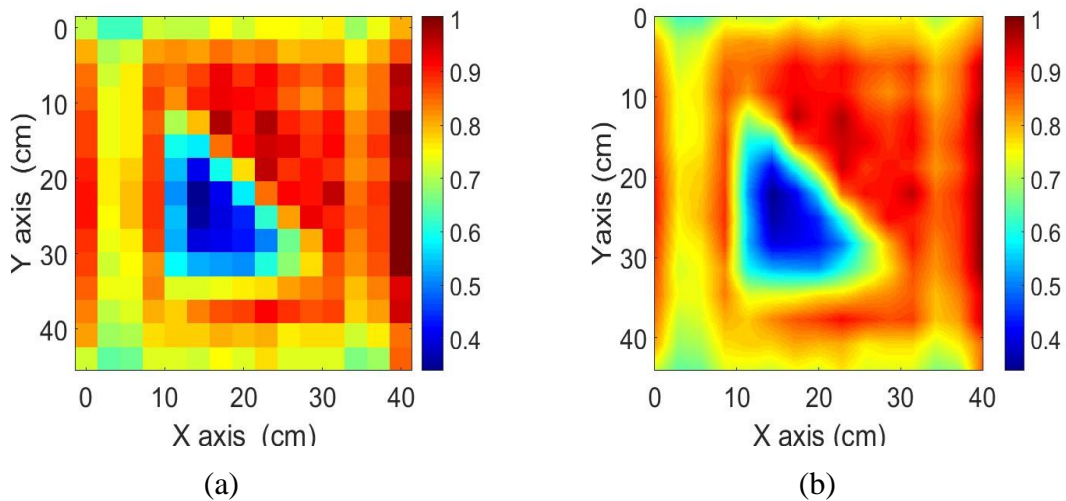


Fig. 6.34 .Simulated hidden Images for Triangle shaped object: (a) Averaged  $15 \times 15$  pixel image and (b) interpolated image constructed from  $6 \times 6$  pixel image

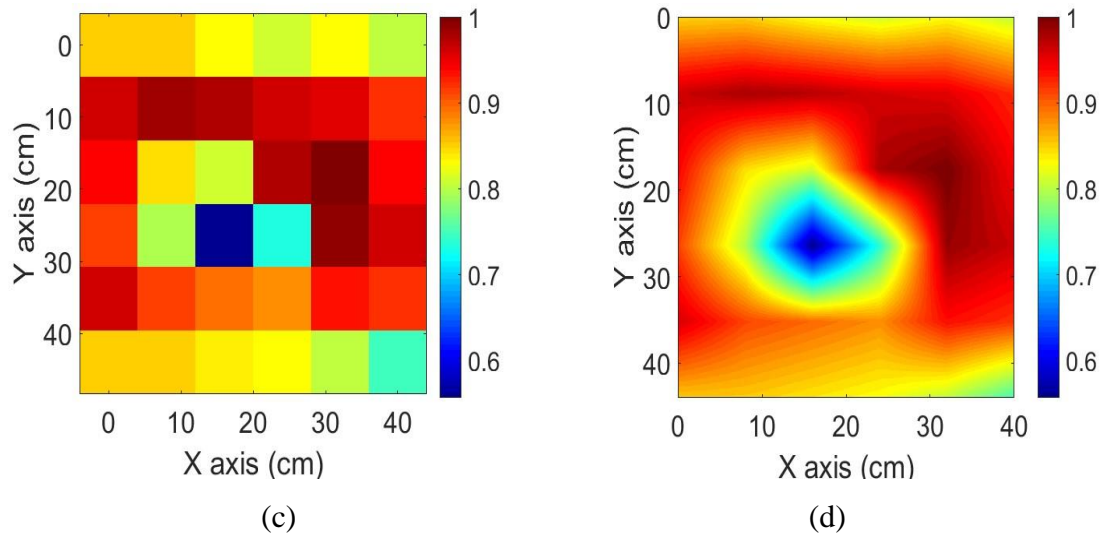


Fig.6.34. Simulated hidden image for Triangle shaped object: (c) Averaged  $6 \times 6$  pixel image and (d) interpolated image constructed from  $6 \times 6$  pixel image

### 6.10 Experimental Setup for Microwave Imaging Detection for Hidden ‘X’ and Triangle Shaped Metallic Object in Wooden Box.

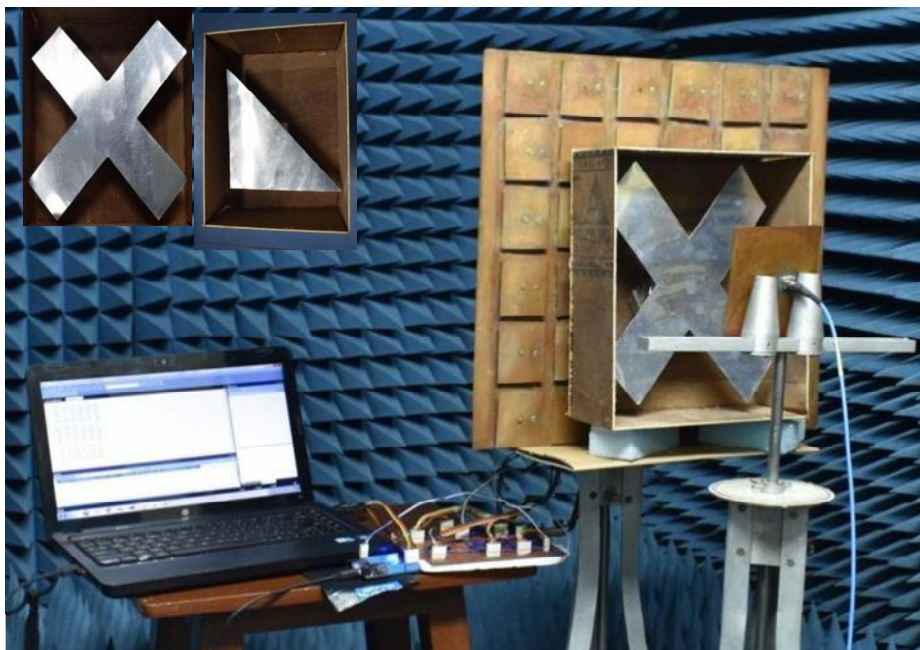


Fig.6.35. Experimental setup for hidden object in wooden box microwave imaging

Experimental setup for the complete imaging system is shown in Fig. 6.35. For mechanical support Styrofoam blocks to wooden box the dimension are width is 30 cm, length is 35cm cm and height is 6cm and thickness is 5mm. A ‘X’ shaped object with 20 cm arms and 5 cm arm



thickness and Triangle shaped object with height is 15cm , base width is 15 cm are made of Aluminum metal sheets are shown in the inset of Fig. 6.35.

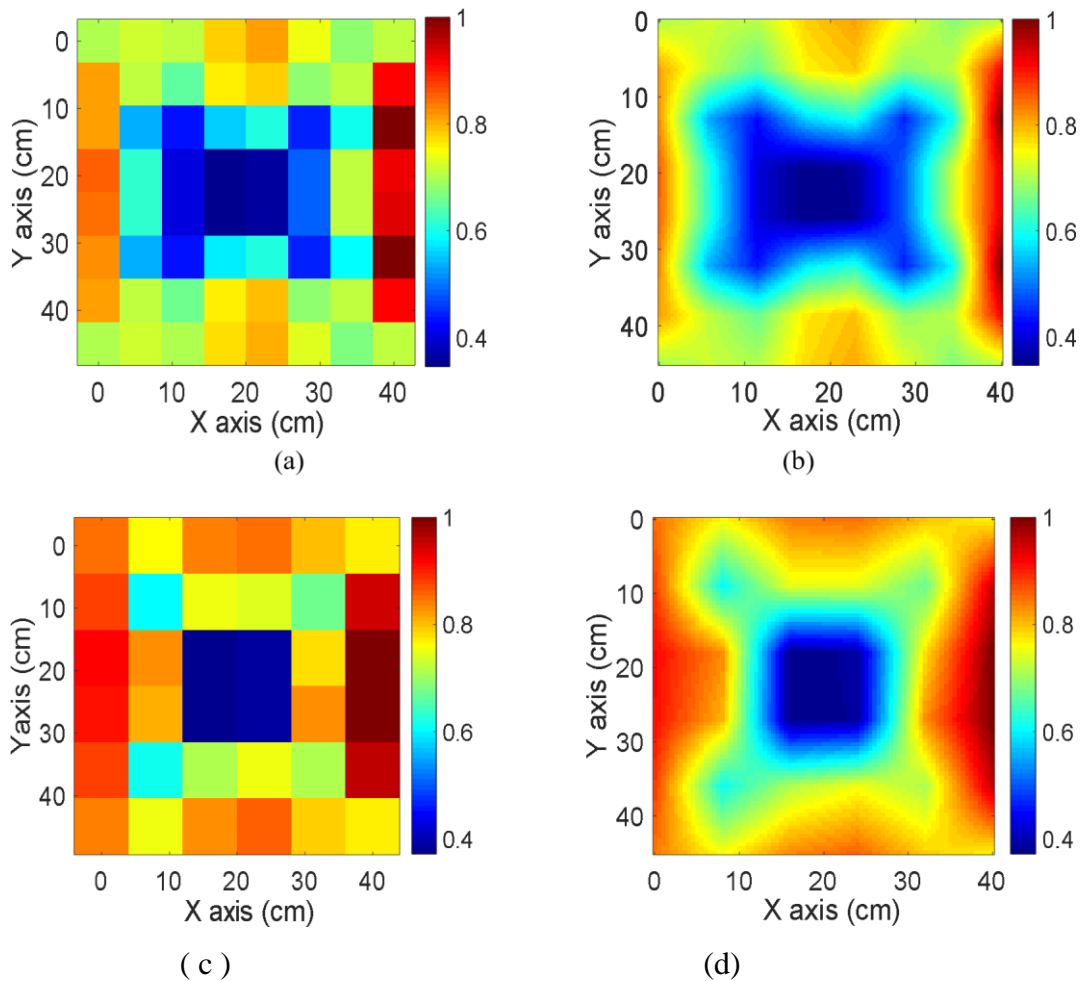


Fig. 6.36. Experimental Hidden Images for 'X' shaped object: (a) Averaged  $8 \times 8$  pixel image, (b) interpolated image constructed from  $8 \times 8$  pixel image, (c) Averaged  $6 \times 6$  pixel image and (d) interpolated image constructed from  $6 \times 6$  pixel image

Hidden object detection is carried out for 'X' shaped metallic object. The averaged  $8 \times 8$  pixel image created from 36 images is shown in Fig. 6.36 (a) and the interpolated version 2D image 'X' shaped object is shown in Fig. 6.36 (b). The normalized  $6 \times 6$  pixel image of the 'X' shaped metallic object constructed from 64 scanning points is shown in Fig. 6.36 (c) and an interpolated version of the same is shown in Fig. 6.36 (d). These two cases, in the first case, a  $8 \times 8$  pixel image is obtained from figure 6.36 (a) and (b), which has more resolution and clearly shows the position and size of a 2D 'X' image object.

For the second case, a  $6 \times 6$  pixel image Fig. 6.36 (c) and (d) is obtained which have a comparatively lesser resolution but has less sensitivity towards different noises than the previous

because it averages the number of images. One more thing can be observed in this figure that an almost not clear shaped image is obtained for a triangle object, which can be rectified if aspect ratios of pixels are considered.

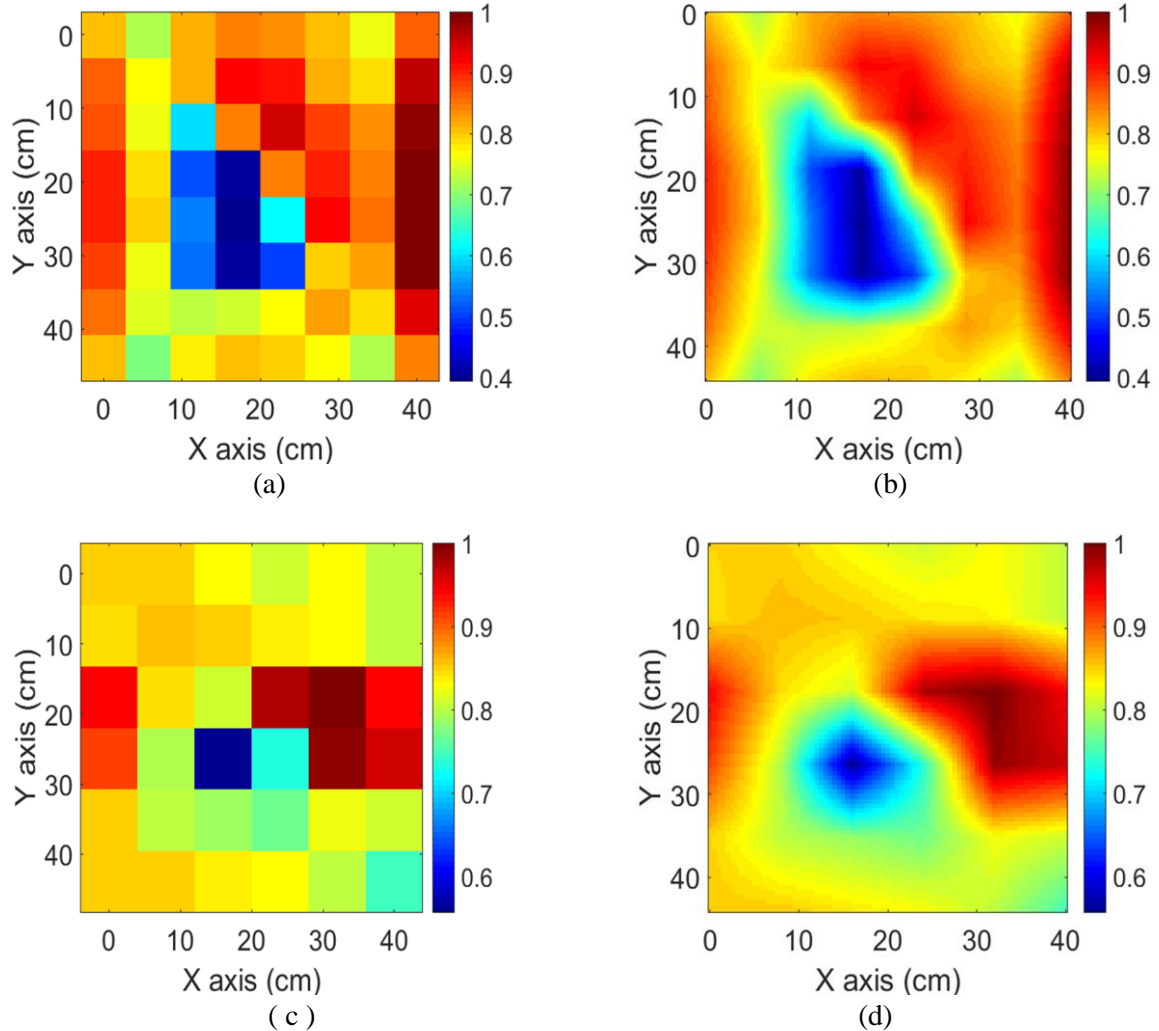


Fig.6.37. Experimental Hidden Image for Triangle shaped object (15cm  $\times$  15cm) : (a) Averaged  $8 \times 8$  pixel image, (b) interpolated image constructed from  $8 \times 8$  pixel image, (c) Averaged  $6 \times 6$  pixel image and (d) interpolated image constructed from  $6 \times 6$  pixel image

A similar experiment is carried out for a hidden triangle metallic imaging object. The averaged  $8 \times 8$  pixel image created from 36 images is shown in Fig. 16.37 (a) and the interpolated version is shown in Fig.16.37 (b). On the other hand, another averaged  $6 \times 6$  pixel image of the circular object constructed from 64 scanning points is shown in Fig. 16.37 (c) and an interpolated version of the same is shown in Fig. 16.37 (d).

Among these two cases, in the first case, a  $8 \times 8$  pixel image is obtained, which has more resolution and clearly shows the position and size of a 2D triangle image object. For the second

case, a  $6 \times 6$  pixel image is obtained which have a comparatively lesser resolution but has less sensitivity towards different noises than the previous because it averages the number of images. One more thing can be observed in this figure that an almost not clear shaped image is obtained for a triangle object, which can be rectified if aspect ratios of pixels are considered.

## 6.10. Conclusion

In this study, an active microwave imaging system is studied and proposed for imaging metallic objects placed within the near field of transmitting and receiving antennas without using any focusing elements like reflectors or lens. In the near field, distribution of EM energy over a different part of objects and on receiver elements is completely nonuniform and large variations of received power at receiver antennas are main problems for ray-tracing. Here these problems are solved by means of averaging the received power from different view angles. Forwardly scattered microwave signals coming through the object from a moving transmitter are captured using a non-movable array of receiver antennas. Thus, this method utilizes both scanning technique and raster imaging technique using sensor array and two images of different resolution are obtained after each scanning. The proposed method is finally verified experimentally for different metallic objects. The images obtained from simulations and experiments are similar in nature and these images provide information regarding the shapes and positions of objects. It is expected that the image will become more prominent if higher resolutions are considered. With suitable modifications like the incorporation of amplifiers and filters may further improve the quality of the images. The system is scalable and similar system can be developed for other frequencies

## References

- [1] C. Pichot, L. Jofre, G. Peronnet and J. Bolomey, "Active microwave imaging of inhomogeneous bodies," in *IEEE Transactions on Antennas and Propagation*, 33(4) (1985) 416–425.
- [2] M. T. Ghasr, M. A. Abou-Khousa, S. Kharkovsky, R. Zoughi and D. Pommerenke, "Portable Real-Time Microwave Camera at 24 GHz," in *IEEE Transactions on Antennas and Propagation*, 60(2) ( 2012) 1114–1125.
- [3] Franchois, A. Joisel, C. Pichot, and J. C. Bolomey, "Quantitative microwave imaging with a 2.45 GHz planar microwave camera," *IEEE Trans. Med. Imag.*, 17(4) ( 1998) 550 – 561.

- [4] D. A. Andrews, S. W. Harmer, N. J. Bowring, N. D. Rezgui and M. J. Southgate, "Active Millimeter Wave Sensor for Standoff Concealed Threat Detection," in *IEEE Sensors Journal*, 13(12) (2013) 4948–4954.
- [5] B. Cooper, R. J. Dengler, N. Llombart, B. Thomas, G. Chattopadhyay and P. H. Siegel, "THz Imaging Radar for Standoff Personnel Screening," *IEEE Transactions on Terahertz Science and Technology*, 1(1) (2011) 169–182.
- [6] Ding, X. Ding, Y. Ye, S. Wu, and Y. Zhu, "High-Resolution Grid-Independent Imaging for Terahertz 2-D Synthetic Aperture Radar with Spatial Under-Sampling", *Progress In Electromagnetics Research, PIER*, 160 (2017) 29–39.
- [7] Yiming Deng, Xin Liu, "Electromagnetic imaging methods for non-destructive evaluation applications," *Journal sensors*, 11(12) (2011) 11774–1808.
- [8] F. Kazemi, F. Mohanna, J. Ahmadi-Shokouh, "Nondestructive high-resolution microwave imaging of biomaterials and biological tissues," *AEU - International Journal of Electronics and Communications*, 84 (2018) 177-185.
- [9] Khanfar, M. Abu-Khousa, N. Qaddoumi, "Microwave near-field non-destructive detection and characterization of disbonds in concrete structures using fuzzy logic techniques," *Elsevier Compos Struct*, 62 (2003) 335–339.
- [10] D. A. Ausherman, A. Kozma, J. L. Walker, H. M. Jones E. C. Poggio, "Developments in radar imaging," *IEEE Transactions on aerospace and electronic systems*, 20(4) (1984) 363– 400.
- [11] M. T. Falconi, D. Comite, A. Galli, D. Pastina, P. Lombardo and F. S. Marzano, "Forward scatter radar for air surveillance characterizing the target-receiver transition from far-field to near-field regions," *MDPI Journal Remote Sens.*, 9(50) (2017)1–22.
- [12] P. Bezousek, V. Schejbal, "Bistatic and Multistatic radar systems," *Radio engineering*, 17(3) (2008) 53 – 59.
- [13] R. C. Conceicao, M. O'Halloran, M. Glavin, and E. Jones, "Comparison of Planar and Circular Antenna Configurations for Breast Cancer Detection Using Microwave Imaging", *Progress In Electromagnetics Research, PIER*, 99 (2009) 1–20.
- [14] T. Ghohipura, M. Nakhkashb, "Optimized matching liquid with wide-slot antenna for microwave breast imaging," *AEU - International Journal of Electronics and Communications*, 85 (2018)192–197.
- [15] D. Yaghjian, "An overview of near-field antenna measurements," *IEEE Trans Antennas Propagate*, 34(1) (1986) 30 – 45.
- [16] M. T. Ghasr, M. J. Horst, M. R. Dvorsky and R. Zoughi, "Wideband Microwave Camera for Real-Time 3-D Imaging," in *IEEE Transactions on Antennas and Propagation*, 65(1) (2017) 258–268.
- [17] P. M. Meaney, M. W. Fanning, Dun Li, S. P. Poplack and K. D. Paulsen, "A clinical prototype for active microwave imaging of the breast," in *IEEE Transactions on Microwave Theory and Techniques*, 48(11) (2000) 1841–1853.
- [18] F. Mirza *et al.*, "An Active Microwave Sensor for Near Field Imaging," in *IEEE Sensors Journal*, 17(9) (2017) 2749–2757.

- [19] Qing Huo Liu et al., "Active microwave imaging. I. 2-D forward and inverse scattering methods," in *IEEE Transactions on Microwave Theory and Techniques*, 50(1) (2002) 123– 133.
- [20] C. Lu and X. G. Zhong, "Image reconstruction of two-dimensional objects inside dielectric walls," *Microwave Optical Technology Letter*, 36(2) (2003) 91– 95.
- [21] B. Mhamdi, K. Grayaa, T. Aguilu, "Microwave imaging of dielectric cylinders from experimental scattering data based on the genetic algorithms, neural networks and a hybrid micro genetic algorithm with conjugate gradient," *AEU - International Journal of Electronics and Communications*, 65 (2011)140–147.
- [22] J. D. Kraus and R. J. Marhefka, "Antennas for all application", 3rd Ed., *Tata McGraw-Hill Publishing Company Limited*, New Delhi, India, 2003.
- [23] E. Nilsson, L. Baath, "Radar Interferometric Measurements with a Planar Patch Antenna Array," *IEEE Sensors J.*, 7(7) (2007) 1025 – 1031.
- [24] CST Microwave Studio Suite, CST Computer Simulation Technology GmbH 2017, <http://www.cst.com> .
- [25] Agilent Advanced Design System, 2009, Agilent Technologies, USA.
- [26] MATLAB - R2013b, <http://www.mathworks.com>

# Chapter 7

## Conclusions and Future Work

### 7.1. Introduction

This chapter concludes the thesis and scope for further investigations are suggested. The thesis started with a brief introduction to wireless energy transfer techniques and microwave imaging methods followed by literature survey on WET and microwave imaging. Planar antenna arrays are investigated for WET. A broadband full-wave rectenna has been investigated using a dual-fed RMSA. A low power detector is proposed for microwave imaging. A two-dimensional microwave imaging system is theoretically investigated using electromagnetic (EM) and circuit co-simulation techniques, and subsequently experimentally verified. The main conclusions drawn from this work are summarized in the following section.

### 7.2. Summary

The contributions made towards the PhD work can be subdivided into two major groups. In this thesis, we have attempted to study different aspects of the interaction of electromagnetic waves for Wireless Energy Transfer (WET) and radar-based imaging.

WET is becoming increasingly popular due to its ability to eliminate the need for wires or connectors, thereby enhancing the mobility of various systems. Microwave-based WET requires suitable antennas and rectennas. To achieve higher power delivery at a distant point, the use of an antenna array can be a viable solution. However, the efficiency of antenna arrays significantly decreases with larger arrays.

In my research, I conducted investigations on planar arrays that incorporate radiating suspended rectangular patch antennas with a corporate feed network. The research conducted in this study focused on designing a suspended planar antenna array for WET applications. The aim was to investigate and compare the WET output power, both through simulation and measurement, between a rectifying antenna array and an array of rectennas.

Rectenna networks are typically single-port networks and not suitable for full-wave rectification. Therefore, the possibility of designing an edge-feed dual-port full-wave rectenna is investigated. Both a two-diode full-wave rectenna and a four-diode full-wave bridge broadband rectenna are investigated for WET. The proposed two-diode full-wave rectenna configuration exhibits better efficiency compared to a conventional half-wave rectenna. Similarly, parametric studies are conducted on the full-wave bridge broadband rectenna to investigate its output properties for different frequencies and distances between transmitter and receiver antennas. The proposed full-wave bridge configuration demonstrates higher efficiency than the two-diode full-wave rectenna and the conventional half-wave rectenna. An edge-feed dual-port full-wave rectenna system has been fabricated for experimental verification. The measured results are compared with the simulated data to validate the performance of the system.

To meet the requirements of low-power detection in microwave imaging, an investigation has been conducted on a low-power small-signal biasing detector. This detector has been specifically designed and implemented for use in microwave imaging.

Furthermore, an investigation has been conducted on near-field microwave imaging systems to explore new methods suitable for non-destructive testing. The investigations have explored various microwave imaging techniques, such as radar imaging and tomographic techniques, to enhance the capabilities of non-destructive testing. In this work, a hybrid system is proposed that utilizes antenna arrays similar to those of optical camera sensors, with a movable illuminating antenna performing ray tracing in the near field.

In this study, an active microwave imaging system is examined and proposed for imaging metallic objects placed within the near field of transmitting and receiving antennas without the use of focusing elements such as reflectors or lenses. In the near field, the distribution of EM energy over different parts of objects and receiver elements is not uniform. A two-dimensional microwave imaging system is theoretically investigated using electromagnetic (EM) and circuit co-simulation techniques, and subsequently experimentally verified. In the case of microwave imaging, scattered signals from objects of different shapes and sizes are captured by an array of rectennas, resulting in multiple, unfocused images. The final images are then constructed by averaging these multiple unfocused images.

Incident and scattered microwave signals coming through the object from a moving transmitter are captured using a non-movable array of receiver antennas. This method combines

scanning and raster imaging techniques using a sensor array, resulting in two images of different resolutions after each scan. The proposed method is experimentally verified using metallic objects of different shapes. The simulated and experimental images exhibit similar characteristics, providing information about the shapes and positions of the objects. It is expected that higher resolutions will further enhance the image quality.

The aim of this thesis includes:

- i. Literature review of different WET system. Study of the advancement and progress in the areas of WET using microwave.
- ii. Investigate possible solutions for full wave rectennas which may provide better efficiency than the conventional rectennas consisting a half wave rectifier circuit.
- iii. Compare efficiencies between rectifying antenna array and array of rectennas
- iv. Design low power microwave detector suitable for microwave imaging
- v. Investigate on near field microwave imaging system for some new method suitable for non-destructive testing

### 7.3 Further investigations

There are scopes for further investigations in the area of planar antenna and rectenna arrays in wireless energy transfer and near-field microwave imaging. Some of these are:

- i. Design optimization: Conducting research to optimize the design of planar antenna arrays for wireless energy transfer and near-field microwave imaging. This includes exploring different antenna geometries, element spacing, and feeding techniques to enhance performance.
- ii. Efficiency enhancement: Investigating methods to improve the efficiency of planar rectenna arrays, which are responsible for converting received microwave energy into usable direct current (DC) power. This can involve optimization of rectification circuitry and improving impedance matching techniques.
- iii. Array beamforming: Exploring beamforming techniques for planar antenna arrays to achieve directional energy transfer and improved imaging capabilities. This involves



developing algorithms and signal processing techniques to steer the transmitted or received beams towards specific targets or areas of interest.

- iv. Multi-band operation: Investigating the feasibility of planar antenna and rectenna arrays operating in multiple frequency bands. This can enable simultaneous energy transfer and imaging in different frequency ranges, allowing for versatile applications and enhanced system flexibility.
- v. Integration with other technologies: Exploring the integration of planar antenna and rectenna arrays with other technologies such as phased array systems, metamaterials, and advanced signal processing algorithms. This integration can lead to improved system performance, increased energy transfer efficiency, and enhanced imaging capabilities.
- vi. Miniaturization and scalability: Investigating techniques to miniaturize planar antenna and rectenna arrays for compact and portable applications. Additionally, exploring scalability options to increase the array size without sacrificing performance, enabling larger coverage areas and higher power transfer capabilities.

-----